The Role of Bone Marrow Mesenchymal Stromal Cell Senescence in Multiple Myeloma

Natalya Plakhova

Myeloma Research Laboratory

School of Biomedicine

Faculty of Health and Medical Sciences

The University of Adelaide

&

Cancer Theme

South Australian Health and Medical Research Institute

A thesis submitted to The University of Adelaide for the degree of Doctor of Philosophy

December 2022

TABLE OF CONTENTS

ABSTRACT

Multiple myeloma (MM) is a malignancy characterised by the uncontrolled clonal proliferation of neoplastic plasma cells (PCs) within the bone marrow (BM). MM PCs rely on mesenchymal stromal cells (MSCs) within the BM for their proliferation and survival. MM is universally preceded by an asymptomatic precancerous condition, monoclonal gammopathy of undetermined significance (MGUS). The risk of progression of MGUS-to-MM increases with advancing age, concurrent to the accumulation of senescent BM-MSCs. Moreover, MSC senescence has been implicated in promoting cancer growth, suggesting that it could play a role in MM progression.

Here, we characterised BM-MSC senescence in *ex vivo* expanded BM-MSCs isolated from BM trephine biopsies from MGUS (median age: 67.5 [range: 42-84]) and MM (age: 70 [52-84]) patients and aged (age: 88 [68-94]) and young (age: 21 [17-26]) healthy subjects by evaluating β-galactosidase activity, proliferation and cellular morphology. These studies confirmed that age-related increases in BM-MSC senescence are a characteristic feature of MGUS and MM. Additionally, there was no significant difference in the number of senescent BM-MSCs between aged healthy subjects, MGUS and MM patients, suggesting that this was not a function of disease stage. Strikingly, we found that the risk of progression to MM is significantly elevated in MGUS patients with increased BM-MSC senescence. Furthermore, we demonstrated that the induction of BM-MSC senescence promoted the proliferation of MM PCs relative to co-culture with non-senescent controls.

Senescent MSCs display a senescence associated secretory phenotype (SASP) characterised by increased production of growth molecules. Notably, we identified that BM-MSC gene

expression of the well-established SASP factor interleukin-6 (*IL-6*) and novel SASP factor Gremlin1 (*GREM1*) at MGUS was predictive of progression to MM in our cohort. However, our studies showed that the MM growth-promoting effects of irradiated senescent BM-MSCs were not mediated by IL-6 and or Gremlin1 *in vitro*. Further RNA sequencing analysis of irradiated murine stroma identified 17 putative SASP factors, which were upregulated with irradiation and are expressed by MM patient BM-MSCs. These include, CXCL-12, GAS6 and IGF-1, which have been previously implicated in promoting MM PC growth.

To investigate whether BM-MSC senescence plays a role in MM PC proliferation *in vivo*, we utilised a mouse model where cre-mediated knockout of enhancer of zeste 2 (EZH2) is driven by the mesenchymal Prrx1 promoter, which has previously been reported to induce senescence of mesenchymal lineage cells *in vivo*. Unexpectedly, our studies revealed that senescent cell burden within the bones and of BM-MSCs of $EZH2^{+/-}$ mice was significantly reduced relative to that of WT controls. Furthermore, we did not detect a difference in Vk*Myc MM tumour growth within the BM following intravenous injection in these animals.

Collectively, our findings suggest that the accumulation of senescent BM-MSCs with advancing biological age could constitute a growth-permissive niche at MGUS and facilitate the progression to MM. Excitingly, this highlights the potential utility of these cells as a novel therapeutic target and provides the impetus for future studies investigating the utility of senolytics and agents that inhibit the pro-tumorigenic effects of SASP to prevent MGUS-to-MM progression.

DECLARATION

I certify that this work contains no material which has been accepted for the award of any other degree or diploma in my name in any university or other tertiary institution and, to the best of my knowledge and belief, contains no material previously published or written by another person, except where due reference has been made in the text. In addition, I certify that no part of this work will, in the future, be used in a submission in my name for any other degree or diploma in any university or other tertiary institution without the prior approval of the University of Adelaide and where applicable, any partner institution responsible for the joint award of this degree. I give permission for the digital version of my thesis to be made available on the web, via the University's digital research repository, the Library Search and also through web search engines, unless permission has been granted by the University to restrict access for a period of time. I acknowledge the support I have received for my research through the provision of an Australian Government Research Training Program Scholarship.

Signed:

Natalya Plakhova 28/11/2022

ACKNOWLEDGEMENTS

Firstly, I would like to thank Professor Andrew Zannettino for and giving me the opportunity to undertake my PhD studies in the Myeloma Research Laboratory and being my primary supervisor throughout this rollercoaster journey. Thank you for taking a chance on me even though I had never done an Honours Degree and believing in me when I had to start over with project 2.0 a year into my candidature.

I would also like to express my gratitude to my PhD supervisors Dr Kate Vandyke and Dr Krzyszstof Mrozik for all your guidance and support throughout my studies and in the preparation of this thesis. To Kate, you have been extremely helpful and supportive throughout this journey by not only helping me with data analysis, planning experiments and reading my extremely lengthy drafts, but most importantly, helping me have a positive outlook throughout my studies. I would not be here today without your support. Thank you for always believing in me and encouraging me to keep going. To Krzys, I am excited and honoured to be your first PhD student (mainly because this means I must be the favourite). Thank you for your help in the lab and during the writing process, but most importantly, thank you for your friendship throughout the years. Being able to openly and honestly discuss how I have been feeling throughout my project has been incredibly encouraging and insightful.

I would also like to thank my lab moms, Sharon Paton, Vicki Wilczek and Rosa Harmer for always supporting me, answering my silly little questions and the all-important life advice.

This has undoubtedly been the hardest experience of my life so far and it has also taught me many things about myself. I could not have possibly done this without all the help and support from my many wonderful work friends. I will cherish these amazing friendships for the rest of my life.

A special thank you to my partner in crime Justine Clark for always being there for me from the start and going to gigs, festivals and tattoo appointments with me to spice up our weekends (and some weekdays) throughout this 5-year journey. When I saw you wearing my Violent Soho shirt in the lab, initially, I wasn't initially sure if we were going to end up being enemies or best friends, but I am glad it ended up being the latter. To Saoirse Benson, thank you for all the endless coffee and pizza dates and Sunday night spirals that prepared us for the week ahead. Also, thank you so much for all the little treats and flowers you surprised me with when you knew I was struggling with my PhD – you always knew how to lift me up and I couldn't have possibly done this without you.

To Alanah Bradey, Dr Mara Zeissig, Dr Kimberley Clark, Dr Khatora Opperman and Dr Clara Pribadi – thank you for making me feel extremely comfortable and welcome when I first started in the lab. I am so grateful for your friendship and will always look up to you. To comrade Jvaughn Duggan, in addition to your technical and mathematical advice, thank you for partaking in communicating with me in a Russian accent when discussing negative results of my experiments to soften the blow. To Laura Trainor, a special thank you for sitting beside me, all our laughs and walks to the Faxitron. Your incredible advice has always guided me, especially when you recommended that I book the Clinic Room for my big supervisor meeting. Also, thank you for your tenacious efforts in facilitating morning tea.

To Emma Cheney, thank you for always letting me borrow your HDMI adapter for all my presentations and letting me help you choose from your outfit options for your special events. To Connor Williams, thank you for all our chats and always checking in on me. ‘It is what it is’- but somehow you made things seem better!

Additionally, I would like to thank Jacqui Scott, Elaine Thomas, Hayley Parkinson, Maya Davies, Caleb Lill, Nick Smith for your wonderful friendship and extremely entertaining lunchtimes.

Many other people outside of the laboratory have made an important contribution to this project. To Dr Randall Grose from the SAHMRI Flow Cytometry Facility, thank you for helping me plan and execute my experiments, making Fridays fun with themed dress ups and most importantly, letting me pick the music when I was running my samples. Furthermore, this project would not have been possible without the help from the SAHMRI Bioresources facility. Particularly, I would like to thank Dylan Harnas for helping me look after my millions of adorable, aged mice. I would also like to thank Prof Stan Gronthos and Dr Dimitrios Cakouros for all of your help with the *in vivo* EZH2 model and all your wisdom, particularly regarding senescence assays. Moreover, I would like to thank Mark Vanderhoek from SAGC for helping me with my RNAseq analysis.

I am also very thankful for the unconditional love and support I received from my friends outside of my laboratory. Although you have not personally experienced writing a PhD thesis, you have always been incredibly understanding and there for me, especially during the times that I was really struggling – Jess Purvis, Kavita Shah, Ashley Biddell and Madeline-Massy Westropp, we all share this achievement.

Jess, believe it or not, this entire thesis has been written on my little sparkly pink laptop, which clearly never saw it coming when I initially purchased it.

Lastly, I would also like to thank my family for your unwavering support throughout this journey. Although you have not always been physically here to support me, you were always just a phone call away and never failed to encourage and motivated me. Daniel – you may be the first 12-year-old to try on the big floppy hat, and I am entirely confident you will be wearing it all day instead of me during my graduation ceremony. Love you loads.

Thank you!!! xxx

ABBREVIATIONS

3D	3-dimensional
α-MEM	α-modified minimum essential medium
β-gal	β-galactosidase
ADM	adrenomedullin
AID	activation-induced-deaminase
AL	amyloid light-chain
AML	acute myeloid leukaemia
Ang-1	angiopoietin-1
ANOVA	analysis of variance
APOBEC	Apolipoprotein B MRNA Editing Enzyme
AREG	amphiregulin
ASCT	autologous stem cell transplant
ATCC	American Type Culture Collection
ATX	autotaxin
AXL	Axl receptor tyrosine kinase
B2M	beta-2-microglobulin
BAP1	BRCA1-associated protein-1
Bcl-2	B-cell lymphoma 2
BCMAs	B cell maturation antigens
BFA	brefeldin A
bHLH	basix helix-loop-helix
BM	bone marrow
BMi1	BMi1 polycomb ring finger oncogene
BMP	bone morphogenic protein
CALCRL	calcitonin receptor like receptor
CAM-DR	cell adhesion mediated drug resistance
CAR	CXCL12-abundant reticular
CBP	p300/CREB-binding protein
CBX	chromobox
CCL1	C-C motif chemokine ligand 1
CCL2	C-C motif chemokine ligand
CCL2	C-C motif chemokine ligand 2
CCL5	C-C motif chemokine ligand 5
CCL5	C-C motif chemokine ligand 5
CCN1	CCN family member 1
CCND2	cyclin D2
CCND3	cyclin D3
CD40 ligand	CD40-L
CDK	cyclin-dependent-kinase
cDNA	copy deoxyribonucleic acid

CFU-F	colony forming unit fibroblast
ChIP	chromatin immunoprecipitation
CHIP	clonal haematopoiesis of indeterminate potential
CLL	chronic lymphocytic leukaemia
CO_2	carbon dioxide
COL14A1	collagen type XIV α 1 chain
CPM	counts per million
CRP	C-reactive protein
CRS	clinical records sheet
CSF2	colony stimulating factor 2
CSR	class switch recombination
CT	computed tomography
CXCL-1	C-X-C motif chemokine ligand 1
CXCL-10	C-X-C motif chemokine ligand 10
CXCL-12	C-X-C motif chemokine ligand 12
CXCL-8	C-X-C motif chemokine ligand 8
CXCR2	C-X-C motif chemokine receptor 2
CXCR4	C-X-C motif chemokine receptor 4
DAPI	4',6-diamidino-2-phenylindole
DCN	decorin
DDR	DNA damage response
Dicer1	Dicer1 miRNA ribonuclease III
DKK1	dickkopf WNT signalling pathway inhibitor 1
DLBCL	diffuse large-B-cell lymphoma
DMEM	Dulbecco's modified Eagle's medium
DNA	deoxyribonucleic acid
dNTP	deoxyribonucleotide triphosphate
ECM	extracellular matrix
EDTA	ethylenediamine tetraacetic acid
EED	embryonic ectoderm development
EFEMP1	EGF containing fibulin extracellular matrix protein 1
EGF	epidermal growth factor
eGFP-luc	eGFP-luciferase
ELOVL2	elongation of very long chain fatty acids-like 2
EMT	epithelial-mesenchymal transition
EV	empty vector
EZH2	enhancer of zeste homolog 2
FACS	fluorescence activated cell sorting
FASST	fibroblasts accelerate stromal supported tumorigenesis
FDR	false discovery rate
FGFR3	of fibroblast growth factor receptor 3
FKBP	FK506 binding protein

FLC	free light chain
FLCr	free light chain ratio
FOV	field of view
G-CSF	granulocyte colony-stimulating factor
Gas6	growth arrest specific 6
GDF-15	growth differentiation factor 15
GM-CSF	granulocyte macrophage colony-stimulating factor
(GRO)α	growth regulated oncogene
GSEA	gene set enrichment analysis
H_2O_2	hydrogen peroxide
H3K27me	histone 3 lysine 27 tri-methylation
H3K4	histone 3 lysine 4
HBSS	Hank's buffered salt solution
HCl	hydrochloric acid
HDAC	deacetylase
HSC	hematopoietic stem cell
HSV	herpes simplex virus
IFN-α	interferon alpha
IFN-β	interferon beta
IFN-γ	interferon gamma
IgA	immunoglobulin A
IGF-1	insuling growth factor 1
IGF-1R	IGF-1 receptor
IGF-II	insulin growth factor II
IGFBP-1	IGF binding protein 1
IGFBP-2	IGF binding protein 2
IGFBP-3	IGF binding protein 3
IGFBP-4	IGF binding protein 4
IGFBP-5	IGF binding protein 5
IGFBP-6	IGF binding protein 6
IGFBP-7	IGF binding protein 7
IgG	immunoglobulin G
IgM	immunoglobulin M
iKO	inducible knock out
IL-10	interleukin 10
IL-13	interleukin 13
IL-18	interleukin 18
IL-1α	interleukin-1 alpha
IL-1β	interleukin-1 beta
IL-6	interleukin 6
IL-7	interleukin 7
IMDM	Iscove's modified Dulbecco's medium

IMiD	immunoomodulatory imide drugs
IMWG	International Myeloma Working Group (
ITGA4	integrin α4
ITGAV	integrin 5
ITGB1	integrin β1
IVC	individual ventilated cage
KD	knockdown
KDM5D	lysine demethylase 5D
KDM6B	lysine demethylase 6B
$LEPR^+$	leptin receptor expressing cells
LFA-1	lymphocyte function-associated antigen 1
LGALS3BP	galectin 3 binding protein
LIMMA	linear models of microarray data
LN_2	liquid nitrogen
LPA1	lysophosphatidic acid recptor 1
LRPAP1	LDL receptor associated protein 1
LSC	leukaemic stem cell
M-CSF	macrophage colony stimulating factor
MBL	monoclonal B cell lymphocytosis
MDK	midkine
MDS	myelodysplastic syndromes
MEF	mouse embryonic fibroblasts
MERTK	MER proto-oncogene tyrosine kinase
MIP-1α	macrophage inflammatory protein alpha
MIP-1β	macrophage inflammatory protein beta
MLL1	mixed lineage leukemia 1
MM	Multiple myeloma
MMP-1	matrix metalloproteinase 1
MMP-12	matrix metalloproteinase 12
MMP-3	matrix metalloproteinase 3
MMP-9	matrix metalloproteinase 9
MRI	magnetic resonance imaging
mRNA	messenger RNA
MRP	Myeloma and Related Paraproteinaemia's
MSAG	Myeloma Australia Medical and Scientific Advisory Group
MSC	mesenchymal stromal cell
MSPC	mesenchymal stem progenitor cell
MUC-1	mucin 1
NANOG	nanog homeobox
NaOH	sodium hydroxide
Ndy1	not dead yet-1
NF	nuclease free

NFκβ	nuclear factor kappa beta
NGF	nerve growth factor
NK	natural killer
NOD *scid* gamma	nonobese diabetic/severe combined immunodeficiency gamma
NOF	neck of femur
NOTCH2	notch receptor 2
NSD2	nuclear receptor binding SET domain protein 2
NTC	no template control
O/N	over night
OCT	optimal cutting temperature
OPG	osteoprotegerin
OPN	osteopontin
OS	overall survival
PARP	poly (ADP-ribose) polymerase
PBMC	peripheral blood mononuclear cells
PBS	Phosphate-buffered saline
PC	plasma cell
PcG	polycomb repressor
PCR	polymerase chain reaction
PD	population doubling
PDGF-α	platelet derived growth factor subunit α
PDGF-β	platelet derived growth factor subunit β
PENK	proenkephalin
PET-CT	positron emission tomography and computer tomography
PI	proteosome inhibitor
PRC1	polycomb repressor complex 1
PRC2	polycomb repressor complex 2
RBC	red blood cell
RISS	Revised International Staging System
RNA	ribonucleic acid
RNAseq	RNA sequencing
RNS	reactive nitrogen species
RO	reverse osmosis
ROC	receiver operating characteristic
ROS	reactive oxygen species
RPMI-1640	Roswell Park Memorial Institute 1640
RT	room temperature
RT-PCR	reverse transcription polymerase chain reaction
SACRB	South Australian Cancer Research Biobank
SAGC	South Australian Genomics Centre
SAHMRI	South Australian Health and Medical Research Institute

SASP	senescence-associated secretory phenotype
SCD1	stearoyl-CoA desaturase 1
SCF	stem cell factor
SDC1	syndecan 1
SerpinE2	serpin E family member 2
SFLC	serum free light chain
SHM	somatic hypermutation
shRNA	short hairpin RNA
SINE	selective inhibitor of nuclear export
SIP	stress-induced premature
siRNA	small interfering RNA
SIRPα	signal regulatory protein alpha
SMM	Smouldering myeloma
SNP	single nucleotide polymorphism
SOX-2	SRY-Box Transcription Factor 2
SPEP	serum paraprotein electrophoresis
SPF	specific pathogen free
SUZ12	suppressor of zeste 12 homolog
TGA	therapeutic goods administration
TIMP1	TIMP metallopeptidase inhibitor 1
TLR	toll-like receptor
TMM	trimmed mean of M-values
TMP	tetramethylpyrazine
TNF-α	tumour necrosis factor alpha
TNF-β	transforming growth factor beta
TP53	tumour protein p53
TPO	thrombopoietin
TTP	time to progression
UPR	unfolded protein response
UV	ultraviolet
VCAM-1	vascular cell adhesion protein 1
VEGF	vascular endothelial growth factor
VEGFR2	vascular endothelial growth factor receptor 2
VLA-4	very late antigen 4
VRD	combination of bortezomib, lenalidomide and dexamethasone
WT	wild type
ZOL	zoledronic acid

PUBLICATIONS

Scientific manuscripts

1. **Plakhova N.**, Panagopoulos V., Vandyke K., Zannettino A. C. W., Mrozik K. M., (2022)., Mesenchymal stromal cell senescence in haematological malignancies, *Cancer and Metastasis Reviews*

2. **Plakhova N.**, Trainor L., Cantley M., Mrozik K. M., Gronthos S., Zannettino A. C. W., Vandyke K., Mesenchymal stromal senescence in multiple myeloma, (2022) *Manuscript in preparation*

3. Clark K., Hewett D. R., Panagopolous V., **Plakhova N.**, Opperman K. S., Bradey A. L., Mrozik K. M., Vandyke K., Mukherjee S., Davies C. G., Worthley D. L., Zannettino A. C. W., (2020), Targeted disruption of bone marrow stromal cell derived Gremlin1 limits multiple myeloma disease progression *in vivo*, *Cancers*

Conference presentations

1. Florey Postgraduate Research Conference, *Poster presentation*, 2019,2020,2021
2. South Australian Health and Medical Research Institute (SAHMRI) showcase annual meeting, *Poster presentation*, 2019, 2020, 2021
3. Myeloma workshop, *Oral presentation*, 2020
4. Australian and New Zealand Bone and Mineral Society (ANZBMS), *Oral Presentation*, 2020
5. EMBL Australia Postgraduate Symposium, *Poster presentation*, 2020
6. Blood Scientific Meeting, *Oral Presentation*, 2022

1 INTRODUCTION

1.1 Multiple myeloma – Clinical Description

Multiple myeloma (MM) is a haematological malignancy of plasma cells (PCs), which are terminally differentiated B-cells responsible for producing immunoglobulins or antibodies. The clonal expansion of neoplastic PCs within the bone marrow (BM) usually culminates in the over-production of a monoclonal immunoglobulin, also known as M protein/paraprotein [1, 2]. In some MM cases, the neoplastic PCs are unable to synthesise immunoglobulin heavy chains, and exclusively produce free light chains (FLCs) [5]. Paraprotein and FLC levels can be measured in a patient's urine and blood as an indirect measure of tumour burden [1]. Moreover, some MM patients present with non-secretory MM, meaning that the MM PCs secrete no measurable monoclonal heavy or light chains [6]. The cause of MM is unknown, although intrinsic genetic aberrations [7] and extrinsic factors within the BM microenvironment have been linked to disease establishment and progression [8-12]. Although recent advances in MM treatment have greatly improved patient outcomes, MM remains largely incurable due to patient relapse.

1.1.1 Incidence and survival

MM is the second most common haematological malignancy and accounts for ~1% of all cancers [1, 13]. Various other factors such as age, sex and race are associated with increased incidence. For example, MM is more common in males (57% of cases) compared with females (43% of cases) [14]. Moreover, while only 37% of patients under 65 years of age are diagnosed with MM, the majority of MM cases (63%) are diagnosed in individuals 66-70 years of age [15]. Additionally, there are racial disparities in MM incidence. For instance, the incidence of MM is 2-3-fold higher in people of African descent compared with Caucasian people [16]. Contrastingly, MM is less common in individuals of Asian descent compared with Caucasians,

although recent reports demonstrate that the incidence of MM is on the rise in some Asian countries such as Korea and Taiwan [17].

In Australia, it is estimated that MM will account for 2.2% of all cancer related deaths in 2022 [18]. In 2017, 1,978 new cases of MM were diagnosed in Australia, with a steady increase of 2,423 cases recorded in 2021 [18]. As the incidence of MM increases with advancing age, peaking at 85-89 years, the increase in the number of MM cases has been attributed to the ageing of the Australian population [18]. In 2022 in Australia, it is estimated that a person has a 0.90% risk of being diagnosed with MM by the age of 85 (1.1% for males and 0.74% for females) [18]. Between 1988 and 1992, the five-year survival rate for MM patients was 28% in Australia, which has increased to 54% in 2013-2017 [18].

1.1.2 Clinical manifestations

The accumulation of monoclonal protein, in conjunction with the proliferation of neoplastic PCs with the BM microenvironment manifests in hypercalcaemia, renal insufficiency, anaemia and bone lesions, which constitute the canonical clinical manifestations of MM, known as CRAB features [19]. Indeed, 80% of MM patients experience a pathological bone fracture and 90% of patients present with bone lesions during the course of their disease [20]. Accordingly, one of the most debilitating symptoms of MM is bone destruction. Specifically, the interaction of MM PCs with the BM microenvironment, via soluble factors and direct adhesion, activates bone-resorbing osteoclasts and suppresses the activity of bone forming osteoblasts, leading to an uncoupling of bone remodelling processes, resulting in bone loss [21]. Several signalling cascades, such as receptor activator of nuclear factor κB (RANK)/RANK ligand/osteoprotegerin, Notch, and Wnt have been implicated in this process [22]. Bone destruction liberates large amounts of calcium, resulting in hypercalcaemia [23], present in

nearly 30% of MM patients at time of diagnosis [24]. Hypercalcaemia, in conjunction with large amounts of MM PC-derived FLCs that deposit in distal and collecting renal tubules manifest in renal insufficiency, affecting 20-40% of MM patients [25]. Furthermore, renal dysfunction can exacerbate increased calcium levels, further compounding hypercalcaemia [23]. In addition, 70% of patients present with anaemia and associated fatigue and weakness at diagnosis [26]. Marrow replacement by MM PCs, accompanied with decreased erythropoietin production by the kidneys and cytokine-mediated marrow suppression are thought to be the underlying causes of anaemia in MM [15]. Additionally, MM patients are subject to recurrent bacterial and viral infections resulting from neutropenia and impaired antibody response because of the reduction in normal plasma cell-derived immunoglobulin production [27].

1.1.3 Clinical diagnostic criteria

1.1.3.1 Multiple myeloma

MM is defined by the presence of ≥10% BM PCs or biopsy proven bony or extramedullary plasmacytomas and presence of at least one myeloma-defining feature, as defined by the CRAB or SLiM criteria. CRAB features are defined as increased serum calcium (corrected serum calcium >0.25 mmol/L above the upper limit of normal or >2.75 mmol/L), renal insufficiency (creatinine clearance 177 μmol/L), anaemia (Hb <100g/L or below the lower limit of normal) or the presence of bone lesions (one or more osteolytic lesions on skeletal radiography, computed tomography (CT), or positron emission tomography CT (PET-CT). SLiM myeloma-defining features include the presence of ≥ sixty% BM PCs on BM biopsy or aspirate, involved/uninvolved serum free light chain (sFLC) ratio of ≥100 with the level of involved sFLC being ≥100 mg/L) and the presence of 2 or more ≥5 mm bone lesions on magnetic resonance imaging (MRI) [28]. Serum paraprotein parameters are not included in the most current definition of MM, as 3% of MM patients present with non-secretory disease while 15-

20% of MM cases produce only FLCs [15, 29]. Prognosis of newly diagnosed MM patients can be predicted based on the Revised International Staging System (RISS), which includes serum measures of β2-microglobulin, albumin and lactate dehydrogenase levels and the presence of high-risk cytogenetic abnormalities [30].

1.1.3.2 Smouldering myeloma (SMM)

Smouldering myeloma (SMM) is an asymptomatic form of MM, defined by serum IgA or IgG paraprotein levels ≥30 g/L or urinary monoclonal protein >500 mg per 24 hours and or the presence of 10-60% BM PCs, in the absence of CRAB or other myeloma-defining features (as in 1.1.3.1) [28].The risk of SMM progression to MM is 10% per year for the first 5 years, 3% per year for the following 5 years and 1-2% per year for the subsequent 10 years [31]. Disease management commonly includes patient monitoring 2-3 months after initial SMM diagnosis [31]. If results are initially stable, patients are subsequently monitored every 6-12 months [31]. As some SMM patients rapidly progress to MM within the first 5 years of diagnosis, while others remain stable for 10 years or more, it is necessary to further stratify SMM patients based on their risk of progression. Several risk models have been proposed to predict the risk of SMM progression. The most frequently used model is the International Myeloma Working Group (IMWG) risk stratification model, which utilises M protein >20 g/L, BM PC >20%, and involved: uninvolved sFLC ratio >20 as cut off parameters, with patients deemed high-risk if they meet at least 2 of these 3 parameters [32]. Specifically, patients classified as high-risk were found to have a ~50% risk of progressing to MM within 2 years [33]. Furthermore, the Spanish Myeloma Group SMM risk model uses the presence of two risk factors: the presence of an aberrant immunophenotype of the PCs (comprising the absence of CD19 and/or CD45 expression, with decreased CD38 and/or increased CD56 expression) in ≥95% BM PCs and the reduction in one or more uninvolved immunoglobulins of ≥25% compared with normal

values (termed immunoparesis) [34]. Using this model, it was found that SMM patients with both risk factors had a median time to progression (TTP) of 23 months, compared with SMM patients with one risk factor, who displayed a median TTP of 73 months [34]. Importantly, the implementation of early treatment for patients with high-risk SMM has been explored in a clinical trial [35]. In a study by Mateos *et al*. [35], high-risk SMM patients who received a diagnosis within 5 years, were stratified into 2 groups, with one group receiving treatment with lenalidomide and dexamethasone, while the other group was only observed. High-risk was defined as either BM PC infiltration of at least 10% with an elevated monoclonal component (defined as serum IgG ≥30 g/L, IgA ≥20 g/L, or a urinary Bence Jones protein level of >1 g per 24 hours) or using the Spanish Myeloma Group SMM risk model described above (≥95% aberrant BM PCs with immunoparesis) [35, 36]. Importantly, this study suggests that lenalidomide/dexamethasone treatment in treatment of high-risk SMM patients may be associated with longer TTP, when compared with patients receiving observation alone. However, the patient cohort included here is inconsistent with current definitions of high-risk SMM, in part because it included patients that would be defined as MM by the current SLiM-CRAB diagnostic criteria, the implications for current clinical management of SMM patients remains unclear. Further research is needed to determine the optimal management approach for this patient population.

1.1.3.3 Monoclonal gammopathy of undetermined significance (MGUS)

Monoclonal gammopathy of undetermined significance (MGUS) is an asymptomatic PC haematopoietic dyscrasia characterised by the presence of an abnormal serum paraprotein or sFLC. In the general population, MGUS is present in 0.3% among those <50 years old [37], with an increase to 3.2% in individuals ≥50 years of age, 5.3% in individuals ≥70 years of age and 7.5% among those aged 85 years or older [38]. Broadly, there are two subtypes of MGUS, which are largely distinguished by the type of immunoglobulin produced by the abnormal PC: IgM MGUS and non-IgM MGUS (which includes IgG, IgA and other rare immunoglobulin

subtypes and light chain only MGUS). Clinically, IgM MGUS is characterised by the presence of an IgM serum paraprotein <30 g/L with BM lymphoplasmacytic infiltration of <10% in the absence of clinical symptoms of an underlying lymphoproliferative disorder. Non-IgM MGUS is characterised by serum paraprotein of <30 g/L or, in the absence of an immunoglobulin heavy chain paraprotein, an abnormal sFLC ratio >1.65, along with <10% BM PCs, in the absence of end-organ damage (CRAB features), amyloidosis or other related lymphoplasmacytic malignancies known to produce paraprotein, such as B-cell lymphoma [28]. Moving forward, unless otherwise specified, references to MGUS in this thesis refer to non-IgM MGUS. IgM MGUS most frequently progresses to Waldenström's macroglobulinemia, non-Hodgkin's lymphoma (NHL), immunoglobulin light chain (AL) amyloidosis and chronic lymphocytic leukaemia (CLL) and, very rarely, IgM MM. In contrast, non-IgM MGUS most frequently progresses to SMM, MM or AL-amyloidosis [13]. Notably, MM is universally preceded by an MGUS stage [39, 40]. However, in most cases, MGUS cases remain stable, and do not progress to any malignancy [41]. Presently, it is unclear what drives MGUS progression, and there is a paucity of predictive biomarkers of progression that can predict an individual's risk of MGUS-to-MM transformation [42, 43]. Nevertheless, population-wide studies have identified several factors associated with an increased risk of progression to MM, SMM, AL-amyloidosis or related disorders. For example, advancing age is a significant risk factor, with a yearly risk of progression of 0.4% per year in MGUS patients less than 60 years of age which increases to 1.0% per year in patients aged 60 years and older [41]. Moreover, markers of increased abnormal PC bulk (M protein ≥ 15g/L, sFLC ratio > 1.65 and PC burden >5%) have been associated with an increased risk of MGUS progression [41, 44, 45]. Furthermore, IgA MGUS is associated with a higher probability of malignant transformation to MM when compared with IgG/light chain MGUS [41, 46, 47]. Additionally, in a large population-based screening study of IgM and non-IgM MGUS patients in Iceland,

high body mass index during midlife has been associated with increased risk of MGUS progression to MM and other lymphoproliferative diseases including Waldenström's macroglobulinemia, NHL, CLL and acute lymphocytic leukaemia [48].

1.1.4 Treatment modalities for MM

The standard clinical management of active MM, as defined in section 1.1.3.1, involves treatment with chemotherapy or novel agents and, in some cases, autologous stem cell transplant (ASCT) as described in Figure 1.1, whereas ongoing monitoring without therapeutic intervention is the current standard for asymptomatic MGUS and SMM [31]. The treatment of MM can vary depending on the risk classification of the patient in addition to other factors such as disease stage, overall health status and age. The upfront treatment for MM patients commonly includes combinations of drugs including corticosteroids (e.g., dexamethasone, prednisolone), alkylating chemotherapeutic agents (e.g., melphalan, cyclophosphamide), proteosome inhibitors (PIs) (e.g., bortezomib, carfilzomib), immunomodulatory imide drugs (IMiDs; e.g., thalidomide, lenalidomide, pomalidomide), in some cases combined with ASCT. In addition, the incorporation of monoclonal antibodies (e.g., daratumumab - which targets CD38 on PCs) to MM treatment regimens have shown significant benefit for newly diagnosed MM in several randomised trials [49-51].

In Australia, high dose chemotherapy and ASCT is the standard upfront treatment for patients <65 years of age and patients between 65-70 years of age with good performance status and organ reserve, as it has been shown to improve MM patient overall survival [52-54]. Clinical tools such as the haematopoietic stem cell transplant co-morbidity index and the International Myeloma Working Group frailty score can be useful for guiding ASCT eligibility [55, 56]. According to the Clinical Practice Guidelines outlined by Myeloma Australia Medical and Scientific Advisory Group (MSAG) [28], if transplant eligible, patients are treated with 3-6

cycles of combination induction therapy prior to transplant. Currently in Australia, the combination of bortezomib, lenalidomide and dexamethasone (VRD) is the standard of care for induction prior to ASCT [28]. If either bortezomib or lenalidomide is contraindicated, induction therapy with triplet drug combination approaches that include either a PI and/or IMiD with a steroid and an alkylating agent is recommended [28].

Patients who are not undergoing ASCT can be considered for VRD therapy [28]. For patients not eligible for ASCT, due to age, comorbidities or frailty, reduced intensity VRD therapy or doublet therapy incorporating IMiDs or PIs with steroids is recommended [28]. These treatment approaches can also be followed by maintenance therapy, which largely depends on initial treatment used [28]. Lastly, patients that are considered ineligible for any treatment are referred for palliative care.

Figure 1.1. Treatment flow chart for newly diagnosed MM. Adapted from [3].

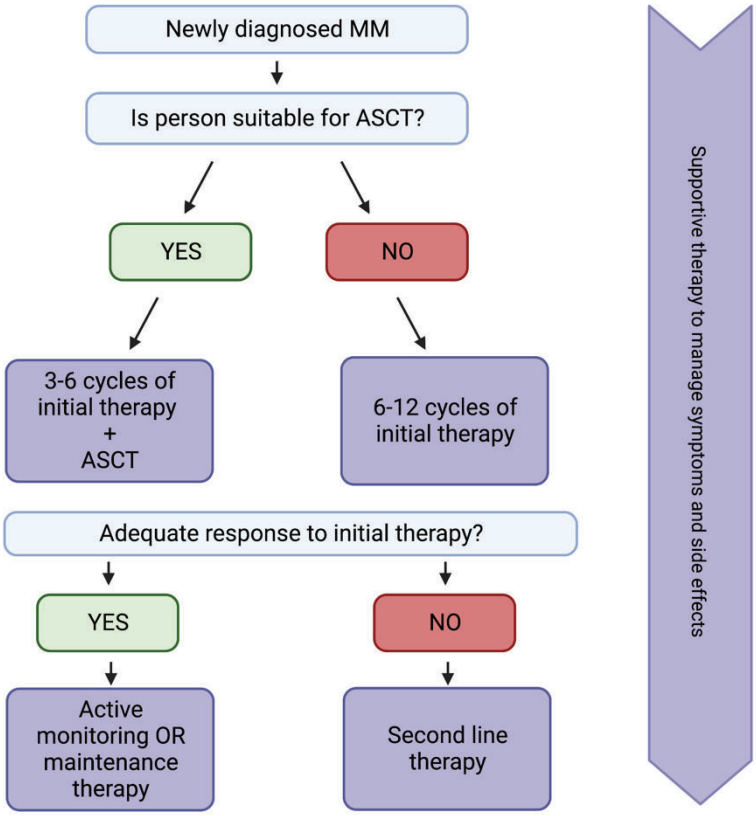
Newly diagnosed MM
Is person suitable for ASCT?
YES
NO
3-6 cycles of initial therapy + ASCT
6-12 cycles of initial therapy
Adequate response to initial therapy?
YES
NO
Active monitoring OR maintenance therapy
Second line therapy
Supportive therapy to manage symptoms and side effects

The mode of action of each of these drug classes are described in the following sections.

1.1.4.1 Alkylating agents

Alkylating agents (melphalan, cyclophosphamide) have been used in MM treatment for over 50 years [57]. These drugs exert their primary function through crosslinking DNA to inhibit DNA replication and transcription, thereby inhibiting cell division and ultimately leading to cellular apoptosis [57].

1.1.4.2 Corticosteroids

Combination regimes that incorporate corticosteroids (dexamethasone, prednisone and its metabolite prednisolone) have been shown to promote MM patient survival [58]. Corticosteroids exert their effect, in part, by binding glucocorticoid receptors in MM cells to inhibit pro-MM signalling pathways such as NFκβ and IL-6 [58].

1.1.4.3 Proteosome inhibitors

Proteosome inhibitors target MM PCs directly by promoting endoplasmic reticulum stress [59]. This mechanism is relatively specific and detrimental to PCs, as they secrete high amounts of immunoglobulin, thereby requiring a well-developed endoplasmic reticulum, secretory apparatus and production of chaperone proteins that mediate appropriate immunoglobulin protein folding and translation [60]. Proper protein folding and prevention of the accumulation of misfolded protein aggregates in PCs is mediated by the unfolded protein response (UPR), with misfolded proteins transported out of the endoplasmic reticulum for degradation by the proteosome [61, 62]. Consequently, inhibiting proteosome function in malignant PCs leads to the accumulation of misfolded immunoglobulin within the endoplasmic reticulum, activating the UPR, with prolonged UPR activation culminating in cell cycle arrest and apoptosis [63, 64]. Therefore, proteosome inhibitors initiate UPR and apoptosis preferentially in malignant

PCs with high immunoglobulin production and minimise toxicity to patient's normal cells *in vivo* [65].

1.1.4.4 IMiDs

IMiDs exert their anti-MM activity by directly targeting MM cells and through their ability to increase anti-tumour immune responses. The latter effect is achieved by IMiD binding to the E3 ligase cereblon in immune cells such as T cells and natural killer (NK) cells [66]. Cereblon is a critical component of the CRL4 complex which possesses ubiquitin ligase activity. IMiD binding to cereblon leads to protein stabilization, which inhibits its own ubiquitination and promotes the degradation of target proteins Ikaros and Aiolos, which alter downstream gene expression of survival genes in PCs and immune regulatory genes in T cells [67, 68].

1.1.4.5 Monoclonal antibodies

Anti-CD38 monoclonal antibodies (e.g., daratumumab) target the CD38 protein expressed on the surface of MM PCs, with antibody binding initiating MM tumour cell death. This is achieved by numerous signalling pathways, including antibody-dependent cell-mediated cytotoxicity, complement-dependent cytotoxicity and antibody-dependent cellular phagocytosis [69, 70].

1.1.4.6 Treatment approaches for relapsed MM

Irrespective of the treatment regimen used, MM patients inevitably relapse, and subsequent treatment strategies are employed. The choice of follow up therapies is largely guided by prior response to treatment, resistance to treatment, patient risk stratification and other associated comorbidities [71]. If the patient has achieved a long-term remission with their initial therapy, one approach for the treatment of relapsed patients is to re-introduce the same combination

therapies used in the frontline context [28]. However, in most cases, switching to a new drug class (IMiD or PI) is recommended, usually in combination with a steroid and, if the patient is rapidly progressing, an alkylating agent [28]. In Australia, in addition to the frontline treatments lenalidomide and bortezomib, patients have access to the PI, carfilzomib, and the IMiD, pomalidomide, in the relapsed setting [28]. Furthermore, recent studies have shown that daratumumab can improve patient outcomes in relapsed/refractory MM patients [72], with the use of this drug approved by the Australian Pharmaceutical Benefits Scheme (PBS) for use at first relapse MM, in combination with bortezomib and dexamethasone [28].

Furthermore, various novel agents may improve relapsed and/or refractory MM patient outcomes. For example, selinexor, a selective inhibitor of nuclear export (SINE) was shown to improve overall response rate in a group of heavily pre-treated, penta-refractory patients [73]. Selinexor has since been approved by the Therapeutic Goods Administration (TGA) in Australia to be used in combination with bortezomib and dexamethasone for the treatment of relapsed and or refractory MM as well as triple class refractory MM [74]. Moreover, venetoclax, a B-cell lymphoma 2 (Bcl-2) protein inhibitor, has shown efficacy in early Phase I clinical trials in treating relapsed/refractory MM, particularly in those with the chromosomal translocation t(11;14) [75-77]. However, in a randomised Phase III trial, it was shown that the addition of venetoclax to bortezomib and dexamethasone therapy in relapsed refractory MM resulted in increased mortality when compared with bortezomib and dexamethasone alone due to increased risk of infection [78]. Furthermore, as a result of this trial, venetoclax is now restricted to patients with t(11:14) given the risk of infection associated with the agent. As such, as of 2020, the treatment of patients with MM with venetoclax is not recommended by the TGA outside of controlled clinical trials [79].

Moreover, the utility of chimeric antigen receptor T cells (CAR-T) cells in MM treatment is currently being explored. CAR-T cells are genetically modified autologous T-cells that have been engineered to express receptors that can detect both specific antigens on cancer cells to flag them as a target for immune destruction. CAR-T cell therapies currently available for MM treatment include ciltacabtagene autoleucel (cilta-cel; Janssen) and idecabtagene vicleucel (ide-cel; Abecma) [28]. While the FDA has approved the use of ide-cel for the treatment of relapsed triple class refractory myeloma in the US, no CAR-T cell therapies have been approved in Australia outside of clinical trial settings [28].

Furthermore, bispecific antibodies are in clinical development for the treatment of MM. Mechanistically, bispecific antibodies bind both antigens expressed on MM PCs and cytotoxic immune cells such as NK and T cells to improve targeting of MM PCs by the immune system. Specifically, teclistamab, elranatamab and AMG-701 have been designed to target B-cell maturation antigen (BCMA), while cevostamab targets Fc receptor-like protein (FcRH5): antigens that are both highly expressed by MM PCs [28]. In addition, Talquetamab has been engineered to target G-protein coupled receptor family C group 5 member D (GPRC5D) expressed by MM PCs [28].

1.1.4.7 Minimal Residual Disease (MRD)

While the introduction of novel therapies continues to improve survival rates in MM, the disease remains largely incurable, with patients prone to relapse even after achieving optimal responses to treatment. Relapse occurs due to the outgrowth of residual MM PCs that do not respond to, and persist beyond, therapy: termed minimal residual disease (MRD). MRD is assessed by next generation flow cytometry (NGF) or NGS analysis in BM aspirates. MRD negativity is defined as the inability to detect tumour cells by flow or NGS in BM aspirates,

with a limit of detection of at least 1 in 10^{-5} cells [80]. MRD is reflective of treatment response depth and may help predict relapse in patients and guide consolidation treatment. In fact, MRD-directed therapy is already being employed for the treatment of ALL, where tailoring consolidation therapy based on MRD load is standard practice [81].

In the context of MM, a meta-analysis of 44 studies that evaluated the prognostic value of MRD status for PFS and OS showed that MRD negativity was associated with significantly improved survival outcomes in newly diagnosed and relapsed/refractory MM [82]. Nevertheless, while MRD are used in routine clinical practice, they are yet to be used to inform or modify MM therapy [83]. However, there is evidence to suggest that MRD-guided therapy can be used improve patient outcomes. For example, MRD-based consolidation therapy has been shown to improve PFS in newly diagnosed and relapsed/refractory MM patients [84]. In line with this, the utility of using MRD to guide the use and duration of post-transplant therapy has been explored in the MASTER clinical trial [85]. In this study, patients classified as MRD negative (10^{-5}) after two assessments did not receive further treatment and were monitored over time. One-year follow up post therapy cessation revealed that only 0-4% of patients with low and intermediate risk cytogenetics experienced MM relapse or the re-emergence of MRD, while the incidence of this was higher (27%) in patients with high-risk cytogenetics. As such, there is potential to use MRD-guided cessation of consolidation therapy post treatment in MM patients with low-risk cytogenetics to reduce the burden and side effects associated with continuous maintenance therapy. Taken together, while further research is required to determine whether MRD-guided consolidation therapy can be incorporated clinically to guide MM treatment, MRD assessment has the potential to become an extremely useful tool in guiding MM therapy in routine clinical practice to improve patient survival rates.

1.1.5 Genetic aetiology of MM

1.1.5.1 Primary genetic events

All PCs initially originate from haematopoietic stem cells (HSC) in the BM. Here, HSC mature into pre-B cells which express a functional B cell receptor, which subsequently enables them to migrate to peripheral lymphoid organs (lymph nodes/spleen) [86, 87]. In peripheral lymphoid organs, B cells are exposed to their cognate antigens, which triggers rapid proliferation in the germinal centre [88]. Here, activated B cells undergo several processes, including affinity maturation to produce highly specific functional antibodies as part of the adaptive immune response. Specifically, the IgH locus in naïve B cells is subject to somatic hypermutation of the immunoglobulin heavy chain and class switch recombination [7]. These processes are mediated by the generation of double stranded breaks in the Ig loci [7]. These processes are outlined in Figure 1.2. Occasionally, during this process, a chromosomal translocation event can lead to the development of an abnormal PC clone, due to the co-localisation of proto-oncogenes with the IgH enhancer [2, 7]. The most common translocation in MM PCs is t(11;14)(q13;q32), which occurs in 15-20% of newly diagnosed MM patients [89, 90]. This translocation leads to the over-expression of the *CCND1* gene, encoding the cyclin D1 protein, which is responsible for promoting cell cycle progression through the G1 phase [91].Patients with t(11;14) translocations are deemed to have standard risk disease [92]. The second most common translocation is t(4;14)(p15;q32), which is detected in approximately 13% of newly diagnosed MM patients [89, 93]. This chromosomal rearrangement leads to the overexpression of the *NSD2* gene, encoding the nuclear receptor binding SET domain protein 2 histone methyltransferase [94, 95]. The upregulation of NSD2 has been shown to contribute to epigenetic reprogramming and subsequent gene expression changes, largely involving PC adhesion, migration, survival and proliferation [96-98]. This includes expression of the cyclin D2 gene (*CCND2*), which promotes the progression through the G1 phase of the cell cycle [91,

96]. Additionally, in 70% of cases, t(4;14)(p15;q32) translocation also leads to the constitutive expression of fibroblast growth factor receptor 3 (*FGFR3*) gene, encoding a receptor tyrosine kinase [94, 95]. The overexpression of functional FGFR3 has been shown to promote MM PC proliferation and prevent apoptosis [99, 100]. The t(14;16)(q32;q23) and t(14;20)(q32;q11) IgH translocations are found in 4% and 1% of MM patients respectively [93, 101, 102] with both translocations resulting in the overexpression of oncogenic MAF transcription factor (MAF and MAFB respectively). MAF transcription factors promote the overexpression of a range of genes such as *CCND2* and *APOBEC* cytidine deaminases, which cumulatively contribute to an increased DNA mutational burden [91, 95, 103, 104]. MM patients harbouring t(4;14), t(14;16) and t(14;20) translocations are classified as high-risk, with these translocations associated with poor prognosis [92, 105, 106]. Lastly, the t(6;14)(p21;q32) translocation, which is present in 1% of MM cases leads to the direct overexpression of *CCND3*, encoding the cyclin D3 gene [91, 93, 101]. Patients with t(6;14) translocations are classified as standard risk [92, 105].

An alternative mechanism for the transformation of MM PCs is hyperdiploidy. Approximately 55% of MM cases are thought to arise due to hyperdiploidy, which is defined by multiple trisomies in odd numbered chromosomes 3, 5, 7, 9, 11, 15, 19 and/or 21 [7, 107]. While it remains unclear what drives hyperdiploidy, it arises during mitosis due to missagregation of chromosomes [108]. Like IgH translocation events, hyperdiploidy has been linked to the upregulation of group D cyclin expression within MM PCs [91]. Hyperdiploidy in general is associated with standard-risk disease [109, 110]. The outlined primary initiating genetic events in MM PCs are summarised in Figure 1.3.

Figure 1.2. Plasma cell maturation. B cells originate from HSCs within the BM, where they undergo maturation to acquire the B cell receptor, necessary for their migration to peripheral lymphoid organs. Here, activated B cells undergo several processes including affinity maturation to produce highly specific functional antibodies as part of the adaptive immune response. Specifically, the IgH locus in naïve B cells is subject to somatic hypermutation. Somatic hypermutation is a process of generating antibody diversity. Somatic hypermutation occurs in immunoglobulin gene segments. Somatic hypermutation leads to small changes at the DNA level augmented by activation induced cytidine deaminase (AID) to change antibody affinity. Occasionally, during this process, this can lead to translocations that lead to the development of an abnormal PC clone.

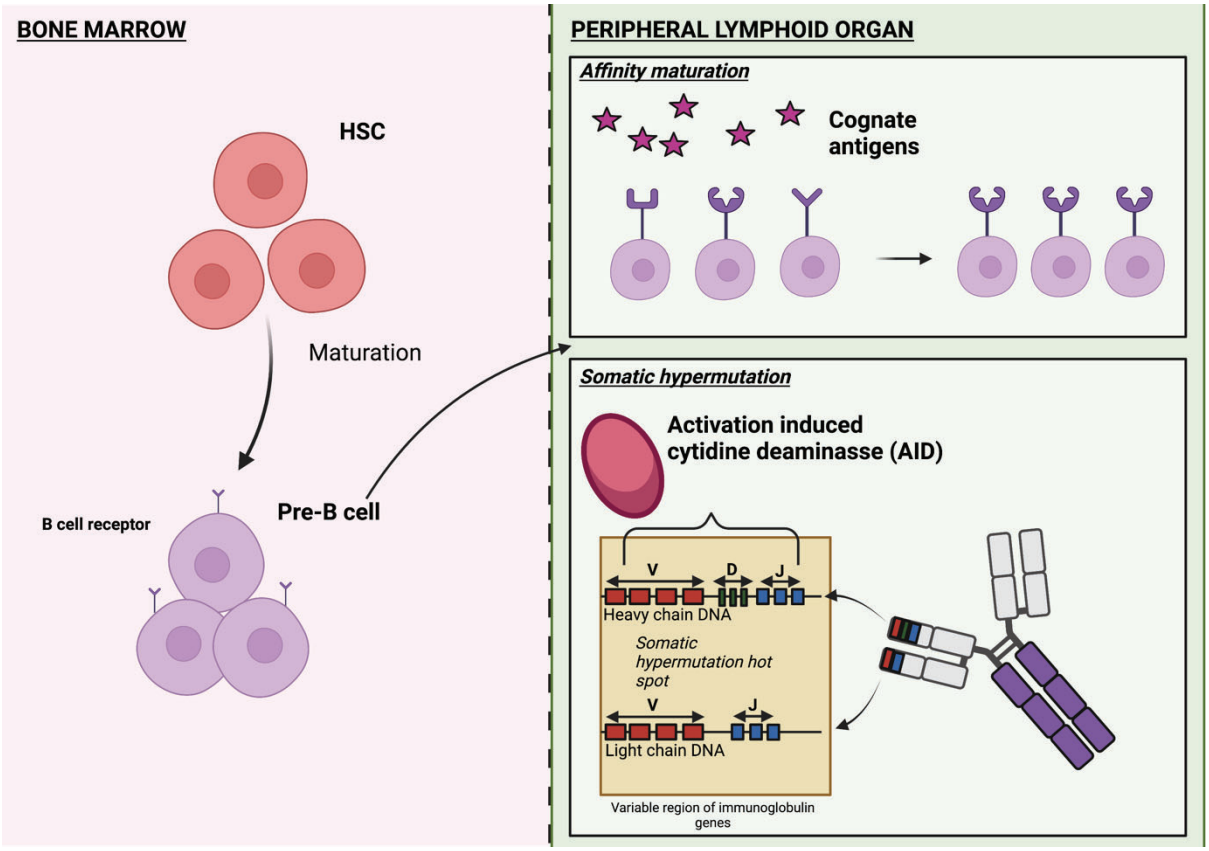
BONE MARROW
HSC
Maturation
B cell receptor
Pre-B cell
PERIPHERAL LYMPHOID ORGAN
Affinity maturation
Cognate antigens
Somatic hypermutation
Activation induced cytidine deaminasse (AID)
V
D
J
Heavy chain DNA
Somatic hypermutation hot spot
V
J
Light chain DNA
Variable region of immunoglobulin genes

Figure 1.3. Primary initiating genetic events in MM PCs. MM initiating events, such as translocations involving the IgH locus and hyperdiploidy (HD) lead to the up regulation of cyclin D1, cyclin D2 or cyclin D3, which accelerate the progression from G_1 to S phase of the cell cycle, thereby accelerating MM PC proliferation. Moreover, the overexpression of functional *FGFR3* has been shown to promote MM PC proliferation and prevent apoptosis. Lastly, the activation of signalling through *APOBEC* contribute to an increased DNA mutational burden.

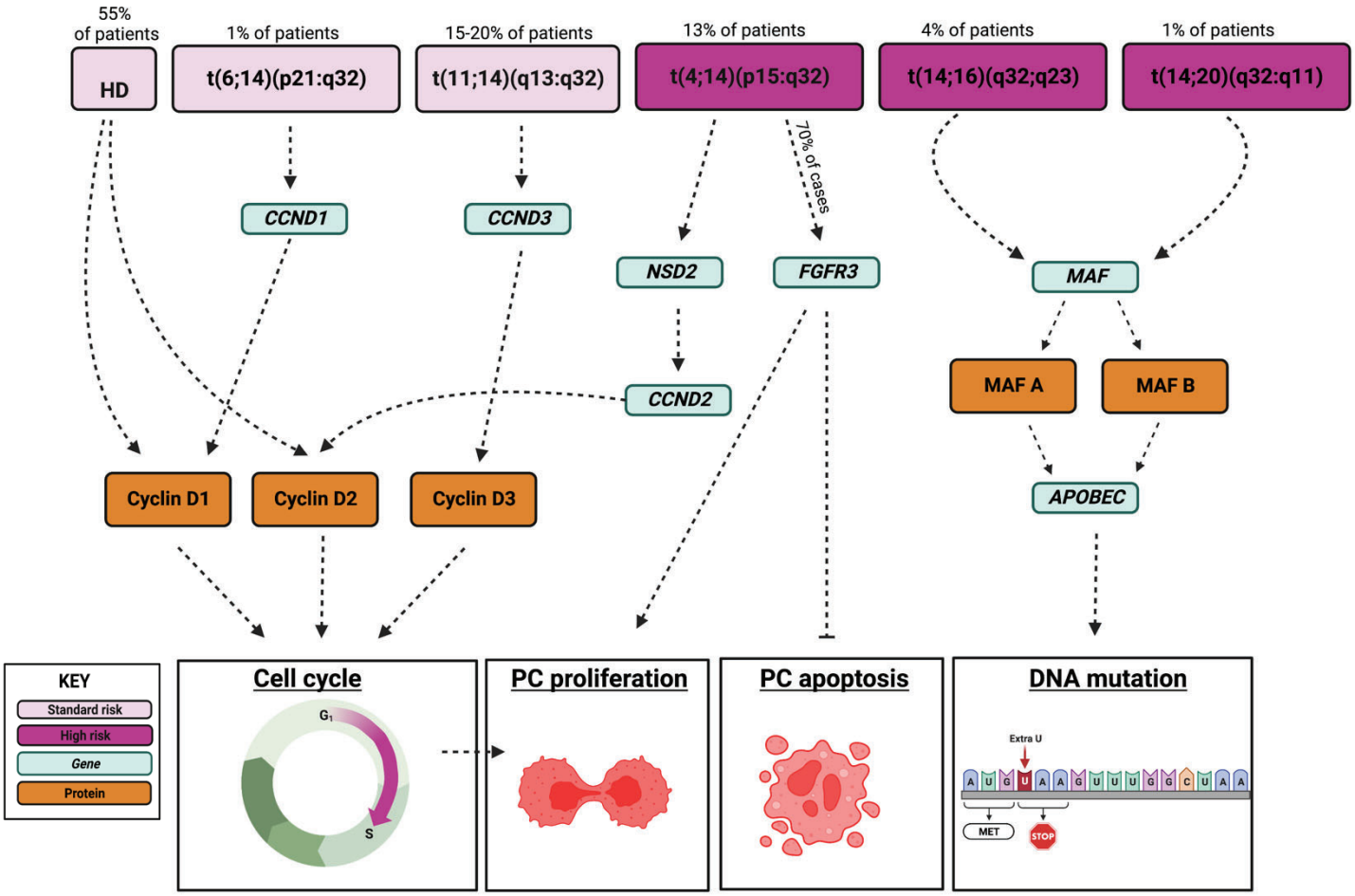
55% of patients
HD
1% of patients
t(6;14)(p21:q32)
15-20% of patients
t(11;14)(q13:q32)
13% of patients
t(4;14)(p15:q32)
4% of patients
t(14;16)(q32;q23)
1% of patients
t(14;20)(q32:q11)
CCND1
CCND3
NSD2
70% of cases
FGFR3
MAF
CCND2
MAF A
MAF B
Cyclin D1
Cyclin D2
Cyclin D3
APOBEC
KEY
Standard risk
High risk
Gene
Protein
Cell cycle
G1
S
PC proliferation
PC apoptosis
DNA mutation
Extra U
MET
STOP

1.1.5.2 Secondary genetic events

Copy number alterations (gains or losses of genomic regions), single nucleotide variants (SNVs), and chromosomal rearrangements involving the *MYC* locus are common secondary genetic events that occur within malignant PCs later in the course of the disease [111]. Moreover, the deletion of 17p13 (del(17p)), which harbours the locus for the tumour-suppressor gene *TP53*, is observed in approximately 10% of MM patients [112-114]. Patients with this deletion display more aggressive disease, shorter overall survival, shorter duration of response after high dose therapy and a high prevalence of extramedullary disease [112-115]. Furthermore, bi-allelic inactivation of p53, which occurs when both copies of *TP53* are compromised, is observed in 3.7% of newly diagnosed MM patients [102, 116]. Bi-allelic mutation and deletion of *TP53* has been reported to be associated with higher rates of relapse [117]. Other secondary genetic changes that have been associated with MM progression include chromosome 13 abnormalities, which are detected in 50% of MM cases (85% of which constitute monosomy and 15% are deletions) [92, 118-120]. While the exact role of chromosome 13 deletion in promoting MM development is unclear, several studies suggest that it is involved in clonal expansion of tumour cells [118, 119, 121, 122]. Notably, approximately 90% of cases harbouring t(4;14)(p16;q32) translocations also harbour chromosome 13 deletion [118, 119, 121, 122]. Indeed, while chromosome 13 abnormalities are associated with shorter patient survival [113, 123-127], this is largely thought to be secondary to the association between del(13q) and the high-risk translocation t(4;14) [128]. Furthermore, gain of 1q (+1q) occurs in 40% of all MM cases, although the specific molecular consequences of this are presently unknown, with a number of studies exploring *CKS1B* [129, 130]. The implication of +1q for OS and PFS of MM patients is currently unclear. Several studies suggest that an amplification of 3 or more copies would constitute high risk, although this requires further confirmation [102, 131]. Moreover, approximately 30% of MM patients present with

chromosome deletions at 1p, which is associated with poor prognosis [132]. Deletion 1p is characterised by deletions in *CDKN2C* and *FAF1* [133].

Next generation sequencing studies of MM PCs have revealed that, despite significant inter-patient heterogeneity, there are consistent patterns of recurrent mutations observed in newly diagnosed patients [107, 135-137]. For example, recurrent mutations observed in newly diagnosed MM patients include *TP53* (6-9% patients), *FAM46C* (9-12% patients) and *DIS3* (10-11% patients) [107, 135, 137]. Furthermore, up to 50% of MM patients have oncogenic mutations involving the pro-proliferative MEK/ERK signalling pathway, including *KRAS* (21-26%% patients), *NRAS* (19-20% patients) and BRAF (6-8% patients), which can be associated with poor prognosis [107, 135, 137-139].

Consequently, primary and secondary genetic events work in concert to drive unchecked proliferation of a mutated PC clone, which manifests in uncontrolled proliferation of neoplastic PCs within the BM microenvironment and the establishment of MGUS and MM.

1.1.6 Drivers of MGUS-to-MM progression

In addition to their critical role in disease initiation, recent studies suggest that genetic aberrations alone may increase risk of progression from MGUS to overt MM. It has been shown that primary initiating events in PCs such as IgH translocations and or hyperdiploidy are already present at MGUS [33, 90, 121, 140, 141]. Notably, some translocations, such as t(4;14), are seen more rarely in MGUS patients (1-5% of MGUS patients) [33, 121, 141] compared with 13% of newly diagnosed MM patients [89, 93], suggesting that this translocation is associated with increased risk of progression to active MM. In contrast, the incidence of t(14;16) is similar between MGUS, SMM and MM patients (approximately 3% in each cohort) [106], suggesting that this translocation does not accelerate disease progression. However, it is

notable that these chromosomal abnormalities alone are insufficient to result in overt MM, as many MGUS patients with these translocations have long term stable disease [90, 142].

Consequently, it was suggested that the development of symptomatic MM is a multistage process involving the acquisition of primary chromosomal abnormalities leading to the development of MGUS, with further sequential genetic hits leading to the subsequent development of SMM and overt MM [143]. In order to understand the genetic basis that underpins progression from asymptomatic disease to overt MM, various studies have compared the genetic landscape of PC samples taken from different patients with MGUS, SMM or MM [12, 128, 144-146]. For example, Walker *et al.* conducted whole exome and whole genome sequencing of PCs from MGUS and high-risk SMM patients who subsequently progressed to MM [12]. Analysis of the number of non-synonymous mutations revealed that MGUS is less genetically complex, with fewer SNVs than MM, while the genetic profile of high-risk SMM PCs resembled that of symptomatic MM [12]. Similarly, whole exome sequencing analysis, coupled with comparative genomic hybridization and single nucleotide polymorphism (SNP) array of primary PCs from MGUS and MM patients revealed that the frequency of non-synonymous mutations detected in MGUS PCs was significantly lower than that of MM PCs [144]. As such, it has been classically thought that MM PCs are characterised by an increased mutational burden compared with that of MGUS PCs, with activating mutations in certain genes driving malignant transformation [143].

In support of this, specific mutations have been shown to be more prevalent in MM patients than in MGUS and SMM. For example, the presence of *TP53* mutations is a recurrent feature seen in up to 10% of MM patients but is rarely detected at MGUS [144, 147]. Additionally, by comparing the genetic profile of PCs from SMM and newly diagnosed MM patients, it was

revealed that fewer *NRAS* and *FAM46C* mutations were detected in SMM samples compared with MM [148]. Moreover, it has been shown that activating mutations in *NRAS* and *KRAS* within PCs are commonly identified in 40% of MM patients, although they are observed in less than 5% of MGUS patients [149-151]. In further support of a direct association between acquisition of mutations and disease progression, the presence of *KRAS* and *DIS3* mutations at SMM is associated with a shorter time to progression to overt MM [147, 148, 152].

Additionally, studies suggest that copy number variants and secondary translocations [144, 147] are observed more frequently in MM than in MGUS or SMM and thus may contribute to MGUS-to-MM transformation. For example, del(1p), del(14q), del(16q) and del(17p) are significantly more frequently observed in MM PCs in comparison to PCs isolated from SMM patients [148]. Furthermore, *MYC* translocations are observed in approximately 15% of MM patients and 6% of SMM patients but are not detected in MGUS patients[147]. Consequently, as the aforementioned chromosomal abnormalities are more commonly present in MM compared with SMM and MGUS, they may play a role in driving MM transformation. In support of this, the presence of del(6q) at SMM is associated with a short time to progression to overt MM [148]. Furthermore, the presence of a MYC translocation has also been identified as an adverse prognostic factor for progression from SMM to MM in some [147, 152] but not all [148] studies.

All MM patients present with MM tumours composed of multiple genetically heterogeneous subpopulations of PCs termed subclones, with between 3 and 11 subclones per patients identified at MM diagnosis [8, 12, 153]. Secondary genetic hits that constitute the key drivers of MM development, such as mutations in *KRAS* and *NRAS*, can be clonal or subclonal in nature, which suggests that they can occur at different stages throughout the course of the

disease [137, 154]. Moreover, studies using SNP arrays on serial PC samples have revealed that the molecular events involved in MM progression are not attained in a linear fashion but through non-linear, branching pathways [153, 155]. This raises the hypothesis that there is Darwinian competition between the abnormal PC subclones, where selective pressures only enable the genetically 'fittest' clones subsequently proliferating and becoming dominant within the tumour [7].

The presence of subclonal heterogeneity is also recognised in MGUS and SMM, suggesting that emergence of subclonal diversity is a very early event in disease development [8, 148, 152, 154]. Notably, studies characterising the genomics of paired MGUS/SMM and MM PC samples have demonstrated that the outgrowth of PCs is characterised by genomic stability, with the acquisition of new mutations being infrequent [8, 156]. For example, a whole-exome sequencing study of serial PC samples from 10 patients at the MGUS/SMM stage and, subsequently, at MM has shown a similar mutational load with disease progression [8]. Specifically, it was revealed that patients at the MGUS/SMM stage exhibit a similar frequency of copy number gains and losses or SNVs at the MM stage [8]. In line with this, whole exome sequencing of MGUS/SMM revealed that mutation load was similar between patients that subsequently progressed to overt MM and those that remained stable for at least 12 months [152, 156, 157]. Furthermore, in studies of paired sequential samples collected from the same patients at MGUS/SMM and MM, the vast majority of non-synonymous SNVs that were detected at the MM stage were also present at the premalignant MGUS/SMM stages, with most patients having no new non synonymous mutations at progression to MM [12, 152, 156].

Likewise, studies analysing subclonal diversity in paired MGUS/SMM and MM PC samples have shown that the subclones that were present at the MM stage were already detectable at

the MGUS and SMM stages [8, 148, 152, 158]. Furthermore, while there was evidence of branching evolution in the development of these subclones, this preceded the development of MGUS and SMM, suggesting that this is an early event in disease development [148, 152, 158]. In paired samples, while some patients show "ebbs and flows" in the abundance of subclones with disease progression from MGUS/SMM to MM, these were generally in relatively minor subclones, with the emergence of a new, dominant clone being a relatively infrequent occurrence [12, 148, 152, 156, 158]. Notably, there is a subset of patients that show a pattern of clonal stability in MGUS/SMM-to-MM progression suggesting neutral, rather than branching, evolution with disease progression in these patients [8, 12, 152, 157, 158].

Taken together, these data suggest that the chromosomal alterations, SNVs and subclonal heterogeneity characteristic of MM are already present at the asymptomatic stages [8, 12, 90, 120, 140, 156, 159, 160]. Consequently, these findings suggest that progression from MGUS/SMM to MM disease is characterised by neutral evolution, where several PC subclones at MGUS/SMM together proliferate and contribute to the MM tumour (Figure 1.4). Therefore, the progression to clinical malignancy may be governed by additional extrinsic factors and not exclusively by intrinsic genetic changes. This highlights the potential role of the extrinsic BM microenvironment in stochastic clone activation and progression to malignant states [8].

Therefore, investigating the dynamic interactions of MM PC with the BM microenvironment is crucial in understanding the mechanism of MGUS-to-MM progression.

Figure 1.4. Schematic of MGUS-to-MM progression. Primary genetic event occurs in plasma cells (PCs) within peripheral lymphoid organ. The transformed PC clones are present at the asymptomatic monoclonal gammopathy of undetermined significance (MGUS) and smouldering myeloma (SMM) stages, with clonal heterogeneity present at the asymptomatic stages of the disease. This implies that the progression to MM may be governed by additional extrinsic factors and not exclusively by intrinsic genetic changes. This highlights the potential role of the extrinsic bone marrow (BM) microenvironment in stochastic clone activation and progression to malignant states. As progression is evident with age, age-related changes to the BM microenvironment may be involved in this process. CRAB: hypercalcaemia, renal insufficiency, anaemia, bone lesions; del(17p): deletion of 17p13; HD: hyperdiploidy; SNV: single nucleotide variant.

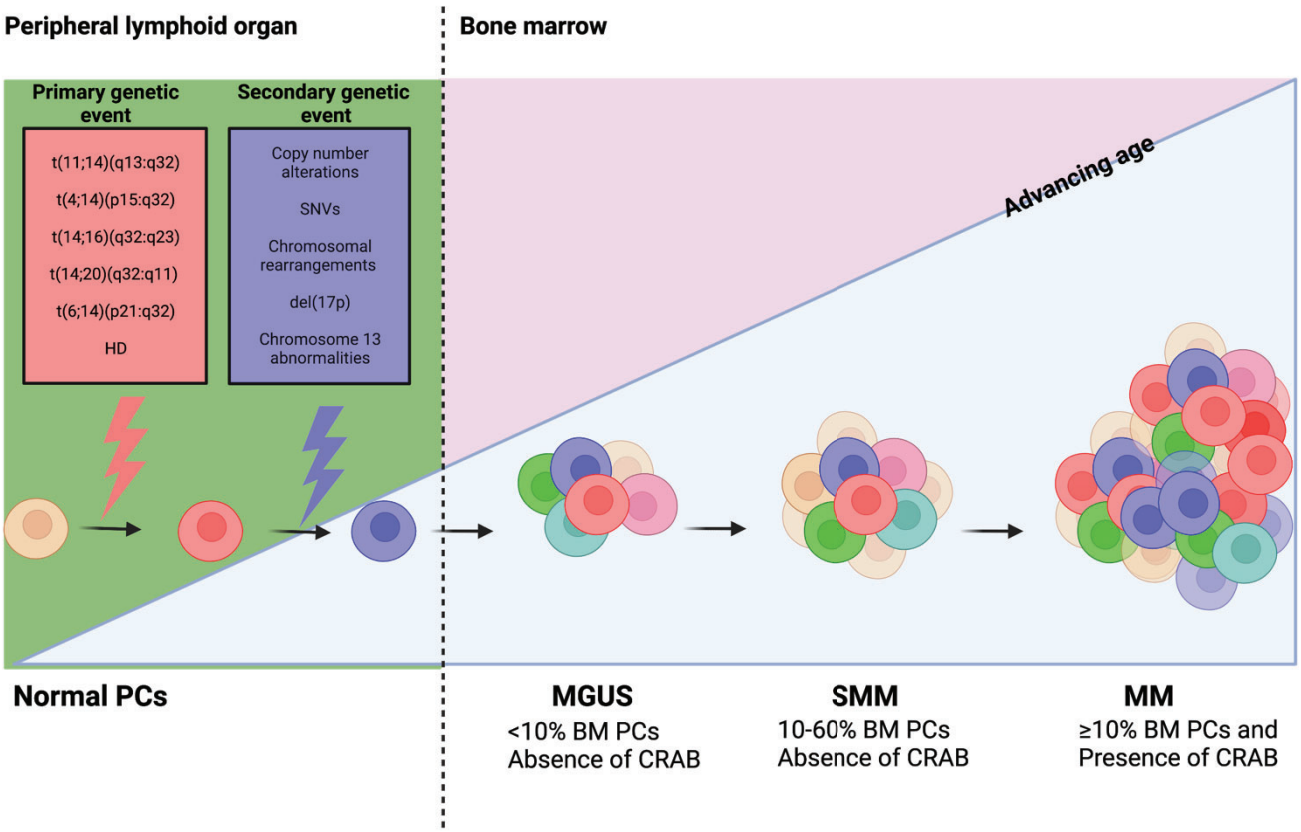
Peripheral lymphoid organ
Bone marrow
Primary genetic event
t(11;14)(q13:q32)
t(4;14)(p15:q32)
t(14;16)(q32:q23)
t(14;20)(q32:q11)
t(6;14)(p21:q32)
HD
Secondary genetic event
Copy number alterations
SNVs
Chromosomal rearrangements
del(17p)
Chromosome 13 abnormalities
Advancing age
Normal PCs
MGUS
<10% BM PCs
Absence of CRAB
SMM
10-60% BM PCs
Absence of CRAB
MM
≥10% BM PCs and
Presence of CRAB

1.2 The BM microenvironment

The BM microenvironment is composed of a wide variety of cell types including differentiated immune cells (macrophages, T cells, natural killer (NK) cells), endothelial cells, stromal cells of mesenchymal origin (encompassing multipotent BM mesenchymal stem cells and their differentiated progeny such as osteoblasts and fibroblasts; hereafter referred to as BM-MSCs), osteocytes, adipocytes and haematopoietic stem cells (HSCs) as well as non-cellular components such as signalling molecules, cytokines, extracellular matrix and mechanical forces [161] (Figure 1.5).

Although the precise interactions of MM PCs and the BM microenvironment are yet to be established, it has been shown that the proliferative fate of MM PCs is greatly dependent on where they "land" within the BM microenvironment [10]. For example, in a study where 5TGM1 MM PC were labelled with a unique heritable DNA barcode and intravenously injected into C57BL/KaLwRijHsd mice, assessment of the final contribution of each tagged 5TGM1 MM PC to tumour burden *in vivo* showed that very few clones proliferate to generate the majority of the bulk of the tumour. In this study, it was estimated that for each proliferative MM PC clone, 16 remained dormant [10]. As this skewing of the growth of individual tumour clones was not observed *in vitro*, this suggests that the BM microenvironment exerts strong selection pressures on MM PC proliferation *in vivo*. Indeed, Lawson *et al.* have investigated the heterogeneity in cell growth and proliferation within populations of MM cells. In this study, the GFP-labelled murine MM cell line 5TGM1-GFP was labelled with DiD membrane dye, to track proliferation and dormancy, and was inoculated in C57BL/KaLwRijHsd mice [162]. While some 5TGM1-GFP cells proliferated *in vivo* and lost their membrane dye (termed DiD^{low}), others remained dormant and retained the DiD label (DiD^{hi}). Importantly, FACS-sorted DiD^{hi} 5TGM1-GFP (dormant) cells isolated from tumour-bearing mice were able to form MM tumour following subsequent inoculation into tumour naïve mice, to a similar extent

as FACS-sorted DiD^{low} 5TGM1-GFP (previously proliferating) cells. This suggests that extrinsic microenvironmental controls, in the host BM, alone can regulate MM PC proliferation. The importance of the BM microenvironment in activating dormant PC isolated from MGUS has also been demonstrated using the humanised MIS$^{(KI)}$TRG mouse model, which features 5 human knock-in genes (encoding macrophage colony stimulating factor [M-CSF], IL-3, GM-CSF, signal regulatory protein alpha [SIRPα] and thrombopoietin [TPO]) to enable the engraftment of various patient derived xenograft tumours. In this study, the MIS$^{(KI)}$TRG mice were further modified by introducing a knock in allele of human IL-6 to recapitulate the human BM microenvironment and allow the growth of IL-6 dependent human MM cells [9]. Specifically, intra-femoral xenografts of MGUS patient derived PCs into MIS$^{(KI)}$TRG6 mice were equally capable as MM PCs to engraft and generate myeloma disease in these animals [9]. These data suggest that MGUS PCs have the same proliferative potential as MM PCs if provided with a supportive microenvironment for their growth. Indeed, studies using the lipophilic dye DiD to track the proliferation or dormancy of the murine 5TGM1 myeloma cell line *in vivo* have found that, following intravenous injection of in C57BL/KaLwRijHsd mice, dormant tumour cells are found localised to endosteal bone surfaces in the BM [162]. In contrast, proliferating 5TGM1 cells were found at variable distances from the endosteal bone. Activation of osteoclastic bone resorption by RANKL administration decreased dormant MM PC numbers, suggesting that remodelling of bone architecture may release these cells from dormancy [162]. Taken together, these studies highlight the importance of the extrinsic BM microenvironment on MM cell fate.

Figure 1.5. MM PC interacts with cellular and non-cellular components of the BM. MM PCs hijack the BM niche and significantly rely on constituents within the bone marrow (BM) microenvironment to promote their proliferation and survival. Solid lines indicate direct cellular interactions. Key cell types, signalling cascades and transmembrane proteins are represented. BM-MSC: bone marrow mesenchymal stem cell; CD40: CD40 molecule; CXCL-12: C-X-C motif chemokine ligand 12; ICAM1: intercellular adhesion molecule 1; IGF-1: insulin like growth factor-1; IL-6: interleukin-6; MM PC: myeloma plasma cell; NK cell: natural killer cell; VCAM1: vascular cell adhesion molecule 1. Adapted from [4].

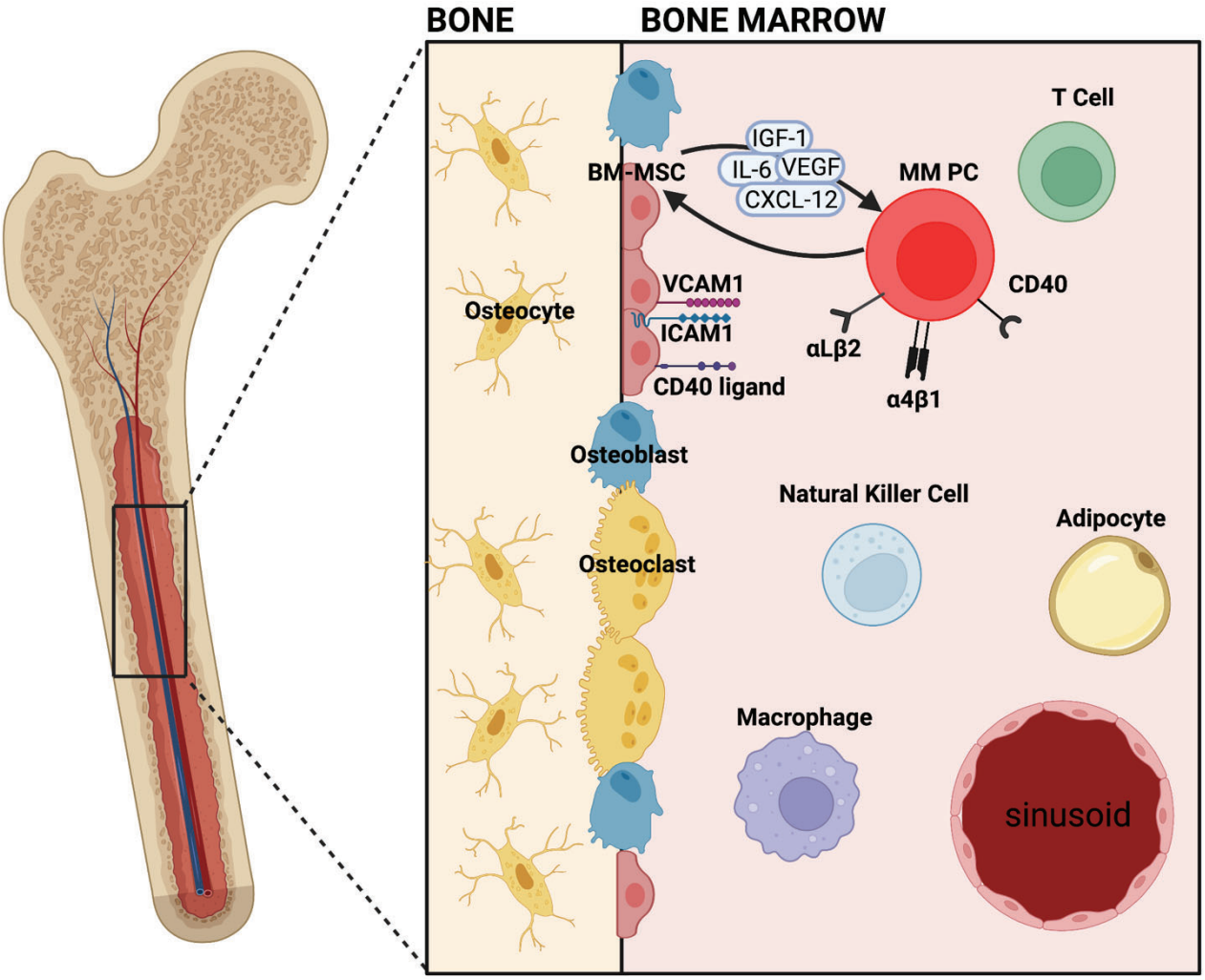
BONE
BONE MARROW
T Cell
IGF-1
IL-6
VEGF
CXCL-12
BM-MSC
MM PC
CD40
VCAM1
ICAM1
CD40 ligand
αLβ2
α4β1
Osteocyte
Osteoblast
Natural Killer Cell
Adipocyte
Osteoclast
Macrophage
sinusoid

1.2.1 The role of BM-MSCs in normal haematopoiesis

To understand how the microenvironment supports MM PC, parallels can be drawn between the supportive niches for MM and those for HSCs [163]. The organisation of the BM microenvironment plays a central role in maintaining the dynamic balance between HSC self-renewal, differentiation, quiescence and proliferation [164]. HSC fate is largely dictated by specific anatomical locations in the BM, termed niches, within which they reside [165]. In normal physiological conditions, the BM niche functions to regulate HSC self-renewal and quiescence, critical to preserving the HSC supply throughout lifetime [166]. The BM niche also enables HSCs to exit quiescence under hematopoietic stress, such as BM injury or inflammation, to undergo subsequent proliferation and differentiation in response to the specific stimulus [167]. During homeostasis, HSCs are largely quiescent [168] and localise within perivascular areas, although there is contention as to whether they specifically reside around the endosteal area around arterioles (endosteal niche) [169] or at sinusoids (vascular niche) [170]. Within the vascular niche, emerging evidence also suggests that quiescent HSCs reside in the peri-sinusoidal rather than peri-arteriolar area [170].

The importance of BM mesenchymal lineage cells on HSC niche maintenance is exemplified by ablation studies. Specifically, ablation of BM stromal cell populations such as C-X-C motif chemokine ligand (CXCL-12)-abundant reticular (CAR) cells [171], Nestin^{+} MSCs [172], leptin receptor expressing cells (LEPR^{+}) cells [173] and nerve/glial antigen 2 expressing (NG2^{+}) cells [169] has been shown to induce HSC cycling and depletion in the BM. Namely, these BM-MSC populations (including NG2^{+}, LEPR^{+} and CAR cells) promote HSC maintenance via secreted factors such as CXCL-12 or stem cell factor (SCF; also known as KIT ligand), which have been shown to regulate HSC niche retention, self-renewal and

trafficking [174, 175]. Furthermore, these BM-MSC populations have been shown to provide structural scaffolding for HSCs [174, 175].

Notably, perturbed interactions between HSCs and the BM niche alter normal haematopoiesis and can lead to haematological malignancies. Indeed, studies have shown that hematopoietic malignancies can develop by modulating supporting cells in the BM microenvironment. For example, constitutive activation of β-catenin in osteoblastic cells can induce myelodysplastic syndromes (MDS) and acute myeloid leukaemia (AML) [176]. Alternatively, the conditional ablation of osteoblasts can accelerate the development of chronic and acute leukaemias in mice [177, 178]. Moreover, conditional deletion of Dicer1 miRNA ribonuclease III (Dicer1) in BM-MSCs is sufficient to distort normal haematopoiesis and result in myelodysplasia which, in some cases, progresses to acute AML *in vivo* [179].

In the context of myeloma, MM PCs may hijack the niche and outcompete HSC, to favour their proliferation and survival within the BM (reviewed in [163]). Much like normal PCs, MM PCs home to CXCL-12-rich regions of the BM microenvironment where they commonly adhere to extracellular matrix and BM-MSCs [180-183]. For example, to facilitate HSC interactions with BM-MSCs, HSCs express adhesion molecules such as integrin α4β1, which enables binding to vascular cell adhesion protein 1 (VCAM-1) expressed by BM-MSCs to promote HSC maintenance within the BM [184]. Notably, MM PCs also express integrin α4β1, integrin αLβ2, and CD40, and thus can also bind VCAM-1, intercellular adhesion molecule 1 (ICAM-1) and CD40 ligand (CD40-L) expressed by BM-MSCs [185]. These interactions result in the mutual modulation of phenotype of both MM PCs and BM-MSCs, which has been shown to promote a myeloma growth stimulating environment. In line with this, several signalling molecules such as CXCL-12, IL-6, vascular endothelial growth factor (VEGF), angiopoietin-

1 (Ang-1) and osteopontin (OPN) have been implicated in healthy HSC maintenance and MM PC establishment and proliferation within the BM [163].

For example, CXCL-12 signalling via the C-X-C motif chemokine receptor 4 (CXCR4) has been implicated in the control of HSC BM homing and retention [175, 186]. In addition to CXCL-12 being an important chemoattractant for HSCs, CXCL-12 signalling has also been reported to promote HSC quiescence [187]. Importantly, it is widely established in the literature that the CXCL-12/CXCR4 axis plays a pivotal role in myeloma PC invasion and drug resistance, with BM-MSC derived CXCL-12 strongly implicated in MM PC adhesion to BM-MSCs, BM-homing and retention in the BM niche and cell adhesion mediated drug resistance (CAM-DR) [180-183, 188-191]. Additionally, IL-6 has been reported to enhance interleukin-3-induced proliferation of HSCs [192], haematopoietic regeneration [193] and B cell differentiation into plasma cells [192, 194, 195]. Notably, IL-6 has been widely reported to promote MM PC growth both *in vitro* and *in vivo* in the literature [196-202]. Moreover, VEGF signalling has been implicated in promoting both the survival and growth of HSCs [203]. Notably, VEGF signalling has been shown to mediate MM PC growth and migration [204], which is enhanced by the increased secretion of IL-6 by BM-MSCs in response to VEGF, further promoting MM PC growth [205, 206]. In addition, while Ang-1 signalling through Tie-2 receptor on HSCs has been reported to regulate HSC quiescence [207], Ang-1 expression by MM PCs is associated with expression of Tie-2 on BM endothelial cells and vascularisation *in vivo* [208]. Lastly, OPN has been implicated in promoting the homing of HSCs to the endosteal surface and suppressing HSC proliferation *in vitro* [209]. In the context of MM, OPN has been described to enhance osteoclast function and angiogenesis [210] as well as synergise with IL-6 to promote MM PC growth [211].

1.2.2 The role of BM-MSCs in supporting MM development

BM-MSCs are a crucial component of the BM microenvironment and are known to significantly impact MM PC proliferation and survival within the BM, as extensively reviewed in [185, 212]. Indeed, numerous studies have shown that primary transformed PCs can be supported *in vitro* using a BM-MSC feeder layer, suggesting that BM-MSCs can prevent primary MM PC apoptosis [213, 214]. In addition, BM-MSCs have also been reported to protect MM PCs from chemotherapy-induced apoptosis [215, 216]. For example, co-culture of MM PC lines with healthy BM-MSCs has been shown to confer resistance to bortezomib-induced apoptosis in human RPMI-8226 and MM5.1 and murine 5T33MMvv and 5T33MMvt MM cell lines, when compared with bortezomib-treated MM cell line monocultures [215]. Similarly, co-culture of U266 and NCI-H929 MM cell lines with BM-MSCs rendered them resistant to daunorubicin-induced apoptosis [216]. Furthermore, intrafemoral co-injection of 5T33MMvv murine MM cells with murine MSCs protected 5T33MMvv MM cells from bortezomib-induced apoptosis *in vivo* compared with animals injected with 5T33MMvv MM cells only [215].

Furthermore, BM-MSCs have been shown to influence MM PC proliferation both *in vitro* and *in vivo*. For example, BM-MSCs isolated from healthy mice have been shown to favour the proliferation of the 5T33MMvv murine MM cell line in direct co-culture *in vitro* relative to MM cells cultured alone [215]. Similarly, BM-MSCs from healthy individuals have been shown to promote the proliferation of human myeloma cell lines (MM5.1 and L363) as well as increase survival and/or proliferation of primary human MM cells in direct co-culture, relative to MM cells in monoculture [215, 217]. Notably, the co-culture of INA-6 MM cell line with healthy donor BM-MSCs was shown to significantly increase MM PC viability [218]. Moreover, the intrafemoral co-injection of 5T33MMvv MM cells with healthy murine BM-

MSCs in a 5T3MM mouse model was shown to significantly promote the proliferation of 5T33MMvv cells *in vivo* relative to the injection of 5T33MMvv cells alone [215]. Similarly, co-injection of IM-9 MM cells with BM-MSCs was shown to substantially increase MM tumour proliferation *in vivo* compared with the injection of IM-9 cells alone in a BALB/c-nu/nu mouse model [219].

Mechanistically, the co-culture of murine BM-MSCs from healthy animals with 5T33MMvv murine MM cell line was found to increase the activation of AKT and ERK proliferative pathways and increase expression of cyclin D2 and CDK4 cell cycle proteins in MM PCs [215]. Co-culture of LP-1 and U266 MM cell lines with BM-MSCs from healthy subjects was shown to increase MM PC clonogenic potential *in vitro*. This was associated with the upregulation of stemness genes *OCT4*, *SOX2* and *NANOG* in MM PCs via the Burton tyrosine kinase [220].

In line with the studies described above, conditioned medium collected from healthy human BM-MSCs has been shown to promote the proliferation of XG1 and MM5.1 MM cell lines, while treatment with conditioned medium from healthy murine BM-MSCs was found to promote the proliferation of the murine 5T33MMvv cell line [215, 221], suggesting that the growth-promoting effect may be mediated, at least in part, by soluble factors. Additionally, the treatment of U266 and ARP-1 human MM cell lines with conditioned medium from healthy donor and MM patient BM-MSCs promoted the translation of eIF4E and eIF4G within MM PCs, with this mechanism suggested to play an important role in the pro-MM effects of BM-MSCs in this study [222]. Indeed, BM-MSCs secrete a range of growth factors and cytokines that are known to promote MM cell viability [218], stemness [220], clonogenic potential [220], proliferation [215] and drug resistance [215, 216] (Figure 1.6).

Figure 1.6. BM-MSCs secrete a plethora of MM growth factors that support MM PC proliferation and survival. MM PCs express integrin α4β1, integrin αLβ2 and CD40 molecule (CD40) receptors on the cell surface, which enables them to bind BM-MSCs via intercellular adhesion molecule 1 (ICAM1), vascular cell adhesion molecule 1 (VCAM1) and CD40 ligand expressed on BM-MSCs respectively. Direct adhesion of MM cell lines to healthy human BM-MSCs promotes the secretion of MM growth factors by BM-MSCs including C-X-C chemokine ligand- 1,-8 and 10 (CXCL-1, CXCL-8 and CXCL-10), C-C motif chemokine ligand-2 and -5 (CCL2 and CCL5), interleukin-6 (IL-6), interleukin 10 (IL-10), tumour necrosis factor alpha (TNF-α), and insulin growth factor 1 (IGF-1) MM growth factors. Furthermore, BM-MSCs secrete a range of growth factors and cytokines that are known to promote MM cell proliferation and survival such as CXCL-12, IL-6, vascular endothelial growth factor (VEGF), angiopoietin-1 (Ang-1) and osteopontin (OPN) which have been implicated in MM PC establishment and proliferation within the BM. Moreover, BM-MSCs from MM patients secrete higher levels of IL-6 and growth differentiation factor 15 (GDF-15) compared with healthy age-matched BM-MSCs, which have been implicated in promoting MM PC proliferation *in vitro* and *in vivo*. Lastly, BM-MSCs from MM patients secrete higher levels of TNF-α compared with healthy age-matched BM-MSCs, which have been implicated in promoting MM PC proliferation *in vitro*.

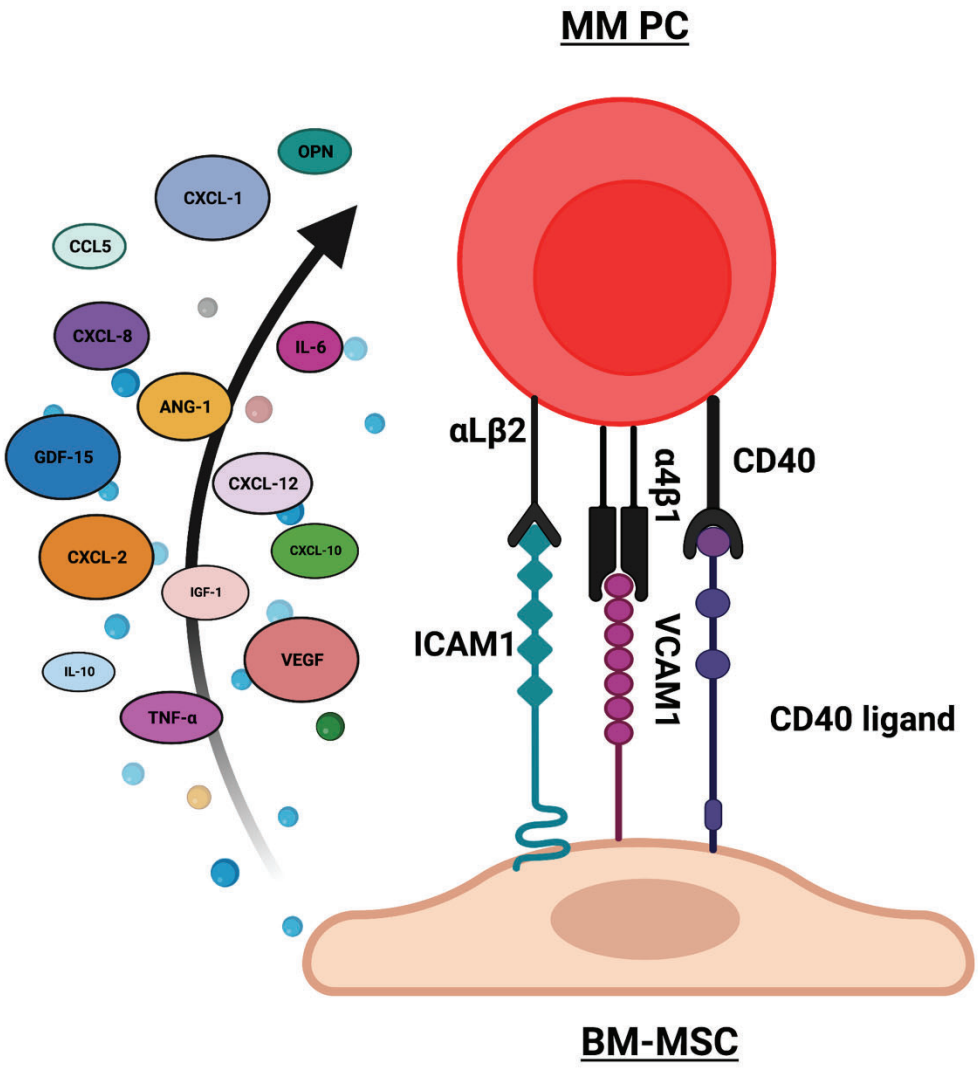
MM PC
OPN
CXCL-1
CCL5
CXCL-8
IL-6
ANG-1
GDF-15
CXCL-12
CXCL-2
CXCL-10
IGF-1
VEGF
IL-10
TNF-α
αLβ2
α4β1
CD40
ICAM1
VCAM1
CD40 ligand
BM-MSC

Alternatively, it has been shown that BM-MSCs may also suppress MM PC proliferation. Studies report that relative to monoculture controls, direct co-culture of BM-MSCs from healthy donors significantly suppresses the proliferation of U266, ARH-77, HS-Sultan and IM-9 myeloma cell lines, [223, 224]. Similarly, exosomes derived from healthy BM-MSCs have been shown to inhibit the proliferation of MM1.S and RPMI-8226 human MM cell lines *in vitro* [225]. This is consistent with previous work showing that BM-MSCs isolated from healthy C57BL6/J mice exert an inhibitory effect on 5TGM1 MM cell proliferation in a 24-hour co-culture [226]. Furthermore, Lawson *et al.* have demonstrated that *in vitro* co-culture of 5TGM1 MM PCs with MC3T3 murine stromal osteoblast-like cells promoted 5TGM1 cell dormancy, as measured by retention of DiD membrane dye [162]. Consequently, MM PC interactions with constituents of the BM niche, especially BM-MSCs plays an important part in modulating MM growth within the BM by either promoting, or suppressing, MM PC outgrowth.

Importantly, there is evidence to suggest that the proliferative fate of MM PCs in culture with BM-MSCs may contextually depend on whether the BM-MSCs are sourced from healthy or MM patients. Indeed, it has been shown that BM-MSCs from MM patients significantly promote the proliferation of MOLP6, U266 and ARP-1 MM cell lines when compared with co-culture with BM-MSCs from age-matched healthy donors [200, 225, 227]. Functionally, BM-MSCs from MM patients display a different gene expression profile to healthy BM-MSCs [200, 228, 229], characterised by the up-regulation of various proteins that have been implicated to promote MM PC growth. In support of this, exosomes released from BM-MSCs of MM patients have been shown to significantly promote the proliferation of MM1.S, RPMI-8226, OPM2, ARP-1 and U266 MM cell lines compared with exosomes derived from healthy human BM-MSCs *in vitro* [225, 230]. For example, IL-6 gene and protein expression is significantly

elevated in MM patient BM-MSCs compared with BM-MSCs from healthy subjects [200, 229, 231-235]. IL-6 has been widely recognised as a growth factor of primary MM cells [196-199] and MM cell lines [200-202]. In line with this, co-injection of U266 MM cells with BM-MSCs transfected with IL-6 siRNA significantly reduced the MM tumour volume and mitotic index in nude mice *in vivo*, compared with animals co-injected with U266 and control untransfected BM-MSCs [202]. Additionally, BM-MSCs from MM patients display a significant upregulation in both gene and protein expression of growth differentiation factor 15 (GDF-15) [200, 229, 231, 234, 236], with studies showing that the supplementation with GDF-15 promotes the survival and clonogenic growth of human MM cell lines and primary human MM cells *in vitro* [236, 237]. Furthermore, pre-treatment of NCI-H929 cells with GDF-15 increases their ability to develop MM tumours *in vivo* [236]. Moreover, survival of mice injected with Vk*Myc MM cells was significantly longer in *Gdf15*-knockout mice, compared with wild-type controls, strongly supporting the role of microenvironmental GDF-15 in MM disease progression *in vivo* [236]. Additionally, BM-MSCs from MM patients express higher levels of tumour necrosis factor alpha (TNF-α) [233, 234] which has been recognised as a survival and proliferation factor for MM cell lines [238].

The interaction between MM PCs and BM-MSCs can induce the production of pro-myeloma factors by the BM-MSCs. Namely, direct adhesion of MM cell lines to healthy human BM-MSCs was shown to promote the secretion of MM growth factors by BM-MSCs including C-X-C chemokine ligand-1 (CXCL-1), CXCL-8 and CXCL-10, C-C motif chemokine ligand-2 (CCL-2) and CCL-5 and interleukin 10 (IL-10), IL-6, TNF-α and insulin growth factor 1 (IGF-1) [215, 223, 239-241]. Taken together, these studies highlight that MM PC crosstalk with BM-MSCs plays an important role in regulating MM PC proliferation, survival and drug resistance.

1.3 The BM microenvironment changes with biological ageing

The risk of progression from MGUS to MM significantly increases with age [41]. As the BM microenvironment is implicated in regulating MM PC growth and survival [8, 9, 162], it is plausible that age-related changes in the BM microenvironment may facilitate this progression.

1.3.1 Cellular senescence

One of the key hallmarks of ageing is the induction of cellular senescence, leading to the accumulation of senescent cells within normal tissues, including the BM [242-244]. Cellular senescence is characterised by irreversible cell cycle arrest, whereby cells cease division but remain viable and metabolically active. Cellular senescence can be induced by cell intrinsic effectors such as telomere shortening, changes in telomere structure, epigenetic changes, chromatin disorganisation, perturbed proteostasis, DNA damage and mitochondrial dysfunction and hypoxia [245, 246]. Cell extrinsic effectors such as oxidative and genotoxic stress, mitogenic signals, inflammation, tissue damage signals, irradiation, chemotherapeutic agents, and nutrient deprivation can also induce cellular senescence [245, 246]. Cellular senescence can either be acute or chronic in nature. Acute senescence response is triggered by a sudden increase in a specific stressor, often during tissue repair and development, generates a sustained DNA damage response (DDR) and involves tightly controlled and coordinated recognition by immune cells, leading to rapid elimination and replacement of senescent cells by healthy cells [247]. In contrast, chronic senescence occurs during ageing due to mild genotoxic stress such as telomere shortening or DNA damage that accumulates over time, triggering a stochastic switch to senescence [248]. While remaining viable, these cells undergo cell cycle arrest and transition into a senescent state, displaying altered metabolic activity and apoptosis resistance [249]. The control of cellular proliferation is achieved at the G1 phase of the cell cycle, which is the point at which senescent cells arrest. As the progression through the

cell cycle requires coordinated efforts of various cyclin/cyclin-dependent-kinase (CDK) complexes, heightened levels of CDK inhibitors can interrupt cell cycle progression by inhibiting cyclin/CDK complex formation. Senescence is initiated through p53-dependent expression of $p21^{Cip1}$ and $p16^{INK4A}$ as well as p53-independent expression of $p14^{INK4A}$ and $p27^{Kip1}$ CDK-inhibitors, with high gene and protein expression of these markers widely used to identify senescent cells [250]. While DNA-damaging stimuli are thought to induce senescence via the $p21^{Cip1}$ pathway, senescence induction via replicative means has been shown to activate the $p16^{INK4A}$ pathway. Furthermore, the heightened activity of senescence associated β-galactosidase (β-gal) enzyme is highly correlated with cellular ageing and is used to identify senescent cells [251]. Moreover, an enlarged, flattened, polygonal cellular morphology is also characteristic of senescent cells [252]. A summary of the features of senescent cells is depicted in Figure 1.7.

In addition to greater induction of cellular senescence with age, there is also a defect in clearing these cells due to the concomitant age-related deterioration of the immune system [253]. Moreover, senescent cells have also been reported to recruit and induce immune cell dysfunction, which may contribute to their retention within tissues [254]. Consequently, chronically senescent cells persist in tissues and organs. Senescent cells can modify tissue microenvironment by expressing a senescence-associated secretory phenotype (SASP), characterised by increased secretion of various cytokines, growth factors and pro-inflammatory mediators to create an inflammatory state [255].

Figure 1.7. Features of senescent MSCs. Senescent bone marrow mesenchymal stromal cells (BM-MSCs) are characterised by increased β-galactosidase activity (blue staining), enlarged morphology, decreased proliferation and increased expression of $p16^{INK4A}$, $p14^{INK4A}$ $p27^{Kip1}$ senescence-associated factors, with high gene and protein expression of these markers widely used to identify senescent cells. Moreover, senescent BM-MSCs are characterised by an altered secretory phenotype termed the senescence associated secretory phenotype (SASP).

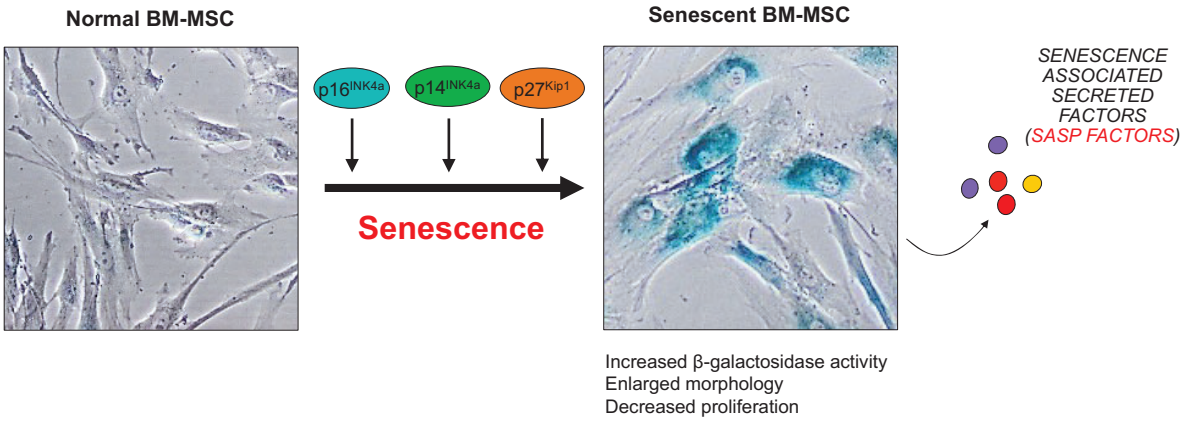
Normal BM-MSC
p16INK4a
p14INK4a
p27Kip1
Senescence
Senescent BM-MSC
SENESCENCE ASSOCIATED SECRETED FACTORS (SASP FACTORS)
Increased β-galactosidase activity
Enlarged morphology
Decreased proliferation

1.3.2 BM-MSCs undergo senescence with advanced biological age

Multiple studies, characterising BM-MSCs from young and aged mice and humans, have shown that BM-MSCs undergo senescence with advancing biological age in both species. For example, the growth kinetics of BM-MSCs derived from young and aged mice show that BM-MSCs isolated from older animals exhibit a decreased proliferative capacity compared with their younger counterparts *in vitro* at an equivalent passage [256, 257]. This is also true in the human context, as BM-MSCs isolated from older patients display significantly reduced growth kinetics *in vitro* compared with BM-MSCs isolated from younger donors [258-260]. Analysis of BM-MSCs isolated from young and aged C57/BL6 mice revealed that cells from aged mice display increased senescence-associated $p16^{INK4A}$, $p21^{Cip}$, p53 and β-gal activity [257] while analysis of BM-MSCs isolated from young and elderly humans revealed an age-related, significant increase in $p21^{Cip1}$ and p53 expression, as assessed by flow cytometry and qRT-PCR [261]. Further, comparison of gene expression of BM-MSCs isolated from young (21-25 year old) and elderly (80-92 years) human donors revealed that biological ageing is associated with a gene expression profile similar to that of replicative senescent cells [262].

1.3.3 Stromal cell senescence as a cancer driver

The incidence of cancer increases 11-fold in individuals over the age of 65, compared with younger individuals, with the median age of cancer diagnosis ranging from 68-72 years [263-265]. Intriguingly, there is strong evidence that senescent stromal cells can promote the proliferation of various cancer cell types (summarised in Table 1.1). For example, co-culture studies suggest that replicatively senescent WI-38 fibroblasts or irradiated senescent primary human mammary fibroblasts significantly induce the proliferation of the malignant breast cancer cell line MDA-MB-231, relative to co-culture with non-senescent controls [266, 267]. Similar findings were observed by Coppé *et al.*, where direct co-culture of weakly tumorigenic

Eph4-v epithelial cells with irradiation-induced and or replicatively senescent fibroblast cell lines WI-38 and hBF promoted their proliferation *in vitro* relative to co-culture with non-senescent control fibroblasts [268]. Moreover, senescent fibroblasts have also been shown to induce the proliferation of premalignant cells in direct co-culture. Namely, HaCAT human epidermal keratinocytes, S1 human mammary epithelial cells and Scp2 mammary epithelial preneoplastic cell lines, all which harbour p53 mutations but do not form tumours *in vivo*, proliferate significantly more in direct co-culture with replicatively senescent WI-38 fibroblasts compared with non-senescent controls [266, 268]. Similarly, Lawrenson *et al.* showed that hydrogen peroxide (H_2O_2)-mediated senescence induction in primary ovarian fibroblast cells significantly promoted the proliferation of partially transformed primary ovarian surface epithelial cells compared with co-culture with non-senescent cells in a 3-dimensional (3D) spheroid culture system [269]. As senescent cells accumulate with age, this may contribute to the age-related progression from cancer precursor conditions to malignancy.

Aside from proliferation, stromal cell senescence has also been linked to conferring other advantages for malignant cells *in vitro*. For example, co-culture of Suit-2 and Capan-1 pancreatic cancer cell lines with irradiated MRC-5 fibroblasts, or irradiated primary pancreatic fibroblasts, significantly enhanced Matrigel invasion of cancer cells when compared with co-culture with non-senescent controls [270]. Furthermore, co-culture of MDA-MB-231 and MCF-7 breast cancer cell lines with irradiation-induced senescent fibroblasts was shown to protect them from chemotherapy and radiotherapy induced apoptosis compared with co-cultures with non-senescent fibroblasts [267].

Additionally, senescent stromal cells have also been implicated in creating a microenvironment supportive of tumour growth of preneoplastic and neoplastic cells *in vivo*. For example, while

injection of premalignant HaCAT or SCp2 epithelial cell lines alone does not result in tumour development in *nu/nu* mice, co-injection of these cells in combination with equal numbers of senescent WI-38 fibroblasts results in significant tumour development compared with co-injection with non-senescent controls [266]. In line with this, co-injection of weakly tumorigenic EpH4-v mouse mammary epithelial cells with senescent murine mammary fibroblasts into mammary fat pads of female *nu/nu* mice significantly promotes tumour formation and vascularisation relative to co-injection with non-senescent fibroblasts or EpH4-v cells alone [268]. Likewise, co-injection of malignant Ha(Pk) epithelial or MDA-MB-231 breast cancer cell lines in combination with senescent WI-38 fibroblasts also significantly promotes tumorigenesis in *nu/nu* mice compared with co-injection with non-senescent cells or tumour cells alone [266]. Similarly, injection of MDA-MB-231 breast cancer cells in nude mice, in combination H_2O_2-treated senescent umbilical cord MSCs, significantly promotes tumour initiation, accelerates tumour growth and leads to a significant increase in tumour xenograft size and weight and tumour in comparison to co-injection with non-senescent MSCs or the injection of tumour cells alone [271]. Analogously, co-injection of MDA-MB-231 cells or PC-3 prostate cancer cells, in combination with HCA2 fibroblasts treated with bleomycin to facilitate senescence induction into *scid* mice, significantly promotes xenograft tumour growth compared with co-injection with non-senescent controls [272]. Co-transplantation of PC-3 cells with irradiation-induced senescent PSC27 fibroblast cells has also been reported to significantly increase xenograft size in *scid* mice compared with co-transplantation with non-irradiated PSC27 fibroblasts [273].

Importantly, the tumour supportive properties of senescent cells in the BM microenvironment have also been explored *in vivo*. For example, Luo *et al.* used a FASST (fibroblasts accelerate stromal supported tumorigenesis) model that utilises a stromal-specific Cre-recombinase,

driven by the collagen-I promoter, to induce targeted stromal senescence in the murine BM by inducing the expression of $p27^{Kip1}$ cell cycle inhibitor [274]. Indeed, when these mice were used in an intracardiac NT2 murine breast cancer model, significantly higher tumour burden was detected in bones of FASST mice compared with littermate controls, suggesting that the accumulation of senescent stromal cells in the BM microenvironment is sufficient to create a hospitable niche for breast cancer cell outgrowth [274].

Notably, studies strongly suggest that senescent stromal cells, and the SASP factors they secrete, can create a favourable localised microenvironment for cancer cell growth [255]. For example, conditioned medium from replicative senescent TIG-3 embryonic fibroblasts and doxorubicin-induced senescent RPE-1 retinal epithelial cells was shown to promote the proliferation of the MCF-7 human breast cancer cell line *in vitro* in comparison with conditioned media from non-senescent cells [275]. Similarly, conditioned medium collected from replicative senescent adipose-derived primary MSCs was shown to promote the proliferation of the LoVo colorectal cancer cell line *in vitro,* relative to conditioned medium from non-senescent cells [276]. Moreover, the treatment of prostate epithelial BPH-1 cell line and prostate cancer DU 145 and PC-3 cell lines with conditioned medium from senescent (H_2O_2-induced) prostate stromal cells significantly promoted prostate cell line proliferation *in vitro,* compared with treatment with conditioned medium from pre-sensecent prostate stromal cells [277]. Collectively, these studies suggest that the proliferative influence of senescent cells is, in part, mediated through secreted SASP factors.

In addition to promoting proliferation, SASP factors can also exert pro-migratory effects on cancer cells. Indeed, it has been shown that conditioned medium from senescent fibroblasts significantly increases the migration of MCF-7 breast cancer cells *in vitro,* compared with

conditioned medium from non-senescent fibroblasts [278]. Furthermore, treatment of non-aggressive human breast cancer cell lines T-47D and ZR-75-1 with conditioned media collected from senescent fibroblasts enhanced invasiveness and induced EMT, when compared with treatment with conditioned medium from pre-senescent fibroblasts, promoting a malignant phenotype in these cell lines [279]. Furthermore, conditioned media collected from senescent fibroblasts significantly enhanced the *in vitro* migratory and invasive properties of ovarian epithelial cells that had been engineered to express the *MYC* oncogene, while having no effect on the parental, non-transformed ovarian epithelial cell lines [269]. These data suggest that senescent cells may provide a localised microenvironment that is required to support the outgrowth of pre-malignant cells that harbour cancer-initiating mutations. Taken together, the accumulation of senescent cells *in vivo* may create a cancer permissive BM niche, enabling the outgrowth of malignant cells in the BM. As senescent cells accumulate with age, this may contribute to the age-related progression from cancer precursor conditions to overt cancers.

Table 1.1.
Evidence for senescent cells promoting malignant and pre-malignant cell growth in various cancer contexts.

Senescent cell type	Method of senescence induction	Assay type	Effect on premalignant/malignant cell type	References
WI-38 fibroblast cell line	Replicative exhaustion	Direct *in vitro* culture	Promote proliferation of breast cancer cell line MDA-MB-231	[266]
Fibroblast cell lines WI-38 and hBF	Irradiation-induced/replicative exhaustion	Direct *in vitro* culture	Promotes proliferation of Eph4-v epithelial cell line	[268]
WI-38 fibroblast cell line	Replicative exhaustion	Direct *in vitro* culture	Promotes proliferation of HaCAT human epidermal keratinocytes, S1 human mammary epithelial cells and Scp2 mammary epithelial preneoplastic cell lines	[266, 268]
WI-38 fibroblasts	Replicative exhaustion	Direct *in vitro* culture	Induces the proliferation of malignant breast cancer cell line MDA-MB-231	[266]
Primary human mammary fibroblasts	Irradiation-induced	Direct *in vitro* culture	Induces the proliferation of malignant breast cancer cell line MDA-MB-231	[267]
Primary ovarian fibroblast	H_2O_2 treatment	Direct *in vitro* 3D culture	Promotes proliferation of partially transformed primary ovarian surface epithelial cells	[269]
MRC-5 fibroblast cell line	Irradiation-induced	Direct *in vitro* culture	Enhances Matrigel invasion of Suit-2 and Capan-1 pancreatic cancer cell lines	[270]
Primary pancreatic fibroblasts	Irradiation-induced	Direct *in vitro* culture	Enhances Matrigel invasion of Suit-2 and Capan-1 pancreatic cancer cell lines	[270]
Primary human mammary fibroblasts	Irradiation-induced	Direct *in vitro* culture	Protects MDA-MB-231 and MCF-7 breast cancer cell lines from chemotherapy and radiotherapy induced apoptosis	[267]
WI-38 fibroblast cell line	Unclear	Co-injection *in vivo*	Promotes proliferation of HaCAT or SCp2 epithelial cell lines	[266]
Primary murine	Unclear	Co-injection *in vivo*	Promotes tumour formation and vascularisation of EpH4-v mouse mammary epithelial cells	[280]

mammary fibroblasts				
WI-38 fibroblast cell line	Unclear	Co-injection *in vivo*	Promotes tumorigenesis of Ha(Pk) epithelial or MDA-MB-231 breast cancer cell lines	[266]
Primary umbilical cord MSCs	H_2O_2 treatment	Co-injection *in vivo*	Promotes MDA-MB-231 breast cancer cell tumour initiation, accelerated tumour growth and led to a significant increase in tumour xenograft size and weight and tumour vascularisation	[271]
HCA2 fibroblast cell line	Bleomycin treatment	Co-injection *in vivo*	Promotes the xenograft tumour growth of MDA-MB-231 breast or PC-3 prostate cancer cell lines	[272]
PSC27 fibroblast cell line	Irradiation-induced	Co-injection *in vivo*	Increases xenograft size post transplantation with PC-3 prostate cancer cell line	[273]
Primary murine stromal cells	FASST mouse model	-	Promotes tumour growth of NT2 murine breast cancer cells *in vivo*	[274]
TIG-3 embryonic fibroblast cell line	Replicative exhaustion	Conditioned media treatment *in vitro*	Promotes proliferation of the MCF-7 human breast cancer cell line	[275]
RPE-1 retinal epithelial cell line	Doxorubicin treatment	Conditioned media treatment *in vitro*	Promotes proliferation of the MCF-7 human breast cancer cell line	[275]
Adipose derived primary MSCs	Replicative exhaustion	Conditioned media treatment *in vitro*	Promotes the proliferation of the LoVo colorectal cancer cell line	[276]
Primary prostate stromal cells	H_2O_2 treatment	Conditioned media treatment *in vitro*	Promotes proliferation of prostate epithelial BPH-1 cell line and prostate cancer DU 145 and PC-3 cell lines	[278]
Human fibroblasts	Irradiation-induced	Conditioned media treatment *in vitro*	Enhances invasiveness T-47D and ZR-75-1 of breast cancer cell lines and induces epithelial to mesenchymal transition	[279]
Primary normal ovarian surface epithelial cells	H_2O_2 treatment	Conditioned media treatment *in vitro*	Enhances the *in vitro* migratory and invasive properties of ovarian epithelial cells that had been engineered to express the *CMYC* oncogene	[269]

H_2O_2= hydrogen peroxide
FASST= fibroblasts accelerate stromal supported tumorigenesis

1.3.4 BM-MSC senescence and its impact on haematopoiesis

Ageing is associated with disruptions in normal haematopoiesis, which is thought to be mediated by increased low-grade inflammatory signalling within the BM. Specifically, there is evidence that a senescent BM microenvironment plays a critical role in promoting BM inflammation and the dysregulation of haematopoiesis with ageing. For example, in a murine model, it has been shown that myeloid skewing can be alleviated when HSCs from aged mice are introduced into a young BM microenvironment. Specifically, transplantation of BM from 17-18-month-old mice into 2-month-old recipients revealed that that when 'aged' HSCs were transplanted into 'young' animals, fewer myeloid cells were generated compared with when 'aged' HSCs were transplanted into aged animals [281]. Moreover, induction of BM-MSC senescence by knockdown (KD) of the endoribonuclease, Dicer1, has been shown to significantly inhibit the ability of BM-MSCs to support HSCs *in vitro* [231, 282]. Dicer1 KD in BM-MSCs also alters haematopoiesis *in vivo* by promoting increased apoptosis and proliferation of primitive HSCs accompanied by a reduction in B cell progenitors and B cells and an increased frequency of myeloid cells, resulting in myelodysplasia [179]. In contrast, reversal of BM-MSC senescence by Dicer1 over-expression enhances their stem cell-supporting properties [282]. Furthermore, SASP secretion by senescent BM-MSCs has been postulated to contribute to age-related haematopoietic decline. For example, inflammatory cytokines CCL5 and IL-6 have been implicated in promoting myeloid skewing and clonal outgrowth of HSCs in mice [281, 283, 284]. Consequently, age-related accumulation of senescent BM-MSCs in the BM microenvironment can significantly impair normal haematopoiesis.

1.3.5 BM-MSC senescence as a driver of haematological malignancy

In addition to playing a role in solid cancers and aberrant haematopoiesis, there is increasing evidence that BM-MSC senescence contributes to the development and progression of haematological cancers. As the growth of transformed pre-neoplastic and neoplastic cells can be influenced by SASP factors, it has been postulated that age-related accumulation of senescent BM-MSCs and SASP leads to clonal outgrowth of transformed cells and malignancy [285]. In the following sections, we discuss evidence for the role of senescent BM-MSCs in blood disorder precursor conditions and haematological malignancies. An overview of the evidence for BM-MSC senescence in various haematological malignancies is provided in Table 1.2.

Table 1.2.
Overview of evidence for BM-MSC senescence in various haematological malignancies.

Molecular or functional BM-MSC characteristic	**Featured haematological disorder (relative to healthy BM-MSCs)**
Enlarged, polygonal and flattened morphology	MDS [282, 286-290] AML [291, 292] MM [229, 231, 289]
Reduced proliferative potential	MDS [282, 286-290, 293] AML [292, 294, 295] MM [229, 231, 232, 289, 296]
Increased β-galactosidase staining	MDS [282, 286-288, 297] AML [291] MM [229, 231, 296, 298]
Increased expression of $p16^{INK4A}$/p53/$p21^{Cip1}$	MDS [282, 287-289] AML [291] MM [229, 231, 233, 289, 296, 298]
Dicer1 downregulation	MDS [282] AML [295] MM [231]
Decreased osteogenic potential	MDS [286, 288-290] AML [294] MM [200, 229, 231, 232, 289, 299]
Senescent MSC promoting the growth of malignant cells	AML [300] MM [200, 219, 231]
Tumour cells inducing BM-MSC senescence	AML [300, 301] MM [219, 231]

AML = acute myeloid leukaemia
BM-MSC = bone marrow mesenchymal stromal cell
MDS = myelodysplastic syndrome
MM = multiple myeoma

1.3.5.1 BM-MSC senescence in myelodysplastic syndromes (MDS) and acute myeloid leukaemia (AML)

The prevalence of various haematopoietic dyscrasias, characterised by precursor conditions of specific age-related haematological cancers, significantly increases with age. For example, 86% of patients with MDS are diagnosed after the age of 60 (median age at diagnosis: 76 years), with only 6% of cases diagnosed in individuals under 50 years of age [302]. Indeed, the malignant state – AML is more prevalent with ageing, with a median diagnosis age of diagnosis of 69 years of age [303-305].

MDS are a group of asymptomatic disorders characterised by ineffective haematopoiesis with varying degrees of cytopenias and dysplasia. MDS is diagnosed based on the presence of one or more cytopenias (anaemia, neutropenia, thrombocytopenia), ≥10% morphologically dysplastic nucleated cells of one lineage and <20% blasts in peripheral blood and BM [306]. MDS can transform into AML, with the diagnosis of AML defined by ≥20% blood and BM involvement of leukaemic blasts, presence of cytopenias and in some cases the presence of genetic abnormalities including t(8;21), inv(16) or t(16;16) [306].

Numerous studies have shown that BM-MSCs from MDS and AML patients display senescent characteristics, including flattened polygonal morphology, a reduced expression of Dicer1, reduced proliferative and osteogenic potential, and increased β-gal activity and elevated $p16^{INK4A}$ and $p21^{Cip1}$ expression [282, 286-289, 291-294, 297, 307]. BM-MSCs from MDS patients have been shown to express increased levels of SASP factors, including IL-6 and TNF-α, compared with those of healthy controls [290, 308]. Further, BM-MSCs from AML patients express increased levels of SASP factors IL-6 [309], IL-7 [310] and CXCL-8 [311] compared with healthy controls.

Notably, increased expression of SASP factors in the BM and blood plasma of MDS patients is predictive of overall survival and progression to AML, supporting a potential role for senescence and SASP factors in MDS to AML transition. For example, several studies have demonstrated that SASP components such as IL-6, IL-7, CXCL-8 and TNF-α are significantly elevated in MDS patient BM and peripheral blood plasma compared with healthy controls [312, 313]. In addition, plasma IL-6 levels in MDS patients are an independent predictor of overall survival and risk of progression to AML [312]. In fact, BM-MSC gene expression of IL-6 gradually increases from MDS to AML [309]. Moreover, blood plasma IL-7 levels have been identified as independent prognostic factors for overall survival in MDS patients [312]. Furthermore, decreased proliferative rate of AML patient-derived BM-MSCs was found to be independently associated with poor patient outcomes such as treatment failure and early relapse [295].

Beyond the association between BM-MSC senescence and MDS to AML transition, there is also evidence that BM-MSC senescence may play an active role in driving progression from MDS to AML. Indeed, senescent BM-MSCs from MDS patients exhibit an enhanced ability to support the survival of leukaemic cells and decreased capacity to support normal haematopoiesis [282, 286, 290, 292]. Moreover, transwell co-culture of mouse myeloid leukaemic cells with senescent BM-MSCs significantly increases leukaemia cell proliferation in comparison to co-culture with non-senescent BM-MSCs [300], suggesting that senescent BM-MSCs promote leukaemic cell proliferation via secreted factors. Importantly, the expression of SASP factors IL-6 and CXCL-8 by BM-MSCs has been implicated in promoting leukaemic cell growth. For example, BM-MSCs from MDS patients exhibit an increased expression of IL-6 compared with healthy BM-MSC controls, with IL-6 previously reported to promote the growth of AML cell line HL-60 [314]. In line with this, the administration of an

anti-IL-6 receptor blocking antibody was shown to inhibit the proliferation of AML cell lines as well as the clonogenic growth of primary AML cells *in vitro* [315]. Knockdown of CXCL-8 in BM-MSCs has also been shown to significantly inhibit the ability of BM-MSCs to promote the survival of primary AML cells in a co-culture setting [316]. The role of CXCL-8 in BM-MSC-mediated promotion of AML cell proliferation has also been explored by blocking the CXCL-8 receptor (CXCR2) on CXCL-8-knockdown HL-60 and THP1 AML cell lines. In this study, treating co-cultures of AML patient-derived BM-MSCs and CXCL-8-knockdown AML cells with CXCR2 inhibitor, SB225002, decreased AML cell line proliferation and colony forming ability, induced cell cycle arrest and induced AML cell apoptosis in a dose-dependent manner, when compared with vehicle treated controls [311].

The functional role of senescent BM-MSCs in AML progression has been directly explored *in vivo* using a p16-3MR mouse model [300]. These mice have been engineered to express the $p16^{INK4A}$ promoter coupled with thymidine kinase, enabling the selective ablation of senescent BM-MSCs by administration of ganciclovir. Strikingly, ablation of $p16^{INK4A}$-expressing senescent BM-MSCs following the engraftment with mouse myeloid leukaemia cells significantly decreased subsequent tumour growth and increased mouse survival, when compared with controls [300], demonstrating the role of senescent BM-MSCs in AML disease progression.

As BM-MSC senescence and secretion of pro-leukaemic SASP factors, including IL-6 and CXCL-8, is evident at the MDS stage, and elevated levels of SASP factors are predictive of MDS-to-AML progression, it is possible that the age-related accumulation of senescent BM-MSCs at MDS provides a permissive, SASP-factor rich growth- activating niche for leukaemic cells which facilitates MDS to AML progression. Taken together, these studies support the

hypothesis that accumulation of senescent BM-MSCs with age in MDS patients may increase the proliferation of the myeloid lineages, increasing the rate of progression to AML in these patients.

1.3.5.2 BM-MSC senescence in MM

Similar to what has been reported in AML, there is mounting evidence that BM-MSCs from newly diagnosed MM patients have a senescent phenotype in culture, compared with BM-MSCs from age-matched healthy volunteers. Furthermore, it has been shown that BM-MSC senescence at MM is associated with MM patient outcomes.

1.3.5.2.1 BM-MSCs from MM patients display senescent phenotypic characteristics

BM-MSCs isolated from newly diagnosed MM patients are morphologically different to age-matched healthy controls and display polygonal, enlarged and flattened morphology compared with spindle-shaped healthy control counterparts [231]. Furthermore BM-MSCs from newly diagnosed MM patients are significantly larger than age-matched healthy control BM-MSCs as determined by flow cytometric cell size analysis [229]. Additionally, BM-MSCs from newly diagnosed MM patients display increased β-gal positivity relative to age-matched healthy BM-MSCs [229, 231]. Specifically, Guo *et al.* showed that increased β-gal staining was observed in 86.7% (26/30) newly diagnosed MM BM-MSC cultures analysed relative to age-matched healthy control BM-MSC cultures [231]. Notably, the proliferative capacity of newly diagnosed MM BM-MSCs was significantly impaired compared with that of age-matched healthy control BM-MSCs. For example, in routine *in vitro* cultures, more than two thirds (66%) of BM-MSC cultures from newly diagnosed MM patients failed to grow *in vitro*, compared with age-matched healthy control cultures, where less than 5% failed to establish *in vitro* [229]. In line with this, the clonogenic ability of newly diagnosed MM BM-MSCs is

significantly reduced by up to 23-fold compared with that of age-matched healthy controls, as quantified by colony forming unit fibroblast (CFU-F) assays [229, 231, 232]. Furthermore, BM-MSCs from newly diagnosed MM patients cease to proliferate earlier (passage 1-3) compared with BM-MSCs from age-matched healthy controls (passage 3-5) [229]. Accordingly, the time to reach confluence is significantly longer for BM-MSCs from newly diagnosed MM patients compared with age-matched healthy controls [232]. Likewise, the doubling time of newly diagnosed MM patient BM-MSCs is at least 2-fold longer than that of age-matched healthy controls [229, 231, 232]. Notably, cell cycle analysis of BM-MSCs from age-matched healthy and newly diagnosed MM patients confirmed that the reduced proliferative rate of BM-MSCs from MM patients is not due to increased apoptosis but is related to an accumulation of cells in the S phase [229].

1.3.5.2.2 The gene expression profile of BM-MSCs from MM patients is characterised by an upregulation of senescence-associated genes

Transcriptomic analysis studies of BM-MSCs from healthy and MM patients revealed that MM BM-MSCs display an altered gene expression profile, compared with their age-matched healthy counterparts [200, 229, 317]. For example, it is thought that the S phase arrest of MM BM-MSCs, described above, is attributed to a reduction in mRNA expression of key S-phase activators such as *CDK2*, *CCNE1* and *CDC25A* in newly diagnosed MM patient BM-MSCs compared with age-matched, healthy control BM-MSCs [229]. Importantly, expression levels of key S-phase inhibitors *CDKN1A, CDKN2A*, *CDKN2B* and *TP53* mRNA and protein, which are frequently used to identify senescent cells, are upregulated in newly diagnosed MM BM-MSCs relative to BM-MSCs from age-matched healthy volunteers [229, 231, 289, 296]. An upregulation of the key senescence marker, $p21^{Cip1}$ protein, levels has also been confirmed in newly diagnosed MM BM-MSCs when compared with age-matched healthy control BM-

MSCs [231]. Moreover, BM-MSCs from MM patients display increased gene expression of *HMGA2*, which encodes a protein involved in the formation of senescence-associated heterochromatin foci [233].

In line with the aforementioned *in vitro* observations, many genes downregulated in newly diagnosed MM BM-MSCs are those involved in cellular processes regulating cell cycle progression, DNA repair, differentiation and metabolism [229]. This includes downregulation of cell cyclins, and cyclin dependent kinases and significant decreases in mRNA expression of osteoblast markers *WNT1*, *WNT3*, *RUNX2* and *ALP* compared with healthy counterparts [229, 231, 232]. Importantly, these gene expression profiles are highly reminiscent of those of replicatively senescent BM-MSCs [318]. Moreover, BM-MSCs from newly diagnosed MM patients express significantly lower *DICER1* mRNA and protein levels compared with age-matched healthy control BM-MSCs [231], with previous reports showing that the attenuation of Dicer1 expression leads to senescence induction in a variety of cell types [319-321]. Furthermore, MM BM-MSCs also display an altered secretory profile compared with that of age-matched healthy control BM-MSCs, closely resembling that of the SASP of senescent BM-MSCs. Gene expression profiling studies have also revealed that the upregulated genes in BM-MSCs from newly diagnosed MM patients encompass those encoding SASP factors, including IL-6, IL-1β, amphiregulin (AREG) and growth differentiation factor 15 (GDF-15) compared with age-matched healthy controls [185, 322].

1.3.5.2.3 Association between serum SASP levels and BM-MSC senescence with MM disease outcomes

Notably, serum levels of canonical SASP factors in the peripheral blood of MM patients have been shown to correlate with MM disease severity and progression. Specifically, serum levels

of IL-6 [323-327], TNF-α [328] and GDF-15 [237, 327, 329-331] are elevated in MM patients compared with age-matched healthy controls. Moreover, serum levels of IL-6 [323-326], GDF-15 [237, 327, 329] and TNF-α [328, 332] in MM patients positively correlate with more advanced stage of the disease according to both Durie-Salmon or ISS classification systems. Furthermore, serum levels of SASP factors have been shown to negatively associate with MM patient survival. For example, in newly diagnosed MM patients, elevated serum levels of IL-6 and GDF-15 are associated with significantly shorter overall survival times compared with patients displaying low serum IL-6 and GDF-15 levels [236, 324, 333]. Although increases in SASP factor expression have been reported to correlate with MM disease severity and progression, it remains to be determined whether these increases are associated with due to the accumulation of senescent BM-MSCs.

Nevertheless, there is evidence to suggest an association between BM-MSC senescence and MM disease outcomes. Specifically, MM patients with high β-gal staining BM-MSCs as defined by ≥4.4% β-gal positive cells at diagnosis had significantly shorter progression-free survival following treatment with bortezomib and dexamethasone than patients with <4.4% β-gal positive BM-MSCs [334]. This finding may suggest an association between elevated MM BM-MSC senescence with increased MM PC proliferation, leading to subsequent relapse, or may suggest that MM BM-MSC senescence confers MM PC resistance to bortezomib and dexamethasone therapy, although this requires further investigation. Furthermore, Berenstein *et al.* showed that BM-MSCs isolated from relapsed MM patients showed increased β-gal staining compared with BM-MSCs isolated from newly diagnosed MM patients (albeit not significantly) [298]. While these findings suggests that elevated BM-MSC senescence may be associated with MM disease relapse, this finding should be interpreted with caution as many chemotherapeutic treatments can induce BM-MSC senescence [335].

1.3.5.2.4 Induction of BM-MSC senescence provides a growth permissive niche for MM tumour growth

While it remains to be determined whether elevated BM-MSC senescence at MM directly promotes increased MM PC proliferation, the artificial induction of BM-MSC senescence *in vitro* has been shown to promote MM tumour growth in co-culture. Notably, co-culture of the NCI-H929 MM cell line with senescence-induced Dicer1 knockdown BM-MSCs significantly enhanced growth of the MM cell line NCI-H929 relative to co-culture with non-senescent BM-MSCs [231]. Moreover, the expression of lysophosphatidic acid (LPA) receptor 1 (LPAR1), and subsequent induction of senescence, in BM-MSCs has been implicated in inducing MM PC growth *in vivo*. LPA signalling via LPAR1 was shown to increase senescence in BM-MSC cultures [219, 336]. Specifically, Kanehira *et al.* have shown that the silencing of LPAR1, via siRNA in human BM-MSCs, significantly reduced the proportion of β-gal positive cells and increased the proliferation of BM-MSCs 3-fold in *in vitro* culture, compared with control BM-MSCs transfected with scramble siRNA [219]. BM-MSCs isolated from MM patients express higher levels of *LPAR1* compared with BM-MSCs from healthy controls [219]. Importantly, the induction of BM-MSC senescence by the artificial over-expression of LPAR1 significantly promoted MM tumour growth *in vivo*. Specifically, co-transplantation of IM-9 MM cells with LPAR1 over-expressing BM-MSC xenografts significantly promoted tumour growth in BALB/c-nu/nu mice when compared with groups co-transplanted with control BM-MSCs [219]. Taken together, these studies suggest that senescent BM-MSCs may increase the proliferation of MM cell lines; however, further studies are required to conclusively demonstrate this.

While studies show that MM patient BM-MSCs display senescent features, and induction of BM-MSC senescence promotes MM PC proliferation leading to poorer disease outcomes, it remains to be deterimined whether the induction of BM-MSC senescence precedes MM development or is a consequence of the disease. Indeed, MM PCs themselves have been implicated in modulating the senescent phenotype of BM-MSCs. For example, transwell co-culture of primary MM cells or MM cell lines NCI-H929, OPM2 and KMS-12-BM with healthy human BM-MSCs for 24 hours was shown to induce a senescent phenotype in BM-MSCs, as defined by increased gene expression of *CDKN1A* and increased β-gal staining, compared with BM-MSCs in monoculture *in vitro* [231]. However, BM-MSC senescence induction by MM PCs has not been consistently reported in the literature. For example, the exposure of primary BM-MSCs from healthy volunteers to RPMI-8226 and MM.1S human myeloma cell lines in a trans-well system was shown to have no effect on $p21^{Cip1}$ and $p16^{INK4A}$ protein expression in BM-MSCs [233]. Moreover, co-culture of primary human BM-MSCs with KMS12B, KMS12PE, MM.1S, NCI-H929, JIM3 and U266 human MM cell lines and primary MM cells was shown to promote BM-MSC proliferation, as assessed by cell cycle progression analysis and Ki-67/PI staining [337]. Furthermore, while the exposure of 3T3-L1 pre-adipocyte murine fibroblast cell line to human MM1.S cell line led to a strong induction of BM-MSC SASP secretion of *Cxcl1*, *Cxcl2* and *Il6* in the murine cells, exposure of 3T3-L1 cells to 5TGM1 murine MM cells did not induce SASP expression [233]. These findings suggest that SASP induction in BM-MSCs may depend on the MM cell line used or may vary between species. Moreover, it has been reported that disease stage may also have implications on the modulation of the senescent phenotype by MM PCs. Specifically, Berenstein *et al.* demonstrated that while co-culture of BM-MSCs from healthy volunteers or HS-5 fibroblast cells with KMS12-PE MM cells did not reduce BM-MSC β-gal expression, co-culture with BM-MSCs from MM patients was shown to significantly reduce BM-MSC β-gal expression

and $p21^{Cip1}$ protein expression and increase cyclin E levels [298]. Taken together, as MM PCs have been shown to both promote and inhibit the induction of senescence in BM-MSCs, it is imperative to determine the senescent phenotype of BM-MSCs of MGUS patients to ascertain whether BM-MSC senescence at MM is a consequence of either advancing age or disease progression.

1.3.6 Conclusions

Although MGUS is a benign asymptomatic haematopoietic dyscrasia, it can sporadically progress to MM, at an average rate of 1% per year, due to unknown causes. A major challenge in the management of MGUS is identifying which patients will remain stable from those who will progress to overt MM as currently, no models exist which can accurately identify low risk MGUS patients with indolent disease from high-risk MGUS patients that are likely to develop overt MM. It is clear that the BM microenvironment plays a pivotal role in the development and progression of abnormal haematopoiesis and haematological cancers. As such, there is a necessity to investigate the microenvironmental differences in stable and progressing MGUS patients to help identify novel biomarkers of progression and understand the underlying influence of extrinsic factors on MGUS-to-MM progression. Evidence suggests that the presence of increased numbers of senescent BM-MSCs is a characteristic feature of haematological cancers including MM, and these cells secrete an altered cytokine profile that closely resembles the SASP. As the risk of development of these haematological cancers increases with age, concurrent age-related increases in BM-MSC senescence may contribute to the progression from benign states to overt malignancies. Most notably, in AML, there is strong evidence for a role of BM-MSC senescence in driving MDS-to-AML progression. While the role of senescent BM-MSCs in MGUS patients remains to be explored, the potential positive effect of senescent BM-MSCs and SASP factors on the proliferation of MM cells

suggests the possibility that age-related increases in BM-MSC senescence may be a driver of MGUS-to-MM progression. Further studies are required to directly confirm the effects of BM-MSC senescence induction on MM tumour outgrowth *in vivo*. Collectively, as the risk of MGUS to MM progression increases with age, it is plausible that the ageing-associated accumulation of senescent BM-MSCs at MGUS can contribute to the creation of a BM niche that is conducive to the outgrowth of MM PCs, leading to transition to overt MM (Figure 1.8). To this end, further studies are required to characterise BM-MSCs from MGUS patients in the context of senescence, and to establish whether these cells play an active role in the transition from MGUS to MM.

Figure 1.8. Schematic model depicting how senescent BM-MSCs may promote the progression of MGUS-to-MM. The acquisition of genetic abnormalities with ageing within plasma cells (PCs) predisposes them to disproportional clonal expansion. These clones reside or home to the bone marrow (BM), where they remain stable for long periods of time. Concurrently, senescent bone marrow mesenchymal stromal cells (BM-MSCs) accumulate with age and constitute senescence associated secretory phenotype (SASP) factor-rich activating niches, resulting in the outgrowth of transformed malignant clones and progression to active malignancy. MGUS: monoclonal gammopathy of undetermined significance; MM: multiple myeloma.

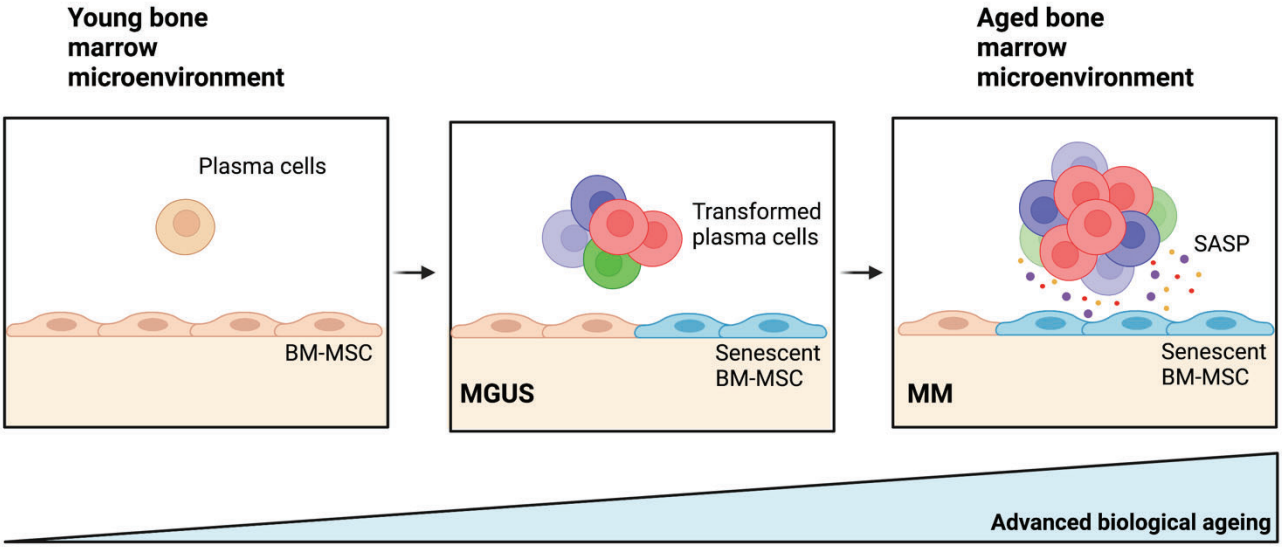
Young bone marrow microenvironment
Aged bone marrow microenvironment
Plasma cells
BM-MSC
Transformed plasma cells
Senescent BM-MSC
MGUS
SASP
Senescent BM-MSC
MM
Advanced biological ageing

1.4 Hypothesis

Age-related increases in BM-MSC senescence within the BM niche leads to the increased proliferation of clonal PCs in MGUS patients, resulting in the outgrowth of malignant clones and the progression to MM.

1.5 Aims

(1) To investigate whether BM-MSCs from MGUS and MM patients display senescent characteristics

(2) To demonstrate the functional importance of age-related BM-MSC senescence in promoting MM PC clonal outgrowth and MM development *in vitro* and *vivo*

(3) To identify factors uniquely secreted by senescent BM-MSCs that stimulate MM PC growth and proliferation, and are associated with MGUS-to-MM transition

2 MATERIALS AND METHODS

2.1 *In vivo* techniques

2.1.1 Generation of EZH2 knockout mice

Ezh2tm1Tara (Ezh2$^{fl/fl}$) mice carrying a transgene in which exons 15 and 20 encoding the SET domain of *Ezh2* are flanked by loxP sites, originally described in Su *et al.* [338] were used in this study. Ezh2tm1Tara (Ezh2$^{fl/fl}$) mice were obtained from the Mutant Mouse Resource and Research Centre (University of California) on a mixed background and were backcrossed to 7 generations to achieve a C57BL/6 genetic background as described previously [339]. The Cre-loxP system [340] was used to conditionally ablate Ezh2 in limb bud mesenchyme by crossing Ezh2$^{+/fl}$ mice with Prrx1-derived enhancer (Prrx1-Cre transgene B6). Cg-Tg(Prrx1-Cre^{+})1Cjt/J (Prrx1 Cre^{+}) mice (The Jackson Laboratory) as described in [339].

The mice were rederived and bred at the SAHMRI Bioresources Facility and were housed in specific pathogen free (SPF) conditions. Five mice or fewer were housed per individual ventilated cage (IVC), with chow and water provided *ad libitum*. The SAHMRI Animal Ethics Committee approved the breeding and use of these animals for experimental purposes under project numbers SAM401.19 and SAM448.19 respectively. Initially, 10 trios of Ezh2$^{wt/fl}$ x Prrx1-Cre^{+} were set up to generate Prrx1-Cre^{+}; Ezh2$^{+/fl}$/C57BL/6 (Ezh2$^{+/-}$) experimental mice and Prrx1-Cre^{+}; Ezh2$^{+/+}$/C57BL/6 (WT control) mice. Mice were genotyped (as described in Section 2.1.2). Prrx1-Cre null EZH2$^{+/fl}$/C57BL/6 and Prrx1-Cre null EZH2$^{+/+}$/C57BL/6 animals were culled. EZH2$^{+/-}$ and WT control mice were aged to 3, 6 and 12-month of age for experimental use (n = 23/genotype/sex at each time-point).

Mice were handled and checked daily after tumour inoculation and a clinical records sheet (CRS) was filled out daily. Animals were provided with enrichment including tunnels and wooden logs. Experienced SAHMRI Bioresources technicians replenished food and water and

performed cage changes as required. Mice were used for tumour experiments as described below. At experiment end points, humane killing of mice was performed by CO_2 followed by cervical dislocation.

2.1.2 Genotyping

Punch biopsies were obtained from the ear pinnae of each animal just prior to weaning (~2-3 weeks of age). The biopsies were stored at -20°C until use. Genomic DNA was isolated from ear biopsies by incubation with 100 µL of 10% Chelex 100 resin (BioRad) at 100°C on a heat block for 20 minutes, with the tubes gently tapped every 5-10 minutes to keep Chelex in suspension. Two hundred microlitres of nuclease free (NF) water (Invitrogen) was added and the samples were centrifuged at 13,000 *g* for 10 minutes at room temperature (RT) and kept on ice until use.

DNA was analysed for the presence of loxP floxed Ezh2 allele and/or presence of Cre-recombinase by qualitative PCR [340, 341]. Briefly, to detect the presence of the floxed insertion Ezh2 allele and the WT Ezh2 allele with no floxed insertion, PCR was performed with each 25 µL reaction containing 5 µL of DNA, 0.2 mM dNTPs, 2.5 mM $MgCl_2$, 0.2 µM forward Ezh2 primer (5'-TGTCATGTCTGGGTCTAATGCTAC-3'), 0.2 µM reverse Ezh2 primer (5'-GGAACCTCGCTATGTGTAACCA-3'), 1x PCR Buffer II and 5 U/µL of AmpliTaq Gold DNA polymerase (Thermo Fisher Scientific) in NF water. The following cycling parameters were used: 94°C for 10 minutes; 35 cycles of 94°C for 30 seconds, 62°C for 30 seconds, 72°C for 45 seconds; followed by 5 minutes at 72°C using a Veriti™ Thermal Cycler (Thermo Fisher Scientific).

To detect the presence of the Prrx1-Cre transgene, PCR was also performed using KAPA2G with each 25 µL reaction containing 1 µL of template DNA, 0.2 µM forward Prrx1 primer (5'-TCCAATTTACTGACCGTACACCAA-3'), 0.2 µM reverse Prrx1 primer (5'-CCTGATCCTGGCAATTTCGGCTA-3') and 12.5 µL of KAPA fast genotyping mix (KAPA Biosystems), containing KAPA2G™ DNA Polymerase, dNTPs and $MgCl_2$, in NF water. The following cycling parameters were used: 94°C for 5 minutes; 35 cycles of 95°C for 15 seconds, 65°C for 30 seconds, 72°C for 30 seconds; followed by 5 minutes at 72°C using Veriti™ Thermal Cycler.

No template control (NTC) reactions were performed for each target gene. The PCR products were then visualised by agarose gel electrophoresis. To detect Prrx1-Cre and Ezh2 bands, gels were cast containing 3 % (w/v) and 1.8 % (w/v) agarose, respectively, in TAE buffer (40 mM Tris base, 20 mM acetic acid and 1 mM ethylenediamine tetraacetic acid (EDTA) and 1:10,000 GelRed® (Biotium) for DNA visualisation. The PCR products (7.5 µL) were mixed with 6x Gel Loading Dye (New England BioLabs), loaded into the gel, resolved by electrophoresis at 90V for 90 minutes, and visualised using a Gel Doc™ XR+ Imager (Bio-Rad). A single band at 100 bp was indicative of Prrx1-Cre expression, with the absence of 100bp band indicative of the Prrx1 null genotype. Presence of two bands at 450bp and 410bp were indicative of the presence of the floxed insertion Ezh2 allele and the WT Ezh2 allele with no floxed insertion respectively ($Ezh2^{+/-}$). Alternatively, the presence of one band at 410bp was indicative of WT genotype.

2.1.3 Vk*Myc MM tumour model

At 3, 6 and 12-months of age, $Prrx1\text{-}Cre^{+}$; $EZH2^{+/fl}$/C57BL/6 ($Ezh2^{+/-}$) mice or $Prrx1\text{-}Cre^{+}$; $EZH2^{+/+}$/C57BL/6 (WT) mice were inoculated with Vk*Myc mouse myeloma cells in whole

BM suspensions. The Vk*Myc MM plasma cell line was developed by inducing an activating mutation in the proto-oncogene MYC gene, a well-established driver of MM disease initiation. This was achieved by coupling the activation-induced-deaminase (AID) to the MYC transgene, which induced the sporadic activation of MYC in B cells of Vk*Myc mice [342]. The Vk*Myc line Vk14451-GFP , which was originally generated by crossing Vk*Myc mice with mice expressing EGFP under the control of gamma1 promoter [343] was kindly provided by Dr Michelle McDonald (Garvan Institute), and Vk*Myc cell stocks were expanded by serial passage *in vivo* in C57BL/6 mice. Briefly, 6–8-week-old C57BL/6 mice were intravenously injected with 100 µL of cell suspension containing $2.5x10^6$ GFP^+ tumour cells/mL. MM tumour was allowed to develop until ethical endpoints were reached. Cell stocks were generated from animals with high tumour burden as determined by serum paraprotein electrophoresis (SPEP) as described in 2.1.5. Whole BM from both tibiae and femurs was extracted as in 2.1.4.1, with the percentage of GFP^+ cells in BM sample determined prior to storage in liquid nitrogen (LN_2) at -80C. Passage 2 Vk*Myc stocks were used in experiments using 3 and 6-month-old animals, whereas passage 3 stocks were used in studies using 12-month-old animals. Vk*Myc cell stocks were thawed into RPMI-1640 containing 10% FCS, centrifuged at 1,400 *g* and subsequently resuspended in PBS to achieve a final concentration of $2.5x10^5$ GFP^+ tumour cells/mL calculated based on the percentage of GFP^+ cells by flow cytometry. Mice were injected intravenously with 100 µL of cell suspension equating to 50,000 MM PCs/mouse.

2.1.4 Detection of GFP^+ tumour cells in mouse tissues by flow cytometry

GFP^+ tumour cells in BM and splenic cell suspensions were quantitated by flow cytometry using either the FACSCanto™ II (BD Biosciences) or LSRFortessa™ (BD Biosciences). In all experiments, cells from a tumour-naïve mouse (that had not injected with tumour cells) were

also analysed to act as a negative control for gating cell populations. Subsequent analysis was performed using FlowJo v10.0.8 software.

2.1.4.1 Isolation of mouse BM cells

Single cell suspensions of BM and spleen from tumour cell-injected mice were analysed for GFP expression by flow cytometry. One tibia and 1 femur per mouse were dissected free from connective tissue and muscle and the proximal and distal ends of the bones were removed using a scalpel blade. BM was collected by repeatedly flushing the bones with 10 mL of chilled PFE buffer (5% FCS and 2 mM EDTA in PBS) using a 10 mL syringe and 26 G needle until the bones were white. The BM cell suspension was then washed in 10 mL of PFE and centrifuged at 1,400 *g* for 10 minutes at 4°C. The BM cell-containing solution was then re-suspended in 500 µL of ice-cold PFE buffer and passed through a 12 x 75 mm style 35 µm cell-strainer cap (Falcon®) into a 5 mL polystyrene round-bottom tubes (Falcon®) and kept on ice until analysis.

2.1.4.2 Isolation of mouse splenic cells

Spleens were excised and cleaned of any connective tissue and a cell suspension was generated by using the plunger of a 10 mL syringe to pass the tissue through a pre-wet 70 µm cell strainer into a 50 mL Falcon® tube. The filter was then washed with 10 mL of chilled PFE buffer. Cells were centrifuged at 1,400 g for 10 minutes and resuspended in 1 mL PBS. Seven and a half millilitres of red blood cell lysis (RBC) buffer (8.26 g/L NH_4Cl, 1 g/L $KHCO_3$, 37 g/L EDTA in H_2O) was added to the spleen suspension, gently mixed by inversion and incubated at RT for 10 minutes. The cell suspension was centrifuged at 5,000 *g* for 5 minutes at RT. The supernatant was aspirated and the pellet was washed with 5 mL ice cold PBS and centrifuged at 1,400 *g* for 10 minutes at 4°C.

The cells were resuspended in 500 µL ice-cold PFE and put through a 12 x 75 mm style 35 µm cell-strainer cap into a 5 mL polystyrene round-bottom tubes for analysis of GFP^+ tumour cells by flow cytometry (as described in section 2.1.4) or were counted and $5x10^6$ cells lysed in 1 mL TRIzol (as described in section 2.7.1.1).

2.1.5 Serum protein electrophoresis

From week 4 post tumour inoculation until the experimental end point, approximately 50 µL peripheral blood was collected from Vk*Myc-injected mice by a tail bleed weekly. The blood was allowed to clot at room temperature and then centrifuged at 2,000 *g* and 4°C for 10 minutes. The serum supernatant was collected and stored at -20°C. Subsequently, the 10 µL serum samples were thawed and the levels of M protein/paraprotein were assessed by performing serum protein electrophoresis (SPEP) using the Hydragel Protein(E) Kit (Sebia), according to the manufacturer's instructions. The amidoblack-stained SPEP gels were imaged on a Gel Doc™ XR+ Imager (Bio-Rad), and the intensity of the paraprotein band/M-spike was quantitated using Image Lab Software v6.0.1 (Bio-Rad).

2.2 *Ex vivo* histological analysis of β-galactosidase activity

2.2.1 OCT embedding

Whole femurs were isolated from 6 and 12-month-old Prrx1-Cre^+; $EZH2^{+/fl}$/C57BL/6 ($EZH2^{+/-}$) or Prrx1-Cre^+; $EZH2^{+/+}$/C57BL/6 (WT) tumour naïve mice and were dissected free from connective tissue and muscle. To facilitate the infiltration of fixative, the proximal and distal epiphyses were removed using a scalpel blade, without disrupting the growth plate. On the day of use, glutaraldehyde fixative solution was prepared by adding 0.6 mL 25% glutaraldehyde (Calbiochem), 0.5 mL 2% NP40 (Sigma), 0.5 mL of 0.5 M EDTA (Chem-supply), 0.1 mL of 1 M $MgCl_2$ (Sigma) and 7.5 mL of 100% sucrose (Sigma) solution made up to 50 mL with

PBS, for a final concentration of 0.3% (v/v) glutaraldehyde, 0.02% (v/v) NP40, 5 mM EDTA, 2 mM $MgCl_2$, 15% (w/v) sucrose in PBS. Bones were fixed for 5 days at 4°C on a rocker in 5 mL of glutaraldehyde fixative solution in 5 mL yellow cap tubes (Starstedt).

Following fixation, the bones were decalcified for ~7 days by incubation with 5 mL of decalcification solution (0.5 M EDTA in PBS at pH 8.0) at 4°C and the solution was refreshed thrice weekly. Decalcification was confirmed by X-ray using the Faxitron LX-60 Cabinet X-Ray System.

Spleens were isolated from 12-month-old Prrx1-Cre^{+}; $EZH2^{+/fl}$/C57BL/6 ($EZH2^{+/-}$) or Prrx1-Cre^{+}; $EZH2^{+/+}$ C57BL/6 (WT) tumour naïve mice and sectioned in half longitudinally, with one half fixed in 5 mL of glutaraldehyde fixative solution for 24 hours in 5 mL tubes at 4°C on a rocker, with the second half used for generation of single cell suspension as described in 2.1.4.2 for subsequent RNA extraction with TRIzol™ and gene expression analysis as described in 2.7.1.1.

Prior to embedding, glutaraldehyde-fixed splenic and decalcified bone tissues were incubated in sucrose as a cryoprotectant. Briefly, 15% (w/v) and 30% (w/v) sucrose solutions were freshly prepared by adding 15 g or 30 g of sucrose, respectively, made up to a final volume of 100 mL of PBS solution and vigorously mixed until the sucrose dissolved. Tissues were washed twice in PBS for 15 minutes prior to incubating in 15% sucrose solution overnight (O/N) at 4°C on a rocker. The following day, the tissues were changed to 30% sucrose and incubated O/N at 4°C on a rocker.

Subsequently, tissues were longitudinally embedded and frozen in optimal cutting temperature (OCT) compound (Tissue-Tek) using 10 x 10 x 5mm cryomolds (Tissue-Tek) using dry ice,

wrapped in aluminium foil to keep away from light and stored at -80°C. Blocks were cryo-cut into 10 μm thick sections and transferred onto slides at the University of Adelaide Histology Facility (Adelaide, Australia). Unstained slides were stored at -20°C.

2.2.2 β-galactosidase staining

Wash buffer was prepared by adding 2 mL of 2% NP40, 0.4 mL of 1M $MgCl_2$ and 2 mL of 1% sodium deoxycholate (Sigma) to 195.6 mL of PBS for a final concentration of 0.02% (v/v) NP40, 0.02M $MgCl_2$ and 0.01% (w/v) sodium deoxycholate in PBS and was kept at 4°C for up to 1 month. To prepare the X-gal solution, 50 mg of 5-bromo-4-chloro-3-indolyl-β-D-galactopyranoside (Sigma) was dissolved in 1 mL of N-N-dimethylformamide (Sigma) and X-gal solution was kept at -20°C wrapped in aluminium foil for up to 1 month. On the day of use, β-gal staining solution was prepared by combining 1 mL of 50 mg/mL X-gal solution with 106 mg potassium ferrocyanide (Univar), 82 mg potassium ferricyanide (Sigma), 1 mL of pH 7.4 1 M Tris (Sigma) and topped up with wash buffer to 50 mL, for a final concentration of 1 mg/mL X-gal, 2.1 mg/mL potassium ferrocyanide, 2.0 mg/mL potassium ferricyanide and 0.02 M Tris.

In order to stain tissue sections for β-gal activity, slides were air dried for 30 minutes in a 37°C ambient air incubator (Ratek). Air-dried slides were washed twice in wash buffer and were then incubated with 50 mL β-gal staining solution O/N in a Coplin jar sealed with Parafilm™ (Bemisa) in a 37°C ambient air incubator in the dark (container wrapped in tinfoil). Slides were washed twice with PBS for 15 minutes and counterstained with Nuclear Fast Red (Merk). Tissue sections were traced with a liquid blocker super pap pen (Daido Sangyo, Co Ltd) and 400 μL of Nuclear Fast Red solution was added per slide for 5 minutes. Slides were washed in reverse osmosis (RO) water for 5 minutes. Tissues were dehydrated by sequential immersion in

increasing concentrations (50%, 75%, 90%, 100%) of ethanol for 2 minutes each and mounted with CV mount (Leica) mounting medium. Slides were imaged using a BX53 Olympus microscope at 10X magnification. The number of β-gal$^+$ blue cells was quantified in 6 fields of view/section . The Osteomeasure (Osteometrics) software (version 3.3.0.2) was used to quantify β-gal$^+$ cells. The number of β-gal$^+$ cells were quantified in 6 separate 500 μm x 500 μm fields of view (FOV) per bone tissue section; 3 FOVs starting 400 μm away from the growth plate adjacent to the cortical bone at the top of the tissue section, with subsequent fields of view descending downwards toward the opposite cortical bone end of the section. Subsequently, 3 additional FOVs were quantified 400 μm away from the first 3 fields of view towards the proximal metaphysis. For splenic analysis, 6 separate 500 μm x 500 μm FOVs were analysed/section (excluding the edge of tissue); 3 FOVs starting 500 μm away from the edge of the tissue section and descending downwards towards the opposite end of the tissue section. Subsequently, 3 additional FOVs were quantified 400 μm away from the first 3 fields of view.

2.3 Cell culture techniques

2.3.1 Maintenance of cells in culture

All cell lines and primary cells were maintained in a humidified incubator maintained at 37°C in the presence of 5% CO_2. All cells were manipulated within a class II biological safety cabinet. Unless otherwise specified, all cell culture reagents were sourced from Sigma-Aldrich and all media were supplemented with 2 mM L-glutamine, 100 U/mL penicillin, 100 μg/mL streptomycin, 1 mM sodium pyruvate and 10 mM HEPES buffer. L-glutamine was replenished in the media every 4 weeks. Media was warmed to 37°C in a water bath prior to use. Tissue culture flasks were sourced from Sigma. Prior to use, all cell lines were tested for mycoplasma infection using a MycoAlert^{TM} Mycoplasma Detection Kit (Lonza) following the manufacturer's instructions. Briefly, 90 μL of MycoAlert^{TM} reagent was added to 90 μL of

sample (conditioned media collected from cells cultured for 2-3 days) in a bioluminescent compatible microplate (Costar) and incubated for 5 minutes at RT. The Wallac 1420 (Wallac luminometer) was used to calculate the initial reading (Reading A). Subsequently, 90 µL of MycoAlert^{TM} substrate was added per sample and incubated for 10 minutes at RT. The Wallac 1420 luminometer was used to record second reading (Reading B). A ratio of Reading B/ Reading A was used to determine mycoplasma contamination. A ratio >1.2 indicated mycoplasma contamination. A ratio 1.0-1.2 indicated possible mycoplasma contamination (cultures were quarantined and retested in a few days). A ratio <1.0 indicated the sample is mycoplasma negative. Only mycoplasma negative samples were used for subsequent experiments. All cell lines were maintained in culture for a maximum of 4 weeks.

2.3.2 Murine MM 5TGM1-luc cell line

The murine MM 5TGM1 PC line was originally kindly provided by Assoc. Prof Claire Edwards (University of Oxford). 5TGM1-luc cells expressing both green fluorescent protein (GFP) and luciferase were previously generated using the retroviral expression vector SFG-NES-TGL [344, 345]. As described previously [346, 347], to generate a basal 5TGM1-luc cell line with enhanced BM tropism, 5TGM1-luc cells were previously injected intravenously into C57BL/KaLwRij (KaLwRij) mice and those which had homed to and proliferated in the long bones of the hind limbs were purified using fluorescence activated cell sorting (FACS) and expanded for use for subsequent *in vivo* and *in vitro* experiments. 5TGM1-luc cells were maintained in Iscove's modified Dulbecco's medium (IMDM) with 20% foetal calf serum (FCS, Thermo Fisher Scientific), which hereafter termed complete IMDM. The cells were sub-cultured every 2-3 days to maintain a concentration of 0.2-2 x 10^6 cells/mL.

2.3.3 Human MM KMM1-luc cell line

The human myeloma cell line KMM1 was kindly gifted by Prof. Andrew Spencer (Monash University). KMM1 cells were maintained in Roswell Park Memorial Institute 1640 (RPMI-1640) medium with 10% FCS (hereafter referred to as complete RPMI-1640 medium) and sub-cultured every 2-3 days to maintain a concentration of 0.2-1 x 10^6 cells/mL.

2.3.3.1 Generating luciferase-expressing KMM1-luc cells

For each transfection, 2 x 10^6 HEK293T cells , sourced from the American Type Culture Collection (ATCC), were seeded in 6 cm culture dishes in 3 mL of Dulbecco's modified Eagle's medium (Sigma) with 10% FCS (complete DMEM) 24 hours prior to transfection and incubated O/N at 37°C with 5% CO_2. The media was aspirated and 2 mL of fresh complete DMEM was added. HEK293T cells were then transfected with 5 μg of the gene-encoding sfg-NES-TGL plasmid and 5 μg of the amphitropic packaging plasmid pEQPAM3 [348] using Lipofectamine 2000 (Invitrogen), according to the manufacturer's instructions. After 48 hours, medium containing retrovirus was collected from the transfected HEK293T cells filtered through a 0.45 μm surfactant-free cellulose acetate membrane filter and added dropwise onto KMM1 cells (4×10^5 cells/infection) in complete RPMI-1640 medium containing polybrene (final concentration of 4 μg/mL) in a 6-well plate. Two millilitres of complete DMEM was replaced on the HEK293T cells. KMM1 cells were incubated O/N at 37°C with 5% CO_2. The infection was repeated the following day and KMM1 cells were incubated with viral supernatant at 37°C with 5% CO_2 O/N. The cells were washed with complete RPMI-1640 and expanded in culture. Following another wash, the KMM1 cells underwent FACS for GFP expression, which indicated successful transduction of the SFG-NES-TGL plasmid, on a FACSAria™ Fusion (BD Biosciences). Subsequent sorts were conducted, where appropriate, until a pooled cell line consisting of > 90% GFP^+ KMM1 cells was obtained. Cell stocks were frozen down in LN_2.

2.3.4 IL-6 supplementation studies

Murine 5TGM1-luc and human KMM1-luc MM cell lines were cultured in the presence of increasing concentrations (0-100 ng/mL) of recombinant mouse IL-6 protein (cat #I9646-5UG, Sigma Aldrich) supplemented into the media and incubated at 37°C with 5% CO_2. 200 ng/mL aliquots of recombinant IL-6 were stored at -20°C and used as required. After 72 hours, MM PC cell numbers were quantified by luciferase activity as described in section 2.3.5.

2.3.5 Quantification of MM cells numbers using bioluminescent imaging

The relative number of myeloma cells per well was quantitated using bioluminescent imaging as described previously [349]. Briefly, 30 mg/mL of D-luciferin (L-8220, BioSYNTH) was diluted to 0.3 mg/mL in appropriate warmed complete RPMI-1640 (human) or complete IMDM (mouse) and 100 µL was added per well. Background controls were established in triplicate by adding 100 µL of luciferin to media-only control wells. Upon addition of luciferin, the plate was incubated in the dark at 37°C with 5% CO_2 for 10 minutes and was then kept at room temperature for 20 minutes prior to measurement of the bioluminescent signal using the Xenogen IVIS Spectrum Bioluminescence Imaging System (Perkin Elmer). Bioluminescent signal from each well, measured in photons/second, was used as a measure of MM cell number per well and was quantitated using Living Image software version 4.4. Bioluminescence of control wells was subtracted from bioluminescence values of each sample well. These values were then normalised to bioluminescent signal of monoculture wells to keep consistency between experiments.

2.3.6 Maintenance of adherent cells

Briefly, adherent stromal cells were washed using in Hank's buffered salt solution (HBSS; Sigma) and incubated with either 1 mL (25cm^2 flask)/3mL (75 cm^2 flask) or 4 mL (150 cm^2

flask) of pre-warmed (37°C) 1 mg/mL collagenase (cat#4196, Worthington) and 1 mg/mL dispase (cat#165859, Roche) in HBSS for ~30 minutes (murine cells) or 1 hour (human stromal cells only). Loose cells were collected and added to a 50 mL Falcon tube and neutralised with 3, 5 or 7 mL of HBSS supplemented with 5% FCS, (depending on amount of collagenase/dispase to be neutralised). Remaining cells in the flask were incubated with either 1 mL (25cm^2 flask)/ 3 mL (75 cm^2 flask) or 4 mL (150 cm^2 flask) 0.05% (v/v) trypsin-EDTA (Sigma) in HBSS for ~1-5 minutes. Flasks were vigorously tapped and loose cells were collected in an appropriate volume of HBSS supplemented with 5% FCS, added to the polypropylene tube and centrifuged at 1,400 *g* for 5 minutes at 4°C. Cells were re-suspended in 1 mL of α-modified minimum essential medium (α-MEM) (Sigma) with 20% FCS supplemented with 100 μM L-ascorbate-2-phosphate (Sigma) (complete 20% FCS α-MEM), counted and seeded at a density of 5-8x10^3 cells/cm^2.

Stromal cell cultures were retrieved from storage in LN_2 and cultured in complete 20% FCS α-MEM culture medium. Primary patient cell cultures were counted and seeded at a density of 5-8x10^3 cells/cm^2. Media was changed the following day if there was a large amount of non-adherent debris in the flask post-thaw. Cells were split twice a week (approximately every 3-4 days). Following each split, the passage number of adherent cells increased by 1.

2.3.6.1 Mouse stromal OP9 cell line

The mouse BM-MSC line OP9 was originally obtained from the ATCC. *Grem1* over expressing and empty vector (EV) OP9 cell lines were previously generated using LegoiT2 lentiviral vector (Plasmid #27343, Addgene) harbouring the murine cDNA for the coding region of Grem1, or vector alone, as described in [11]. OP9-Grem1/EV cell lines were

maintained in complete DMEM. Medium was renewed every 2-3 days and cells were split when the cells reached 70-80% confluence at a sub-cultivation ratio of 1:5.

2.3.6.2 Primary murine-derived BM stromal cells

Primary BM-MSCs were isolated by plastic adherence from bone chips of healthy, non-tumour bearing mice and cryopreserved. Briefly, long bones (tibiae and femurs) were isolated from 8-week-old C57BL6/KaLwRijHsd mice or 6-12-month-old Prrx1-Cre^{+}; EZH2$^{+/fl}$/C57BL/6 (EZH2$^{+/-}$) mice or Prrx1-Cre^{+}; EZH2$^{+/+}$/C57BL/6 (WT) animals. Long bones were dissected and cleaned free from muscle and connective tissue using a scalpel blade. Bones were finely cut into small fragments with a scalpel to generate bone chips. Bone chips obtained from 2 x tibiae and 2 x femurs were pooled and transferred into a 75cm^2 flask and maintained in 10 mL of complete 20% FCS α-MEM. Primary cultures were maintained for 7-10 days until they were passaged as described in section 2.3.6. BM-MSC cultures were passaged at least twice before use in *in vitro* assays.

2.3.6.3 Primary human BM stromal cells

BM-MSC cultures were isolated by plastic adherence from trabecular bone fragments as previously described [350] and expanded prior to cryopreservation. Posterior iliac crest trephines were collected from previously untreated patients with asymptomatic MGUS (*n* = 29 [19 M; 10 F]; age-range = 42-84 years; median age = 67.5 years) or newly diagnosed symptomatic MM (*n* = 11 [7 M; 4 F]; age-range = 52-84 years; median age = 70 years) seen between 4/1/2000 and 10/10/2014, who consented, through the South Australian Cancer Research Biobank (SACRB), to donate additional samples collected during their routine diagnostic bone marrow biopsy. Sample use for this project was approved by the CALHN (HREC/18/CALHN/684; no. R20181011). Samples were collected from MM patients prior to

the initiation of treatment. All patients provided informed consent in accordance with the Declaration of Helsinki. Clinical follow up was provided by the Myeloma and Related Paraproteinaemia's (MRP) Database (CALHN HREC ref # 16351).

Upon receipt of trephine biopsy, the trephine was removed from the sterile pot and placed in a sterile petri dish. Using 2 scalpel blades, the trephine was chopped into small pieces and placed in a 25 cm^2 flask in 8 mL of α-MEM with 10% FCS and 100 μM L-ascorbate-2-phosphate (complete 10% FCS α-MEM). The tissue culture flask was incubated at 37°C with 5% CO_2 for ~10-14 days until adherent BM-MSCs appeared. Trephine chips were removed from the flask by 2 x washes with 8 mL HBSS supplemented with 5% FCS and 8 mL of complete α-MEM 10% FCS was replenished. When BM-MSCs reached 70-80% confluency, cells were harvested as described in section 2.3.6, above. The cells were seeded in 12 mL of complete 10% FCS α-MEM in a 75cm^2 flask, which was termed passage 1. Cells were passaged to passage 2 and at 70-80% confluency, frozen down and stored in LN_2 for further use.

BM-MSC cultures from healthy young (age ≤ 26 years) non-tumour volunteers (*n* = 14; [8 M; 5 F; 1 unknown]; age-range = 17-26 years; median age = 21 years) were obtained from posterior iliac crest BM aspirates. Aspirates were taken after obtaining informed consent according to the procedures approved by the human ethics committee of the RAH, SA (Protocol # 940911a). Briefly, bone marrow aspirates were diluted 1:3 in complete α-MEM 20% FCS and passed through a 70 μm strainer to retain bone chips. The strainer was rinsed twice with complete α-MEM 20% FCS medium to collect the bone chips. The bone chips were cultured in 5 mL complete 20% FCS α-MEM in 25 cm^2 flask for 7-14 days undisturbed prior to expansion and passage as described above. Once expanded to passage 1, samples were cultured in complete α-MEM containing 10% FCS.

BM-MSC cultures from aged (age ≥ 60 years) non-tumour controls from aged volunteers were kindly provided by Prof Gerald Atkins (University of Adelaide). Briefly, plastic-adherent BM-MSCs were isolated from intertrochanteric trabecular bone samples from patients undergoing hip arthroplasty for neck of femur fractures (*n* = 11 [4 M; 6 F; 1 unknown]; age-range= 69-94 years; median age = 88 years) [351], as approved by CALHN HREC protocol HREC/13/RAH/33 No: 130114) and were cultured to passage 2-4.

2.4 Senescence induction techniques

2.4.1 Hydrogen peroxide (H_2O_2) treatment

Passage 3 BM-MSCs from young non-tumour volunteers and murine KaLwRij BM-MSCs were seeded at $6x10^3$ cells/cm^2 in 6 well plates and cultured for 2 days to achieve 60-70% confluence. Subsequently, BM-MSCs were treated with 0-800 μM H_2O_2 (Merck) in complete α-MEM 20% FCS medium for 2 hours. Treatment media were aspirated and wells washed twice with PBS. Cells were then cultured in complete α-MEM 20% FCS medium for 96 hours. Subsequently, cells were stained for β-gal activity as described in section 2.5.1 and RNA was extracted by lysing cells in TRIzol™ as described in section 2.7.1.1 for gene expression analysis of senescence markers.

2.4.2 Doxorubicin treatment

Passage 3 BM-MSCs from young non-tumour volunteers or murine KaLwRij BM-MSCs were seeded at $6x10^3$ cells/cm^2 in 6 well plates and cultured for 2 days to achieve 60-70% confluency. Subsequently, the complete α-MEM 20% FCS culture medium was supplemented with 0-200 nM doxorubicin (Hospira Australia) for 1 hour per day for 3 consecutive days. Briefly, after the 1 hour treatment, doxorubicin containing media was aspirated and cells were washed twice with 1 x PBS and replenished with complete α-MEM 20% FCS. Subsequently, cells were stained for β-gal

activity as described in section 2.5.1 and RNA was extracted by lysing cells in TRIzol™ as described in section 2.7.1.1 for gene expression analysis of senescence markers.

2.4.3 Irradiation of murine BM-MSCs

KaLwRij BM-MSCs were cultured to passage 2-3, as described in section 2.3.6., harvested with 0.05% (v/v) trypsin-EDTA in HBSS and re-suspended at $1x10^5$ cells/mL in complete α-MEM 10% FCS medium in 50 mL tubes (Falcon®). Re-suspended cells were irradiated at 30 Gy and 60 Gy using the RS2000 Biological Irradiator (Rad Source) which was used to induce DNA damage and subsequent senescence induction in BM-MSCs. The RS2000 irradiation system was operated at 160 keV with a tube current of 25 mA. An irradiation dose of 4.5 Gy/minute was used; cells irradiated for 6.6 minutes to achieve 30 Gy or 13.3 minutes to achieve 60 Gy. Irradiated cells were re-seeded at $1x10^4$ cells/cm^2 in a T75 flask and left in culture. In senescence induction by irradiation experiments (sections 2.4.3 and 2.4.4), mouse BM-MSCs were seeded at $6x10^3$ cells/cm^2 in 6-well plates, with β-gal (section 2.5.1) staining carried out 4,5,6,7 and 10 days after irradiation parallel to MM PC co-culture studies (section 2.6). Media were refreshed at day 3 post irradiation. At 24-hours and 4,5,6,7 and 10 days post-irradiation, cells were detached from the flask as discussed in section 2.3.6, with cells from 3 wells of the 6-well plate washed twice in PBS and lysed in 1 mL TRIzol™ as described in section 2.7.1.1 for gene expression analysis of senescence markers.

After the initial optimisation experiments, mouse BM-MSCs were irradiated at 60 Gy, and seeded at $2.5x10^4$ cells/cm^2 in 6-well plates for analysis of β-gal activity or gene expression. β-gal staining was conducted at 4-days post irradiation (as described in 2.5.1) and RNA was collected 24-hours post irradiation (as described in 2.4.3 and 2.4.4). Twenty-four hours post irradiation, irradiated

mouse BM-MSCs were seeded at $2.5x10^4$ cells/cm^2 in 96-well black-walled flat bottom plates (Corning Life Science) for co-culture with MM PCs, as described in section 2.6.1.

2.4.4 Irradiation of human BM-MSCs

Passage 2-3 human BM-MSCs were cultured as described in section 2.3.6 and re-suspended in an appropriate volume of complete α-MEM 10% FCS medium to achieve the concentration of $1x10^5$ cells/mL prior to irradiation. Re-suspended cells were irradiated at 30 Gy and 60 Gy, as described above. Irradiated cells were re-seeded at $1x10^4$ cells/cm^2 in a T75 flask. In senescence induction by irradiation experiments (sections 2.4.3 and 2.4.4), human BM-MSCs were seeded at $6x10^3$ cells/cm^2 in 6-well plates, with β-gal (section 2.5.1) staining carried out 4,5,6,7 and 10 days after irradiation parallel to MM PC co-culture studies (section 2.6.2). Media were refreshed at day 3 post irradiation. At 24-hours and 4,5,6,7 and 10 days post-irradiation, cells were detached from the flask as discussed in section 2.3.6, with cells from 3 wells of the 6-well plate washed twice in PBS and lysed in 1 mL TRIzol™ as described in section 2.7.1.1 for gene expression analysis of senescence markers.

After the initial optimisation experiments, human BM-MSCs were irradiated at 60 Gy, and seeded at $2.5x10^4$ cells/cm^2 in 6-well plates for analysis of β-gal activity or gene expression. β-gal staining was conducted at 10-days post irradiation (as described in 2.5.1) and RNA was collected 7 days post irradiation (as described in 2.7.1.1). Seven days post irradiation, irradiated mouse BM-MSCs were seeded at $2.5x10^4$ cells/cm^2 in 96-well black-walled flat bottom plates for co-culture with MM PCs, as described in section 2.6.2.

2.4.5 Culture of patient BM-MSCs for replicative senescence assessment

Passage 4 (end of week 2 in culture) human BM-MSCs obtained from young and aged non-tumour controls and MGUS and MM patients were seeded at 6 x 10^3cells/cm^2 in a 25cm^2 flask in triplicate in complete 20% α-MEM medium and were cultured for 3 days. On day 3, cells were harvested and 3 independent cell counts were conducted. Cells were subcultured every 3 days and passage number was calculated as described in section 2.3.6. Population doublings were calculated using the following formula: PD= $\frac{log\ (cells\ harvested/cells\ seeded)}{log2}$. Population doubling of ≤0 indicated senescence. For assessment of senescence in human BM-MSC cultures, passage 5 (start of week 3 in culture) BM-MSCs were seeded at 1x10^4 cells/cm^2 in a 6-well plate in and allowed to adhere O/N. Cells were then stained for β-gal activity (as described in section 2.5.1) or cells were detached from the flask as discussed in section 2.3.6 and counted, with 1 x 10^6 cells washed twice in PBS and were lysed in 1 mL TRIzol, as described in section 2.7.1.1.

2.5 *In vitro* characterisation of BM-MSC senescence

2.5.1 Senescence-associated β-galactosidase (β-gal) staining

Staining for β-gal activity was carried out using the Senescence β-galactosidase Staining Kit #9860 (Cell Signalling Technology) according to the manufacturer's protocol. All reagents were kept at -20°C and were subjected to multiple freeze/thaw cycles. The cells were washed twice with 2 mL PBS per well. The 10X Fixative Solution provided in the kit was thawed at RT for ~15 minutes and diluted 1:10 using RT PBS and 1 mL of 1X Fixative Solution was added per well of a 6-well plate and was incubated at RT in the dark for 15 minutes. The Fixative Solution was aspirated and the wells were washed with 2 mL PBS per well twice prior to the addition of staining solution.

The 10X Staining Solution provided in the kit was thawed and warmed to 37°C in the waterbath for 15 minutes and vigorously shaken for 15 seconds prior to 1:10 dilution in RT PBS. Solutions A and B 100X stocks provided in the kit were thawed at RT for ~15 minutes and briefly vortexed prior to use. Twenty milligrams of 5-bromo-4-chloro-3-indolyl β-D-galactopyranoside (X-gal) provided in the kit was weighed out in a 1.5 mL tube (Eppendorf) and diluted in 1 mL of N-N-Dimethylformamide (Sigma) for a final concentration of 20 mg/mL. The tube was gently inverted several times to ensure the powder went into solution, wrapped in aluminium foil and kept in the dark. The diluted X-gal solution was kept at -20°C and discarded after one month.

For each well of the 6-well plate, 930 µL of diluted 1X Staining Solution was added to 10 µL 100X Solution A, 10 µL of 100X Solution B and 50 µL X-gal solution in a 50 mL tube (Falcon®), wrapped in aluminium foil and protected from light. The final β-gal staining solution was adjusted to pH 6.0 (± 0.1) with either 2.5M NaOH or 1M HCl. One millilitre of prepared β-gal staining solution was added/well. The plate was sealed with Parafilm™ to prevent evaporation and wrapped in aluminium foil to protect from light. The plate was incubated O/N at 37°C in the ambient air incubator (presence of CO_2 can alter pH). The following day, the β-gal solution was aspirated and wells washed with 2 mL RT PBS. One microliter of 5 mg/mL stock of 4′,6-diamidino-2-phenylindole (DAPI) (Life Tech) DNA nuclear stain was diluted in 5 mL MilliQ to achieve a concentration of 1 µg/mL. One milliliter of 0.001 mg/mL diluted DAPI solution was added/well and incubated in the dark at RT for 10 minutes. The DAPI solution was aspirated and 1 mL of PBS was added/well prior to imaging using an IX53 Olympus fluorescence inverted microscope at 20X magnification with images were taken with Olympus XC50 camera. The number of β-gal positive cells was counted in 3 separate fields of view per well in triplicate wells.

The percentage of β-gal positive cells was calculated as a proportion of total cells in field of view identified by co-staining with DAPI nuclear stain.

2.6 *In vitro* co-culture assays

2.6.1 Murine co-culture system

OP9 or primary murine BM-MSCs were seeded at $2.5x10^4$ cells/cm^2 in triplicate in a 96 well black walled flat bottom plate in 100 µL of media and allowed to adhere O/N. OP9 cultures were seeded in complete DMEM while primary murine cells were maintained in complete α-MEM with 20% FCS. The medium was aspirated and $1x10^4$ cells/well of 5TGM1-luc MM PC (100 µL of $1x10^5$ cells/mL) suspended in complete IMDM was added to the stromal cell cultures. After 72 hours of co-culture or monoculture controls at 37°C with 5% CO_2, the 5TGM1-luc cells were enumerated by measuring luciferase activity as described in section 2.3.5.

2.6.2 Human co-culture system

Primary human BM-MSCs were seeded at $2.5x10^4$ cells/cm^2 in triplicate in a 96 well black walled flat bottom plate in complete α-MEM 20% FCS and allowed to adhere O/N. The medium was aspirated and $1x10^4$ cells/well of KMM1-luc MM PC in 100 µL of complete RPMI was added to the stromal cell cultures. After 72 hours of co-culture and MM cell monoculture (controls) at 37°C with 5% CO_2, the KMM1-luc cells were enumerated by measuring bioluminescent signal as a measure of luciferase activity as described in section 2.3.5.

2.6.3 IL-6 blocking studies

Murine and human MM PCs were co-cultured (as in 2.6.1 and 2.6.2) with irradiation-induced senescent (as described in sections 2.4.3 and 2.4.4) KaLwRij and human BM-MSCs respectively in the presence of 0.05 μg/mL neutralising anti-IL-6 antibody (cat #AF-406-NA, R&D systems) or mouse IgG control (lot # 154781, Jackson Immunoresearch) antibody supplemented in the culture medium on the day the MM cells were seeded (Day 0). MM PC proliferation was assessed after 72 hours by luciferase activity as described in section 2.3.5 and results were normalised to mouse IgG control for replicate experiments.

2.6.4 Grem1 blocking studies

Murine and human MM PCs were co-cultured (as in 2.6.1 and 2.6.2) with irradiation-induced senescent (as described in sections 2.4.3 and 2.4.4) KaLwRij and human BM-MSCs respectively. Prior to seeding MM PCs onto BM-MSCs, BM-MSCs were pre-treated with 1 μg/mL of neutralising anti-Grem antibody Ab7326 (UCB-Pharma) or IgG control Ab101.4 (UCB-Pharma) supplemented into complete α-MEM 20% FCS medium and the plate was incubated at 37°C with 5% CO_2 for 45 minutes. BM-MSCs were washed with 200 μL of PBS, which was aspirated prior to seeding of MM PCs. Cells were co-cultured for 72 hours at 37°C with 5% CO_2 in 100 μL complete IMDM (mouse) or complete RPMI (human). MM PC proliferation was assessed after 72 hours by luciferase activity as described in section 2.3.5. Results were normalised to mouse IgG control for replicate experiments.

2.7 Molecular biology

2.7.1 RNA techniques

2.7.1.1 Total RNA isolation

RNA was isolated from cultured primary mouse and human BM-MSCs (as described in sections 2.3.6.2 and 2.3.6.3), senescence-induced BM-MSCs as described in section 2.4 or cell

suspensions isolated from whole splenic tissues (described in section 2.1.4.2). To extract RNA, 1 mL of TRIzol™ Reagent (Invitrogen) was added to 1-6 x 10^6 cells to facilitate cell lysis and was stored at -80°C until use. TRIzol™ lysed samples were thawed at RT prior to use. Upon the addition of 0.2 mL of chloroform, the TRIzol™ and chloroform were mixed by vigorous shaking and incubated for 2-3 minutes at room temperature. Samples were centrifuged at 4°C for 15 minutes at 12,000 *g* to separate phases and the RNA-containing aqueous phase was collected. Total RNA was precipitated by the addition of 0.5 mL isopropanol and 2 µL (20 µg) ribonuclease-free glycogen (Roche) and incubated on ice for 1 hour. The RNA was pelleted by centrifugation at 12,000 *g* and 4°C for 10 minutes and then washed with 75% (v/v) ethanol. The RNA was resuspended in 20 µL TE buffer (Invitrogen) and incubated at 55°C for 10 minutes to facilitate solubilisation. The concentration of RNA in solution was determined by measuring the absorption at 260 nm on a NanoDrop™ 8000 Spectrophotometer (Thermo Fisher Scientific). RNA was stored at -80°C until use.

2.7.1.2 RNA-sequencing

Total RNA was extracted from paired non-irradiated and irradiated (section 2.4.3) KaLwRij BM-MSCs samples from 3 independent donors using TRIzol™ Reagent, as described in section 2.7.1.1). RNA quantity was determined using the Qubit™ RNA Broad Range Assay Kit and the Qubit™ 2 Fluorometer (Thermo Fisher Scientific), according to the manufacturer's instructions. RNA quality was determined using the RNA 6000 Nano kit (Agilent) on a Bioanalyzer 2200 (Agilent); all samples were confirmed to have an RNA integrity number > 8. Library construction and RNA-sequencing were performed by the South Australian Genomics Centre (SAGC) (South Australian Health and Medical Research Institute [SAHMRI], Adelaide). Briefly, RNA-seq libraries were prepared using the NEXTflex™ Rapid Directional mRNA-Seq Kit, NEXTflex™ Bundle (including RNA-Seq Barcodes 1-24 and

NEXTflex™ poly(A) beads;BIOO Scientific), according to the manufacturer's instructions. Libraries were sequenced (1 x 75bp single end reads) with the NextSeq® 500 (Illumina). Quality control assessment of raw.fastq files was performed using FastQC [352]. Raw single-end FASTQ reads were aligned to the GRCh38/mm10 version of the mouse genome using STAR. After alignment, mapped sequence reads were summarised to the mm10 gene intervals using the tool feature Counts, available through the package RSubread. Raw counts were converted to counts per million (CPM). CPM values were normalised using the trimmed mean of M-values (TMM) using edgeR, followed by data filtering for low counts, by only including genes with >2 CPM in at least 3 samples.

Differential gene expression analysis was then undertaken using limma-voom [353] in R v3.5.1. To identify significantly enriched or depleted groups of genes with the induction of senescence via irradiation, gene set enrichment analysis (GSEA) was performed using the GSEA software (UC San Diego) available at <https://www.gsea-msigdb.org/gsea/index.jsp> [354, 355]. To identify novel SASP factors, the list of the differentially expressed genes with irradiation was further triaged to genes encoding cell surface or secreted ligands, using the ConnectomeDB2020 database [356].

2.7.1.3 DNAse treatment of RNA

All RNA samples were DNAse treated with RQ1 DNAse (Promega) prior to reverse transcription according to manufacturer's instructions. Briefly, per 20 µL RNA sample, 2.5 µL of RQ1 RNAse free DNAse and 2.5 µL of RQ1 RNAse free DNAse 10X reaction buffer was added and thoroughly mixed prior to a 30-minute incubation on a heat block at 37°C. 2.5 µL of DNAse stop solution was added and thoroughly mixed to terminate the reaction. The

samples were incubated at 65°C on a heat block for 10 minutes. Subsequently, the samples were chilled on ice prior to cDNA synthesis or stored at -80°C until required.

2.7.1.4 cDNA synthesis

To qualitatively assess messenger RNA (mRNA) levels, reverse transcription polymerase chain reaction (RT-PCR) was performed. Firstly, total RNA (2 µg) was reverse transcribed into single-stranded complementary DNA (cDNA) using SuperScript™ IV Reverse Transcriptase (Invitrogen). The RNA sample was resuspended in a total volume of 14 µL with NF water (Invitrogen) and 1 µL each of random hexamers (50 µM; Merck) and deoxyribonucleotide triphosphate (dNTP) mix (10 mM; Merck) were added and mixed thoroughly. The solution was incubated at 65°C for 5 minutes and immediately chilled on ice for at least 2 minutes. A mix containing 5 µL of 5x RT buffer (Invitrogen), 1 µL of 0.1 M DTT (Invitrogen) and 1 µL of SuperScript™ IV enzyme (200 U) was then added to the denatured RNA. This reaction mixture was incubated for 10 minutes at 23°C, 10 minutes at 55°C and 10 minutes at 80°C using a Veriti™ Thermal Cycler. The resulting cDNA was then diluted to a total volume of 100 µL with NF water and either used immediately for downstream applications or stored at –20°C. Negative control (minus reverse transcriptase) reactions were performed concurrently for all samples.

2.7.2 Quantitative reverse transcription polymerase chain reaction (RT-qPCR)

Following cDNA synthesis, performed as described in section 2.7.1.4, RT-qPCR was performed. Each 15 µL qPCR reaction contained 2 µL of cDNA, 1x RT^2 SYBR® Green qPCR Mastermix (QIAGEN), 0.5 µM forward primer and 0.5 µM reverse primer in NF water in a 96-well clear PCR plate (Bio-Rad). Primer sequences for mouse and human are listed in Table 2.1 and 2.2, respectively. All cDNA samples were analysed in triplicate and minus reverse

transcriptase and no template control reactions were included for each sample and target gene, respectively. Reactions were performed on the CFX Connect™ Real-Time PCR Detection System (Bio-Rad) using the following cycling parameters: 50°C for 2 minutes; 95°C for 15 minutes; 40 cycles of 95°C for 15 seconds, 60°C for 25 seconds and 72°C for 10 seconds; and 72°C for 3 minutes. A melt curve was then performed in which there was an incremental increase of 0.5°C/5 seconds from 65°C to 95°C. Standard curves were generated to determine the reaction efficiency of each primer pair. Normalisation and relative expression analysis were performed, with the reaction efficiency taken into account, using Q-Gene software [357]. Gene expression levels were calculated relative to *ACTB* (human) and *Gapdh* mouse as the endogenous control using the $2^{-\Delta CT}$ method [358].

Table 2.1

Human primer sequences for PCR.

Gene	**Primer sequence**
ACTB	Forward: 5'-GATCATTGCTCCTCCTGAGC-3' Reverse: 5'-GTCATAGTCCGCCTAGAAGCAT-3'
CDKN2A ($p16^{INK4A}$)	Forward: 5'-GAAGGTCCCTCAGACATCCCC-3' Reverse: 5'-CCCTGTAGGACCTTCGGTGAC-3'
CDKN2A ($p14^{INK4A}$)	Forward: 5'-CCCTCGTGCTGATGCTACTG-3' Reverse: 5'-ACCTGGTCTTCTAGGAAGCGG-3'
CDKN1A	Forward: 5'-ATTAGCAGCGGAACAAGGAG-3' Reverse: 5'-CTGTGAAAGACACAGAACAG-3'
IL6	Forward: 5'-TCTGGCTTGTTCCTCACTACT-3' Reverse: 5'-AACCTGAACCTTCCAAAGATGG-3'
GREM1	Forward: 5'-AGGCCCAGCACAATGACTCAG-3' Reverse: 5'-GTCTCGCTTCAGGTATTTGCG-3'
IGF1	Forward: 5'-TCTTCAGTTCGTGTGTGGAG-3' Reverse: 5'-CAGCCTCCTTAGATCACAGC-3'
EZH2	Forward: 5'-GGGACAGTAAAAATGTGTCCTGC-3' Reverse: 5'-TGCCAGCAATAGATGCTTTTTG-3'

Table 2.2

Mouse primer sequences for PCR

Gene	**Primer sequence**
Gapdh	Forward: 5'-AGGTCGGTGTGAACGGATTTG-3' Reverse: 5'-TGTAGACCATGTAGTTGAGGTCA-3'
Cdkn2a (p16)	Forward: 5'-TCTGCTCAACTACGGTGCAG-3' Reverse: 5'-ATCGCACGATGTCTTGATGT-3'
Cdkn2a (p14)	Forward: 5'-CCCACTCCAAGAGAGGGTTT-3' Reverse: 5'-TCTGCACCGTAGTTGAGCAG-3'
Cdkn1a	Forward: 5'-GAACATCTCAGGGCCGAAAAC-3' Reverse: 5'-CTGCGCTTGGAGTGATAGAA-3'
Il6	Forward: 5'-GCACTCCTTGGATAGAGCCC-3' Reverse: 5'-ACGAGGATTCTTGCACTGGG-3'
Grem1	Forward: 5'-GCGCAAGTATCTGAAGCGAG-3' Reverse: 5'-CGGTTGATGATAGTGCGGCT-3'
Prrx1	Forward: 5'-GAACTCTGAGGAGAAGAAGAAGAG-3' Reverse: 5'-GCAGTCACGTCTCCTGAGTAG-3'

2.8 *In silico* analysis and statistics

2.8.1 Publicly available microarray data

The analysis of gene expression in BM-MSCs from MM patients was done using the publicly available microarray dataset GSE36474 [229] encompassing *n*=4 MM donors (aged 47, 52, 56 and 65 years). Raw microarray data (CEL files) were downloaded from Gene Expression Omnibus (NCBI) <http://www.ncbi.nlm.nih.gov/geo/query/acc.cgi?token=ltazpowigoiekji&acc=GSE36474> and were normalised with the robust multi-array average (RMA) algorithm using the Bioconductor package affy in R (version 3.03) and $\log_2$ transformed. . Expression was filtered by genes expressed at >log (100) in at least 3 of 4 MM BM-MSC donors. To identify potential SASP factors, the list of genes expressed by MM BM-MSCs was restricted by ligands that were upregulated in irradiated murine KaLwRij stroma as described in section 2.7.1.2.

2.8.2 Statistical analysis

Unless otherwise described, statistical analysis was performed using GraphPad Prism v8.0.0 (GraphPad Software) and differences were statistically significant when $P < 0.05$. When two groups were being compared for a single variable, a parametric paired *t*-test, a parametric unpaired *t*-test or a non-parametric Mann-Whitney U test was used, as appropriate. When three or more groups were being compared for a single variable, a parametric one-way ANOVA with Tukey's post-hoc multiple comparisons test or a non-parametric Kruskal-Wallis test with Dunn's multiple comparisons test was used. For time-course experiments, groups were compared using a two-way ANOVA with Sidak's or Tukey's multiple comparisons test. Correlation was assessed using Pearson's correlation coefficient. For categorical variables, The Fisher's exact test was used to compare between groups.

Unless otherwise noted, progression to MM was analysed using Kaplan-Meier curves and the log-rank test. MGUS patient progression to MM was defined clinically by the development of CRAB features (hypercalcaemia, renal insufficiency, anaemia and bone lesions [19]) and/or initiation of therapy for their myeloma. Patients were censored at the time of last clinical follow up. Univariate and multivariable analyses of factors associated with progression to MM were conducted using IBM SPSS version 26. Initially, the proportional hazards assumption was tested, and univariate Cox regressions were conducted to identify factors that were significantly associated with progression to MM ($p < 0.1$). These factors were then included in a multivariable Cox proportional hazards model.

3 CHARACTERISING THE SENESCENT PHENOTYPE OF BM-MSCs FROM MGUS AND MM PATIENTS

3.1 Introduction

MM is a cancer of antibody-producing PCs that aberrantly proliferate in the BM. MM is an age-related cancer, with the average patient age of 70 years at diagnosis [39]. MM is universally preceded by the benign condition MGUS [39, 40], although MGUS is also a precursor condition for other plasma cell disorders (e.g., smouldering myeloma, AL amyloidosis, plasmacytoma) [37, 38].

The average yearly risk of progression among MGUS patients to plasma cell dyscrasias is 0.8% [41]. The mechanism underlying the transition of MGUS to MM is presently unknown, although has been widely speculated to be the consequence of sequential acquisition of driver mutations in PCs [12, 153, 359-361]. Despite this, recent research from our laboratory has shown that genetic aberrations alone may not be sufficient to drive malignancy. Specifically, a recent whole exome sequencing study from our laboratory of paired MGUS-MM patient samples revealed that PC subclones responsible for MM progression are already present at the asymptomatic stages, suggesting that the extrinsic BM microenvironment plays a critical role in malignant transformation [8].

While the underlying triggers for MGUS progression are largely unknown, several risk factors for progression have been reported. For example, paraprotein levels ≥15g/L and PC burden >5% [41, 45] have been recognised as hallmarks of malignant transformation of MGUS patients. Moreover, other presenting features, such as IgA immunoglobulin (compared with IgG or light chain only), as well as serum free light chain (SFLC) ratio ≥1.65, have been reported to be associated with increased rates of malignant transformation of MGUS [41, 44, 46]. Furthermore, advanced biological age has been identified as a risk factor for MGUS progression. Indeed, the risk of MGUS progression to MM and other plasma cell disorders

increases from 0.4% patient years in younger patients (age<60 years) to 1.0% in older patients (age≥60 years) [41].

The association between age and increased risk of progression from MGUS to MM suggests that ageing related changes in the BM may create a supportive microenvironment that encourages PC growth and disease progression. One of the key hallmarks of ageing is the concept of 'inflammaging', a condition whereby individuals, with advancing age, display chronic activation of the innate immune system and a sterile low-grade inflammation, in the absence of overt infection [362]. In the BM, this increased inflammatory signalling is thought to contribute to abnormal haematopoiesis including clonal haematopoiesis of indeterminate potential (CHIP) [363], myeloid skewing [364], reduced lymphopoiesis [365], reduction in erythropoiesis [366] and decreased BM cellularity [367]. One of the critical contributors to this inflammatory BM microenvironment is senescent BM-MSCs [248, 362], which accumulate in the BM with advancing age [368, 369].

Cellular senescence is induced by activation of cyclin-dependent kinase inhibitors, including $p21^{Cip1}$, $p16^{INK4A}$, $p14^{ARF}$, $p15^{INK4b}$ and $p27^{Kip1}$, which inhibit cell cycle progression through p53 and RB-dependent and -independent pathways (reviewed in Kumari *et al.*, 2021) [245]. As senescence can be induced by various pathways that depend on senescence-inducer and cell type, the expression of one or more of these factors at the gene or protein level can help define whether a cell has undergone senescence. The senescent state corresponds with a decrease in proliferation ability, flattened and enlarged morphology and increased activity of β-gal enzyme. Importantly, cellular senescence is associated with increased secretion of growth factors and pro-inflammatory cytokines via the SASP [268, 370, 371].

Notably, BM-MSC senescence is a feature of MM. Several studies have reported that BM-MSCs, isolated from MM patients, display increased senescent characteristics compared with healthy counterparts, which include increased β-gal positivity, flattened and enlarged cell morphology and a reduced proliferative and osteogenic potential [200, 229, 231, 232, 289, 296, 298, 299, 334]. Furthermore, BM-MSCs from MM patients exhibit a significantly altered gene expression profile, compared with BM-MSCs from non-cancer (healthy) individuals [200, 229, 296]. This altered gene expression includes downregulation of many genes involved in regulation of cell cycle progression and DNA repair including genes, such as *CCND1, CCNB1, CCNE2, CCNH, CDK1, CDK2, CDK4, CDK6, CDC25A, CDC25B, CDC25C* and *MKI67* [229, 296]. Conversely, BM-MSCs from MM patients display elevated levels of signalling molecules and receptors involved in senescence induction pathways such as *CDKN1A*, *CDKN2A*, *CDKN2B*, *TP53, DICER1* and *LPA1* [229, 231, 289, 296]. In line with this, BM-MSCs from MM patients also display an altered secretory profile compared with that of BM-MSCs from age-matched non-cancer (healthy) controls, closely resembling that of the SASP of senescent human BM-MSCs [228, 229, 231, 334, 372]. Specifically, BM-MSCs from MM patients express higher levels of IL-6, TNF-α, CXCL-8, AREG, IL-1β and GDF-15 relative to healthy controls, all of which are well established SASP factors [200, 229, 231-236]. As such, the gene expression profile of BM-MSCs isolated from MM patients is highly suggestive of replicatively senescent MSCs [229, 318].

Clearly, age-related BM microenvironment changes have a significant effect on haematopoiesis with advancing age. As MM PCs hijack the haematopoietic niche to promote their proliferation and survival [163], it is possible that age-related changes to the BM microenvironment can influence MM growth within the BM, especially as MGUS-to-MM progression is correlated with advancing age. Notably, it is evident that BM-MSC isolated from

MM patients are characterised by a senescent phenotype. This raises the possibility that increased BM-MSC senescence may be associated with myeloma development and could play an active role in this process. Although the phenotype of MGUS patient BM-MSCs is yet to be defined in the context of senescence, analysis of patient BM-MSC growth characteristics have shown that CFU-F expansion is reduced in MGUS BM-MSC cultures relative to age-matched controls, indicative of lower clonogenic ability compared with healthy counterparts [200]. Furthermore, IL-6 has been shown to be upregulated in BM stromal cell culture supernatants from MGUS patients, while it was undetectable cultures from age-matched normal donors [373]. As such, characterising the phenotype of BM-MSCs from MGUS patients may reveal insights into whether the increased BM-MSC senescence observed at MM precedes MM progression or occurs as a consequence of MM disease. In this chapter, we characterise the senescence-related phenotype of BM-MSCs from patients with MGUS and MM to assess the potential association between senescence and risk of disease progression. We also investigate the senescent phenotype of BM-MSCs isolated from young and aged non-cancer donors to understand whether the senescent phenotype of BM-MSCs at MGUS/MM is likely influenced by the presence or burden of MM PCs or is a consequence of advanced biological ageing.

3.2 Results

3.2.1 BM-MSCs from both MGUS and MM patients are characterised by a senescent phenotype comparable to that of aged non-cancer control BM-MSCs

To evaluate the level of BM-MSC senescence within individuals, MSC cultures were established by plastic adherence from samples of trabecular bone fragments [374]. BM-MSC cultures from healthy young non-cancer volunteers (age <35 years) were obtained from posterior iliac crest BM aspirates, while BM-MSC cultures from aged non-cancer controls (age ≥60 years) were sourced from intertrochanteric trabecular bone samples from patients

undergoing hip arthroplasty for neck of femur fractures [351]. BM-MSCs from non-IgM untreated MGUS and MM patients were obtained by culturing trabecular bone collected from posterior iliac crest BM trephine biopsies of patients. The clinical characteristics of individuals included in this study are described in Table 3.1.

Table 3.1.
Characteristics of BM-MSC patient donors used in the study.

	Non-cancer controls <35 years *n*=14	**Non-cancer controls 60+ years *n*=11**	**MGUS *n*=29**	**MM *n*=11**
Age (years)				
Median	21	88	67.5	70
Range	17-26	68-94	42-84	52-84
Sex				
Male (*n*)	8	4	19	7
Female (*n*)	5	6	10	4
Unknown (*n*)	1	1	0	0
M (%)	57	37	66	64
F (%)	37	55	35	36
BM PC burden (%)				
Median	-	-	5	42
Range	-	-	1-9	9-80
Paraprotein type				
IgG	-	-	18	3
IgA	-	-	8	1
sFLC only	-	-	2	2
Unknown	-	-	0	5
Paraprotein level (g/L)				
Median	-	-	8.5	24
Range	-	-	0-28	0-54
Involved SFLC level (mg/L)				
Median	-	-	27.5	718
Range	-	-	8-638	82-19368
SFLC ratio				
Median	-	-	2.78	15.9
Range	-	-	1.11-63.8	4-2778.6
β-2-microglobulin, (mg/L)				
Median	-	-	2.2	3.3
Range	-	-	1-4.8	2.1-18.9
Creatinine level (µmol/L)				
Median	-	-	80	83
Range	-	-	1.14-173	45-270
Haemaglobin level (g/L)				
Median	-	-	137	99

Range	-	-	82-154	89-135
Calcium level (mmol/L)				
Median	-	-	2.32	2.33
Range	-	-	2.01-37	2.11-2.65
Albumin level (g/L)				
Median	-	-	35	33
Range	-	-	26-43	26-48

BM PC = bone marrow plasma cell
SFLC = serum free light chain

The median age of young non-cancer donors was 21 years (range: 17-26 years; *n*=14 [8 male [M], 5 female [F], 1 unknown), while the median range of aged non-cancer donors was 88 years (range: 68-94 years; *n*=11 [4 M, 6 F, 1 unknown]). The median age of MGUS and MM patients used in the study was 67.5 years (range: 42-84 years; *n*=29 [19 M, 10 F]) and 70 years (range: 52-84 years; *n*=11 [7 M, 4 F]), respectively. There were approximately twice as many males as females in our MGUS and MM cohorts, in line with the sex-based prevalence of the disease in the literature [18, 375, 376].

BM-MSCs were passaged twice per week, with *in vitro* analyses conducted at the start of week 3 in culture (passage 5). Morphologically, BM-MSCs isolated from aged, non-cancer controls displayed an enlarged, flat, polygonal morphology characteristic of senescent cells [377] while BM-MSCs isolated from younger non-cancer controls displayed a spindle-shaped morphology (Figure 3.1A-B). Like older, non-cancer donor BM-MSCs, BM-MSCs from MGUS and MM patients displayed a large and flat polygonal morphology characteristic of senescent cells (Figure 3.1A-B). BM-MSC cultures were stained for β-gal activity, a marker of cellular senescence, with the percentage of β-gal positive (blue) cells calculated as a proportion of total cells as identified by DAPI co-stain (Figure 3.1A-C). Consistent with the senescent-like morphology, BM-MSC cultures from older donors displayed a 6.4-fold increase in the proportion of β-gal positive cells relative to younger donors (p=0.015; Kruskal-Wallis test with Dunn's multiple comparisons test; Figure 3.1C). Specifically, while the number of β-gal positive cells was relatively low in BM-MSC cultures from younger donors, with less than 3.40% of cells staining β-gal positive (median: 1.70% β-gal positive; range: 0.00-3.40%), cultures from older donors displayed up to 50.8% β-gal positive cells (median: 10.8%; range: 3.90-50.8%) (Figure 3.1C). BM-MSCs from MM patients displayed 11.8-fold higher β-gal staining compared with young non-cancer controls (median: 20.0% β-gal positive; range: 7.90-

60.0%; p=0.00060; Kruskal-Wallis test with Dunn's multiple comparisons test; Figure 3.1C). Notably, BM-MSCs from MGUS patients display 7.5-fold greater β-gal staining than younger non-cancer controls (median: 12.7% β-gal positive; range: 2.40-43.5%, p=0.0030, Kruskal-Wallis test with Dunn's multiple comparisons test; Figure 3.1C). The percentage of β-gal positive cells was not significantly different between BM-MSCs from MM or MGUS patients, or aged non-cancer controls. To further characterise the senescent phenotype of BM-MSCs, qPCR analysis evaluating the expression of the replicative senescence marker *CDKN2A* was also performed at passage 5. The median expression of *CDKN2A* was approximately 2-fold higher in older non-cancer control BM-MSCs (median: 0.00890; range: 0.00450-0.0220) compared with younger non-cancer control BM-MSCs (median: 0.00470; range: 0.00230-0.0130), although this did not reach statistical significance (p=0.14; Kruskal-Wallis test with Dunn's multiple comparisons test; Figure 3.1D). Similarly, median *CDKN2A* expression levels in BM-MSCs from MGUS (median: 0.00870; range: 0.00240-0.0440) and MM (median: 0.00870; range: 0.00490-0.0390) were similar to that of aged non-cancer control BM-MSCs (Figure 3.1D).

Furthermore, as senescent cells are characterised by proliferative arrest [248], we assessed the proliferative rate of BM-MSCs as an additional independent measure of senescence induction. Notably, the median population doubling rate of BM-MSCs isolated from aged non-cancer controls (median: 0.110 population doublings/day; range: 0.000-0.510) was approximately 3.9 times slower than that of young non-cancer controls (median: 0.430; range: 0.210-0.640; p=0.0075; Kruskal-Wallis test with Dunn's multiple comparisons test; Figure 3.2A), supporting the suggestion that BM-MSCs from older donors are more senescent than BM-MSCs from younger donors. The proliferative rate of BM-MSCs isolated from MGUS and MM patients was 2.0 times and 4.6 times slower, respectively, compared with BM-MSCs of younger non-cancer controls (MGUS

median: 0.220; range: 0.000-0.670; p=0.077; MM median: 0.0920; range: 0.000-0.310; p=0.043; Kruskal-Wallis test with Dunn's multiple comparisons test; Figure 3.2A) and was not significantly different from that of aged non-cancer controls.

Figure 3.1. BM-MSCs from both MGUS and MM patients are characterised by a senescent phenotype comparable to that of aged non-cancer control BM-MSCs. (A) BM-MSCs isolated from the bone marrow of young non-cancer controls (<35 years), aged non-cancer controls (60+ years), newly diagnosed MGUS and newly diagnosed MM were passaged twice a week for 3 weeks, with *in vitro* analysis conducted at the start of week 3 in culture (passage 5). Cells were seeded at $6x10^3$ cells/cm^2 in 6-well plates and were stained for β-gal (blue) activity after 24 hours of culture. Representative images are shown. Scale bar: 300 μm, (**B)** scale bar: 75 μm. (**C)** Graph depicts the percentage of β-gal-positive cells, calculated as a proportion of total cells (identified by DAPI co-stain) for young non-cancer controls (*n*=6), aged non-cancer controls (*n*=11), newly diagnosed MGUS (*n*=22) or MM (*n*=9) patients. Each point represents the mean of manual counts of 3 independent fields of view for each donor. **(D)** RNA was extracted from *ex vivo* cultured BM-MSCs at passage 5 from young non-cancer controls (*n*=11), aged non-cancer controls (*n*=8), newly diagnosed MGUS (*n*=25) and MM (*n*=10) patients. Expression of *CDKN2A* was analysed by real-time PCR. Data presented as mRNA expression normalised to *ACTB*. Graphs depict median and interquartile ranges, **p*<0.005, ***p*<0.001, ****p*<0.0001, Kruskal-Wallis test with Dunn's multiple comparisons post-test.

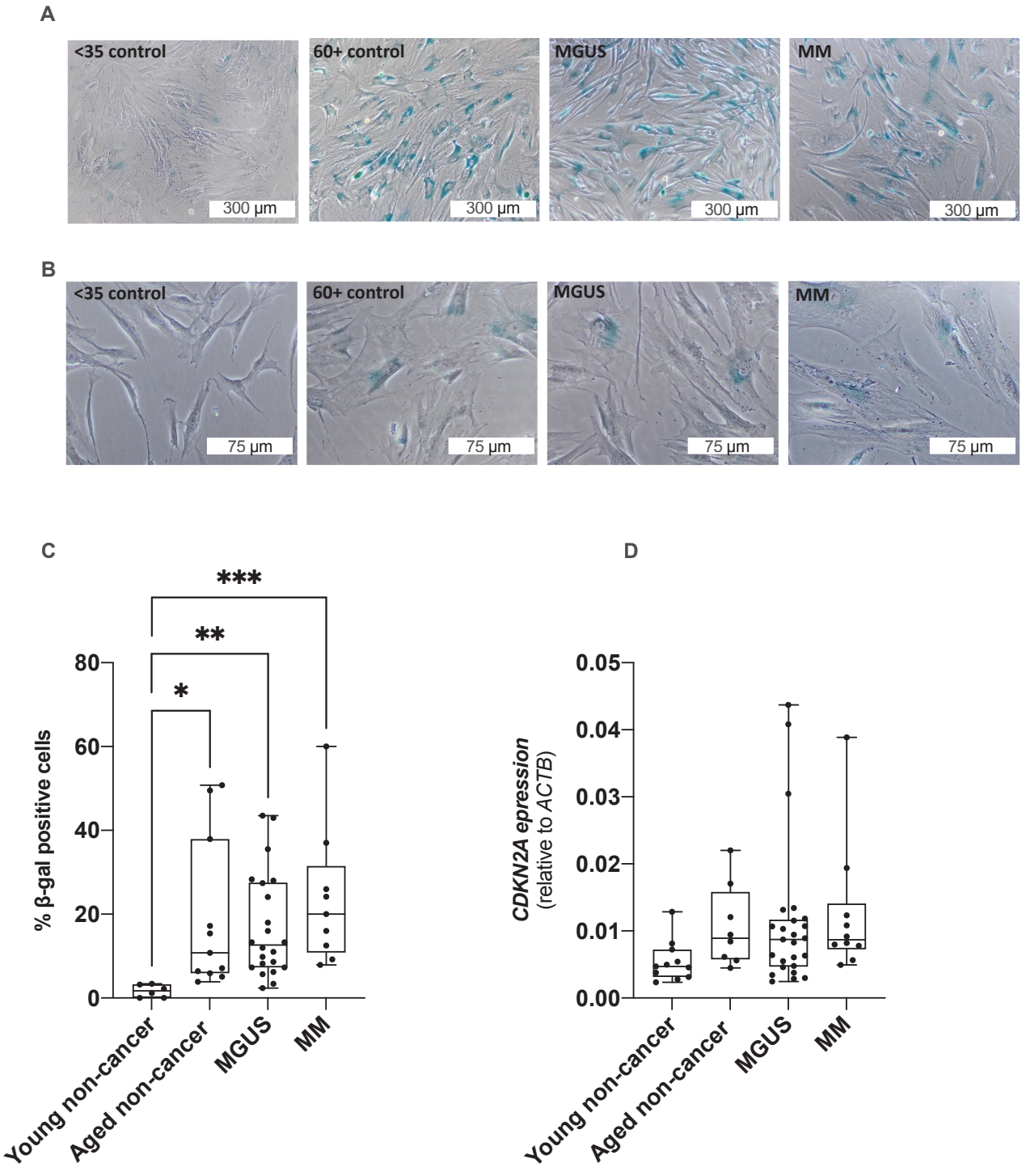
A
<35 control
60+ control
MGUS
MM
300 µm
B
<35 control
60+ control
MGUS
MM
75 µm
C
% β-gal positive cells
0
20
40
60
80
*
**
***
Young non-cancer
Aged non-cancer
MGUS
MM
D
CDKN2A epression
(relative to ACTB)
0.00
0.01
0.02
0.03
0.04
0.05
Young non-cancer
Aged non-cancer
MGUS
MM

To complement the senescence characterisation studies, we also assessed the replicative capacity of BM-MSCs, by determining the passage at which BM-MSCs underwent proliferative arrest by passaging cells twice weekly until they ceased proliferating. Notably, while BM-MSCs from healthy young donors continued to proliferate until passage 13 or more (median: passage 15; range: 13-22), BM-MSCs from MGUS or MM donors were found to reach proliferative arrest at an earlier passage (MGUS, median: passage 8; range: 4-22; p=0.0023; MM, median: passage 11; range: 3-18; p=0.022; Kruskal-Wallis test with Dunn's multiple comparisons test, Figure 3.2B). Aged non-cancer controls were not evaluated beyond passage 5 in this study, due to lower numbers of cells available for these samples; however, 5/11 of the older donors had ceased proliferating by passage 5, consistent with more rapid senescence in these cultures, when compared with those of young donors. Taken together, these results demonstrate, for the first time, that BM-MSCs from MGUS patients display evidence of BM-MSC senescence. Furthermore, these studies reveal that the extent of BM-MSC senescence at MGUS is equivalent to that of aged non-cancer controls, suggesting that BM-MSC senescence at MGUS/MM is associated with age and not disease stage.

Figure 3.2. MGUS and MM BM-MSCs display similar proliferative capacity to that of BM-MSCs from aged non-cancer controls. (**A)** Passage 5 BM-MSCs were seeded at $6x10^3$ cells/cm^2 in 75cm^2 flasks and, after 3 days were harvested, counted and the number of population doublings was calculated for young non-cancer controls (*n*=8), aged non-cancer controls (*n*=11), newly diagnosed MGUS (*n*=23) and MM (*n*=7) BM-MSCs. Number of population doublings was calculated from the difference between the number of cells harvested and the number seeded using the formula PD= log[(harvested)/(seeded)]/log2. Population doubling of ≤0 indicated senescence. **(B)** BM-MSCs cultures were isolated from young non-cancer controls (*n*=8), newly diagnosed MGUS (*n*=13) or MM (*n*=8) patients were seeded at $6x10^3$cells/cm^2 in 75cm^2 flasks and passaged twice weekly until cessation of proliferation. Graphs depict median and interquartile ranges, **p*<0.005, ***p*<0.001, Kruskal-Wallis test with Dunn's multiple comparisons post-test.

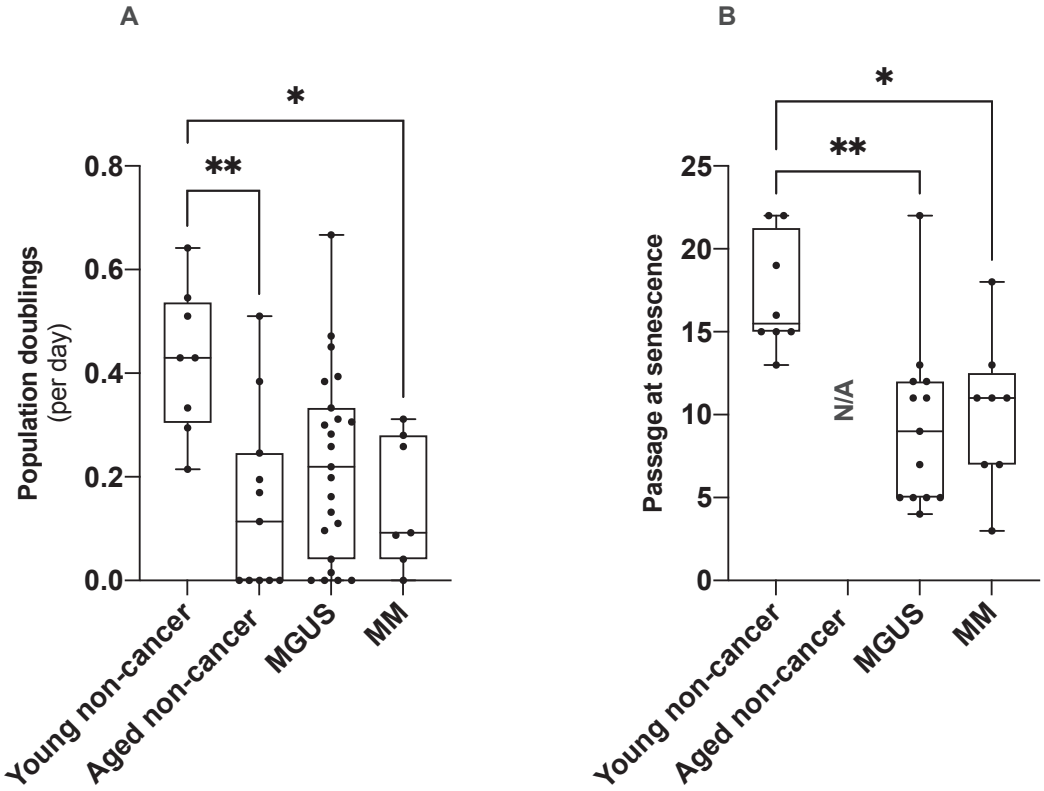
A
B
Population doublings
(per day)
0.8
0.6
0.4
0.2
0.0
**
*
Young non-cancer
Aged non-cancer
MGUS
MM
Passage at senescence
25
20
15
10
5
0
N/A

3.2.2 Senescent characteristics observed in BM-MSCs from newly diagnosed MGUS and MM patients correlate with patient age

Having shown that early senescence is a feature of BM-MSCs from older donors compared with younger healthy controls, we then investigated whether the level of BM-MSC senescence observed at the MGUS and MM stage is associated with patient age. Notably, the percentage of β-gal positive BM-MSCs significantly positively correlated with donor age in MGUS and MM patients (p=0.0091; Pearson correlation; R=0.51; 95 % CI: 0.14, 0.75; Figure 3.3A). Furthermore, there was an inverse correlation between patient age and BM-MSC proliferation rate, as assessed by population doublings per day (p=0.055; Pearson correlation; R=0.14; 95% CI: -0.017, -0.0002; Figure 3.3B). Moreover, there was a significant inverse association between donor age and the passage at which BM-MSCs reached senescence in MGUS and MM patients (p=0.00020; Pearson correlation; R= -0.59; 95% CI: -0.85, -0.087; Figure 3.3C). Taken together, these data suggest that BM-MSC senescence in MGUS and MM patients is strongly associated with patient age.

Figure 3.3. BM-MSC senescence correlates with donor age in MGUS and MM patients. BM-MSCs isolated by plastic adhesion from BM trephine biopsies from newly diagnosed MGUS donors (black) and newly diagnosed (red) MM donors. The correlation between donor age (x-axis) and (**A)** BM-MSC senescence by β-gal positivity, (**B)** BM-MSC population doublings, and (**C)** the passage of BM-MSC senescence is shown for MGUS (*n*=25, 16 and 4 patients, respectively) and MM (*n*=6, 7 and 8 patients, respectively). Pearson correlation, simple linear regression line of best fit.

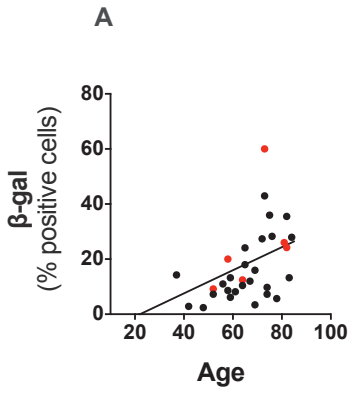

P=0.0019, R=-0.61, 95% CI [-0.81,-0.27].

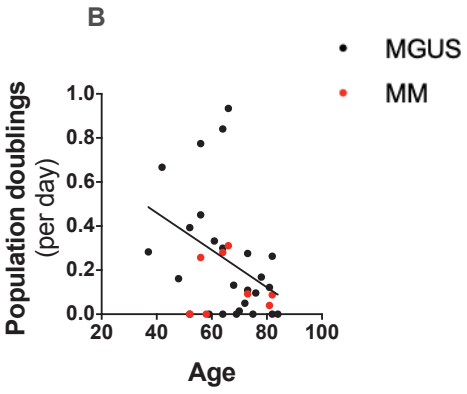

P=0.055, R=0.144, CI [-0.017,-0.0002]

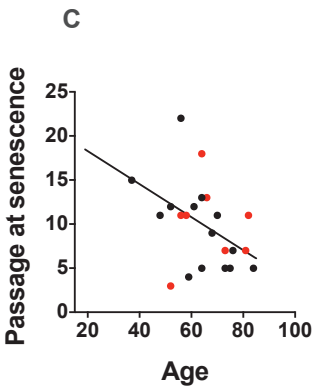

P=0.0002, R= -0.59, CI [-0.85, -0.087]

3.2.3 The risk of progression to active MM is elevated in MGUS patients with highly senescent BM-MSCs

Given BM-MSC senescence in MGUS and MM patients is associated with age, and the risk of MGUS-to-MM progression increases with age [41], elevated BM-MSC senescence may be associated with increased risk of MGUS-to-MM progression. To this end, we investigated whether elevated BM-MSC senescence at the MGUS stage is associated with increased risk of progression to overt MM disease. In this study, progression to active MM was determined clinically as development of CRAB features [including increased serum calcium (corrected serum calcium >0.25mmol/l above the upper limit of normal or >2.75mmol/l), renal insufficiency (creatinine clearance 177 μmol/L), anaemia (Hb <100g/L or below the lower limit of normal), presence of bone lesions (one or more osteolytic lesions on skeletal radiography, CT or PET-CT and high involved: uninvolved serum light chain ratio (≥100) [28] and/or initiation of therapy for their MM. Of the 28 MGUS patients, for whom follow up data were available, 13 patients progressed during follow-up while 15 remained stable at the time of last follow-up, with a median follow-up of 262 weeks (range: 14.0-694 weeks). To identify whether BM-MSC β-gal staining level at MGUS was predictive of MGUS-to-MM progression, we conducted receiver operating characteristic (ROC) curve analysis of MGUS BM-MSC β-gal staining and time to progression to overt MM. ROC curve analysis demonstrated that the level of β-gal staining was able to differentiate between patients who were likely to progress, compared with those who displayed stable disease (AUC: 0.83; 95% CI: 0.65-1.00; p=0.00035; Figure 3.4A). To this end, a cut-off of 10% β-gal-positive cells provided a specificity of 0.64 and sensitivity of 0.89. The time to progression was assessed in the MGUS patient cohort following stratification into patients displaying low levels of β-gal positive BM-MSCs (<10% positive cells; β-gal^{lo}) and those with high β-gal positive BM-MSCs (≥10% positive cells; β-gal^{hi}) at diagnosis and (Figure 3.4B-C). Notably, 1 out of 10 MGUS patients in the β-gal^{lo} group

(10%) progressed during follow up, while 8 of 13 patients in the β-gal^{hi} group (61.5%) progressed. Kaplan-Meier analysis revealed that MGUS patients with high (≥10%) β-gal BM-MSC positivity were 5.8 times more likely to progress to MM (HR: 5.8; 95% CI: 1.54-21.8) compared with patients with low (<10%) BM-MSC β-gal expression (p=0.048, log-rank test; Figure 3.4C). The median time to progression of β-gal^{hi} patients was 336 weeks, while median time to progression was not reached in the β-gal^{lo} patients. The baseline demographics of β-gal^{lo} and β-gal^{hi} MGUS patients are shown in Table 3.2.

Table 3.2
Baseline patient characteristics of β-gal^{lo}and β-gal^{hi} MGUS patients

	β-gal^{lo} (*n*=10)	**β-gal^{hi} (*n*=13)**	***p*-value (<0.05)**
Age[1]	60 (42-78)	72 (34-84)	0.1
Paraprotein level[1]	8.0 (0.99-16.0)	8.0 (0-28)	0.45
Paraprotein type[2] IgA IgG Light chain only	 2 7 1	 5 7 1	0.41
SFLC ratio[1]	1.8 (1.1-4.0)	22.4 (1.6-63.8)	0.015
PC burden[1]	2.5 (1.0-6.0)	6.0 (2.0-9.0)	0.0016
β-galactosidase staining[1]	6.8 (2.4-9.8)	27.4 (10.4-43.5)	<0.0001

PC= plasma cell
SFLC= serum free light chain
[1]Unpaired t-test
[2]Fisher's exact test

Figure 3.4. The risk of progression to active MM is elevated in MGUS patients with highly senescent BM-MSCs. Newly diagnosed MGUS patients were stratified on their mean β-gal activity at passage 5. Cut offs defined by ROC analysis **(A)** (Youden's J coefficient). β-gal^{lo} classified as <10% positive cells (*n*=10 patients), β-gal^{hi} ≥10% (*n*=13 patients). **(B)** Representative images of β-gal staining (blue) of BM-MSCs isolated from newly diagnosed MGUS patients at passage 5 in the β-gal^{lo} and β-gal^{hi} groups. Scale bar: 300 μm. **(C)** Kaplan-Meier survival plots of β-gal^{lo} and β-gal^{hi} groups compared with log-rank test. MGUS progression defined as time of

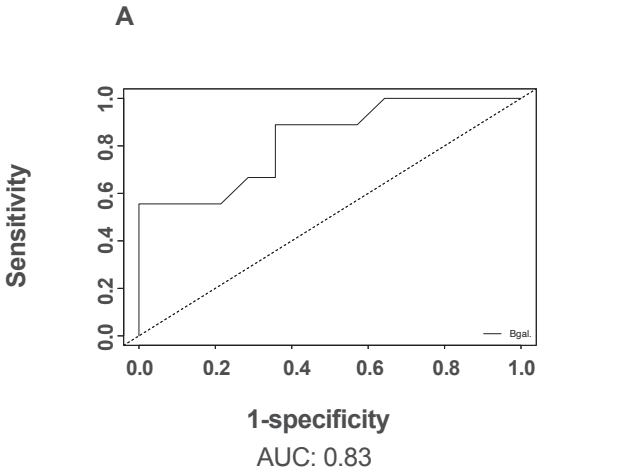

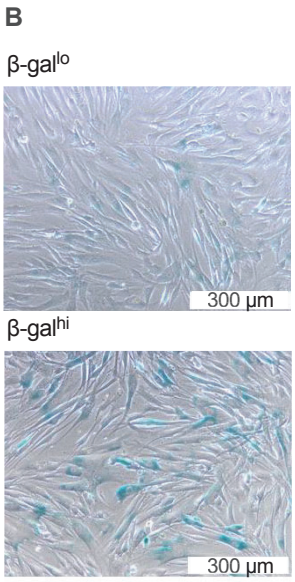

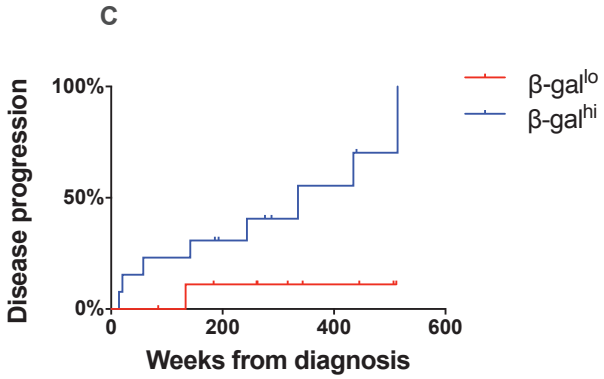

P=0.048, HR=5.8(1.54-21.8)

To determine whether elevated BM-MSC β-gal staining was associated with other factors known to be associated with risk of progression in MGUS patients, we compared paraprotein type, paraprotein level, SFLC ratio and BM PC % in the β-gal^{lo} and β-gal^{hi} patients. Analysis of the baseline levels of the known prognostic factors revealed that the poor prognostic factors SFLC ratio (p=0.015, unpaired t-test) and PC burden (p=0.0016, unpaired t-test) were significantly higher in the β-gal^{hi} cohort compared with the β-gal^{lo} cohort. While the median age in the β-gal^{hi} cohort was higher than that of the β-gal^{lo} MGUS patients (median age, β-gal^{lo}: 60 years; β-gal^{hi}: 72 years), this was not statistically significant (p=0.10; unpaired t-test). Moreover, no significant difference in paraprotein levels was observed between the β-gal^{lo} (median paraprotein: 8.0; range: 0.99-16) cohort compared with the β-gal^{hi} MGUS cohort (median paraprotein: 8.0; range: 0.0-28.0; p=0.45; unpaired t-test). The prevalence of IgA paraprotein, which is associated with increased risk of progression in MGUS patients [46], was elevated in the β-gal^{hi} (62.5% of patients in β-gal^{hi} group) relative to the β-gal^{lo} (25.0% of patients in β-gal^{lo} group) MGUS patient group (p=0.41, Fisher's exact test). However, overall, there was no significant difference in paraprotein type between the β-gal^{hi} and β-gal^{lo} MGUS patient groups.

Analysis of the high-risk MGUS clinical features among β-gal^{lo} and β-gal^{hi} MGUS patient groups is shown in Table 3.3.

Table 3.3
High risk clinical features of β-gal^{lo}and β-gal^{hi} MGUS patients

	β-gal^{lo} (*n*=10)		**β-gal^{hi} (*n*=13)**		[1]**Statistical analysis (*p* value <0.05)**
	Number	Percent (%)	Number	Percent (%)	
Age ≥60 years	*n*=5	50.0	*n*=10	76.9	0.22
Paraprotein level ≥15(g/L)	*n*=1	11.1 (1 unknown)	*n*= 3	27.3 (2 unknown)	0.61
Paraprotein type IgA IgG/Light chain only	*n*=2	20.0	*n*=5	38.5	0.67
SFLC ratio≥1.65	*n*=4	57.1 (3 unknown)	*n*=7	87.5 (5 unknown)	0.46
PC burden>5%	*n*=1	10.0	*n*=7	58.3 (1 unknown)	0.11

PC= plasma cell
SFLC= serum free light chain
[1]Fisher's exact test

We did not observe a significantly higher proportion of MGUS patients displaying any indicator of poor prognosis in the β-gal^{hi} group compared with the β-gal^{lo} group. This included no significant difference in the percentage of MGUS patients classified as high-risk by age (β-gal^{lo}: 50.0% aged ≥60 years; β-gal^{hi}: 76.9% aged ≥60 years; p=0.22; Fisher's exact test), paraprotein level (β-gal^{lo}: 11.1% of patients paraprotein level ≥15(g/L); β-gal^{hi}: 27.3% of patients paraprotein level ≥15 (g/L); p=0.61; Fisher's exact test) or paraprotein type (β-gal^{lo}: 11.1% IgA; β-gal^{hi}: 38.5% IgA; p=0.67; Fisher's exact test) as assessed by β-gal. Moreover, no significant differences were seen in the proportion of MGUS patients with SFLC ratio ≥1.65 (β-gal^{lo}: 57.1%; β-gal^{hi}: 87.5%; p=0.46; Fisher's exact test). Notably, 10.0% of β-gal^{lo} patients were characterised by PC burden >5% in comparison with 58.3% of β-gal^{hi} patients; however, this did not reach statistical significance (p=0.11; Fisher's exact test). In order to determine whether BM-MSC senescence was an independent predictor of risk of progression in MGUS patients, we utilised univariate and multivariable Cox proportional hazard models (Table 3.4).

Table 3.4
Univariate and multivariable analysis of factors associated with high risk of progression of MGUS patients

	High risk group	*Univariate analysis*		*Multivariable analysis*	
	***n* (%)**	***p*-value[1]**	**HR (95% CI)**	***p*-value[1]**	**HR (95% CI)**
Age ≥60 years	65.5	0.37	0.56 (0.16-1.98)	-	-
Paraprotein level ≥15(g/L)	20.8	0.42	1.75 (0.46-6.71)	-	-
Paraprotein type IgA IgG/Light chain only	28.5	0.71	0.77 (0.19-3.01)	-	-
SFLC ratio≥1.65	66.7	0.37	33.07 (0.015-73202.8)	-	-
PC burden>5%	59.3	0.023	10.99 (1.39-86.89)	0.35	2.98 (0.31-28.85)
β-galactosidase staining≥10%	56.5	0.085	6.30 (0.76-51.28)	0.28	3.47 (0.36-33.4)

BM PC= bone marrow plasma cell
SFLC = serum free light chain
[1]Cox-proportional hazards models, Hazard ratio (HR), CI: confidence interval.

In univariate analyses, β-gal staining ≥10% in BM-MSCs at MGUS was significantly associated with increased risk of progression to MM (p=0.085). Several known parameters associated with increased risk of MGUS-to-MM progression, including age ≥60 years (p=0.37), serum paraprotein levels ≥15g/L (p=0.42), IgA paraprotein type (p=0.71), SFLC ratio ≥1.65 (p=0.37) were not predictive of risk of progression in our MGUS patient cohort. However, BM PC burden >5% was identified as predictive of risk of progression (p=0.023) in our MGUS patient cohort. ROC analysis suggested that MM PC >5% could detect patients that will progress to MM 82% of the time (sensitivity 0.82) with a false positive rate of 10% (specificity 0.9). Consequently, the two significant variables (β-gal staining and PC burden) were included in multivariable analyses (Table 3.4). The multivariable analysis indicated that when both β-gal level and MM PC burden were included together in the model, they were not significant predictors of risk of progression, suggesting that these variables are not independent of each other. Consistent with this, BM-MSC β-gal staining significantly correlated with the bone marrow tumour burden (MM PC %) in the MGUS cohort (p=0.0030; Pearson correlation; R=0.60; CI [0.24-0.82]; Figure 3.5A), suggesting that these two variables are interrelated. However, the association between β-gal staining and MM PC % was not observed in the MM cohort (p=0.15; Pearson correlation; R=-0.56; CI [-0.91-0.24]; Figure 3.5B). Nevertheless, given the small number of MM patients included in this analysis, the relevance of this is unclear. In summary, these data show, for the first time, that BM-MSC senescence, as quantified by β-gal staining, is a strong predictor of risk of progression in MGUS patients and is associated with PC burden in these patients.

Figure 3.5. BM-MSC β-gal activity positively correlates with bone marrow PC infiltration in MGUS, but not MM, patients. The percentage of CD138-positive PCs in bone marrow samples of MGUS **(A)** and MM **(B)** as determined by histopathological analysis of patient bone marrow trephine biopsies was correlated with β-gal activity in *ex vivo* cultured BM-MSCs at passage 5. The trephines used for histopathology and for BM-MSC culture were collected at the same time. Graphs depict PC% (y-axis) vs β-gal percentage (x-axis), *n*=22 MGUS and *n*=8 MM, Pearson correlation, simple linear regression line of best fit.

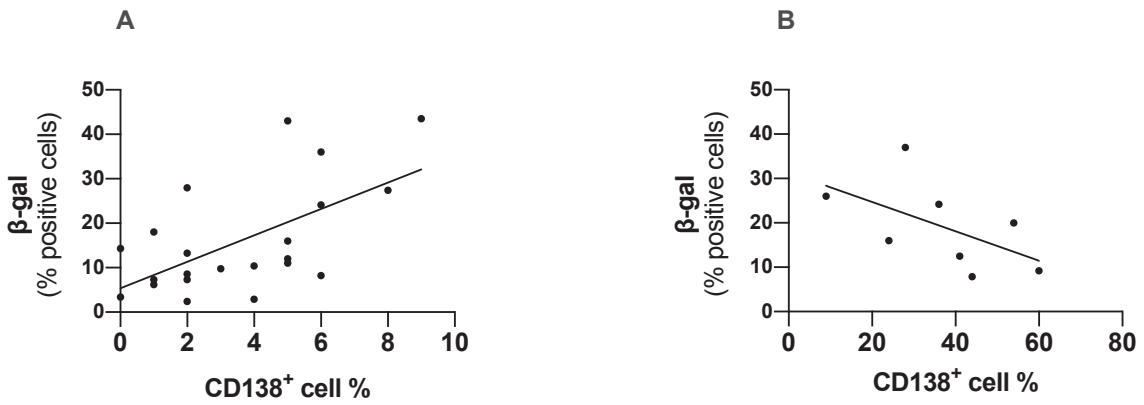

P=0.0029, R=0.60, CI [0.24-0.82]

P=0.15, R=-0.56, CI [-0.91-0.24]

3.3 Discussion

As MM is a highly debilitating, incurable condition, developing an understanding of the drivers of MGUS progression is essential to identifying new therapeutic targets. To date, advanced age ≥ 60 years, serum paraprotein levels ≥15g/L, IgA paraprotein type, abnormal SFLC ratio (SFLCr ≥1.65) and bone marrow PC burden >5% have been recognised as predictors of MGUS-to-MM progression on a population basis. Moreover, in a recent study, elevated serum levels of BCMA in MGUS patients (≥ 77 ng/mL) were associated with shorter PFS of MGUS patients, although these results require further validation [378]. Nevertheless, none of these factors are sufficiently stringent to predict risk of progression in an individual patient. As such, the identification of biomarkers predictive of MGUS-to-MM progression would help guide the frequency of MGUS disease monitoring, which would, in turn, ensure more rapid detection of MM progression and assist with therapeutic decision making.

Advancing biological age is a risk factor for progression of various solid [263-265] and haematological cancers including MM, AML and CLL [303-305]. The accumulation of senescent cells in the tumour microenvironment with ageing has been implicated in promoting malignant cell outgrowth in solid cancers [266, 271-277, 279, 379] as well as haematological malignancies such as AML [300]. In MM, it has been reported that increased senescence of BM-MSCs is a feature of established MM disease [200, 229, 231, 232, 289, 296, 298, 299, 334]. However, to date, there is a paucity of knowledge concerning whether increases in senescent BM-MSC populations precede MM development and, in turn, play a role in promoting the transition from indolent MGUS to active MM. Consequently, the studies presented in this chapter aimed to characterise senescence in BM-MSCs from MGUS patients and to explore whether there was association between increased BM-MSC senescence at MGUS and progression to overt MM. Furthermore, as MM PCs have been implicated in

inducing BM-MSC senescence [231], we also explored whether the extent of BM-MSC senescence at MGUS and MM was a function of age or a consequence of disease stage.

Consistent with the age-related induction of BM-MSC senescence reported in the literature [258-260], our studies found that relative to young non-cancer donors, BM-MSCs of older non-cancer donors displayed evidence of increased senescence, including enlarged, polygonal and flattened cellular morphology, β-gal positivity, diminished *in vitro* proliferative capacity and early proliferative arrest in culture *in vitro*. Similarly, and in line with previous reports [229, 231, 289, 296, 298], we showed that BM-MSCs isolated from MM patients displayed senescent characteristics as described above. Moreover, consistent with previous studies, we found that MM BM-MSCs displayed increased *CDKN2A* expression levels as BM-MSCs from aged non-cancer control donors [200, 298]. Notably, we showed, or the first time, that BM-MSC from MGUS patients displayed a senescent phenotype, similar to that observed in MM. Importantly, we also showed that the senescent features of MGUS and MM BM-MSCs were consistent with those observed in aged haematologically normal, non-cancer controls, indicating that the induction of BM-MSC senescence is not influenced by MM disease development, but is a reflection of donor age.

In contrast to previous studies that identified increased senescence in BM-MSCs from MM patients when compared with those of age-matched non-cancer controls [229, 231, 296, 298], we did not observe significant morphological differences, or increased β-gal staining of MM BM-MSCs when compared with aged, non-cancer BM-MSCs. Similarly, and contrary to previously published reports [229, 231, 232], we found that the proliferative rate of MM BM-MSCs did not significantly differ from BM-MSCs obtained from aged non-cancer controls. These differences may be explained by the fact that BM-MSC samples obtained from aged

non-cancer controls in our study were collected from older patients (median: 88; range: 68-94 years) compared with that of our MGUS cohort (median: 67.5; range: 43-84) and MM (median: 70; range: 52-84) patients. Additionally, as the aged non-cancer control BM-MSCs used in our study were collected from patients undergoing total hip arthroplasty for fragility fractures of the femoral neck, it is possible that these cells display other differences related to the fracture phenotype that may confound our senescence analysis. Indeed, Tsangari *et al.* showed that bone samples taken from elderly fragility fracture patients are characterised by increased mRNA expression levels of the SASP factor, IL-6, relative to age-matched bone samples taken from individuals without evidence of skeletal disease [380]. Moreover, in line with the dysregulation of bone formation and resorption in fracture patients, the RANKL/OPG mRNA ratio was significantly higher in fragility fracture patients compared with controls [380]. Taken together, the correlation between BM-MSC senescence and patient age in the MGUS and MM cohorts in our study indicate that patient age is, at least in part, responsible for the variability in senescence in our patient cohorts.

Strikingly, here we showed, for the first, time that BM-MSC senescence in MGUS, as quantified by β-gal staining is significantly associated with increased risk of subsequent progression to MM. Our results suggest that β-gal staining cut-off of 10% is able to differentiate patients who are likely to progress, from those who are likely to have stable disease. Notably, 1 in 10 donors with lower percentages of β-gal positive cells progressed to MM during follow up, while 8 in 13 in the β-gal^{hi} group progressed, suggesting that elevated BM-MSC senescence at MGUS may be an indicator of subsequent progression to active MM. Thus, while high β-gal BM-MSC staining has an excellent sensitivity, accurately identifying 89% of all progressing patients, its specificity was suboptimal, as 36% of high β-gal patients did not go on to progress during follow up. In contrast, low β-gal BM-MSC had an excellent specificity for identifying

patients who would subsequently have long-term stable disease, with a false positivity rate of only 10%. Consequently, analysing BM-MSC β-gal staining at MGUS could be clinically informative in identifying MGUS patients who are likely to remain stable and not progress to overt MM. Furthermore, β-gal BM-MSC staining at MGUS had similar predictive power of disease progression as MM PC >5% in our cohort. Specifically, while MM PC >5% has been reported as predictive of MGUS progression, this test was able to detect MGUS patients likely to progress to MM 83% of the time (sensitivity 0.83), with a false positive rate of 43% (specificity 0.57).

Using a multivariable Cox model, we showed that when β-gal staining and MM PC burden were used in combination, they were not significant predictors of survival, suggesting that the predictive value of both variables are interdependent. Indeed, the percentage of β-gal positive cells significantly correlated with MM PC % at MGUS. Accordingly, these data suggest that greater numbers of senescent BM-MSCs, in close proximity to abnormal PCs, may promote their PC proliferation at MGUS. Indeed, several studies have shown that stromal cell senescence can promote the outgrowth of premalignant and malignant cells in various cancer contexts both *in vitro* and *in vivo,* as will be discussed in Chapter 4.

Notably, MM PCs have been shown to modulate senescence in BM-MSCs in some, but not all, studies. For example, the exposure of primary BM-MSCs from healthy volunteers to RPMI-8226 and MM.1S human myeloma cell lines in a trans-well system were shown to have no effect on $p21^{Cip1}$ and $p16^{INK4A}$ protein expression in BM-MSCs [233]. Additionally, direct co-culture of the human MM cell line KMS12-PE decreased MM BM-MSC β-gal activity and $p21^{Cip1}$ protein expression while having no effect on β-gal expression activity in healthy donor BM-MSCs or HS-5 fibroblasts [298]. In contrast, transwell co-culture of primary MM cells, or

MM cell lines NCI-H929, OPM2 and KMS-12-BM, with healthy human BM-MSCs for 24 hours was shown to induce a senescent phenotype in BM-MSCs, as defined by increased gene expression of *CDKN1A* and increased β-gal staining, compared with BM-MSCs in monoculture [231]. These findings suggests that MM cells may, under some conditions, increase BM-MSC senescence to further compound the senescent phenotype and promote the expression of MM growth supporting cytokines.

Our studies showed that β-gal staining of BM-MSCs isolated from MGUS and MM patients strongly correlates with patient age, while the proliferative rate (as measured by population doublings) and proliferative senescence (defined as the passage at which cells reach proliferative arrest) of BM-MSCs inversely correlated with patient age. Therefore, while we cannot rule out the possibility that MM PC-driven increases in senescent BM-MSCs may, in part, be responsible for the association between β-gal staining and PC numbers in the MGUS patients, our findings suggest that advancing age is a more important driver of the senescent BM-MSC phenotype than the effect of MM PC on BM-MSC. Moreover, as we didn't observe a significant association between β-gal staining and MM PC % at MM, we contend that MM PCs are less likely to be responsible for the induction of BM-MSC senescence. In addition, the lack of association between senescent BM-MSCs and the percentage of MM PCs at MM may suggest that at the overt cancer stage the MM PCs are less reliant on the BM microenvironment for their outgrowth as compared with the premalignant MGUS state.

As shown in our univariate analysis, the known risk factors associated with increased risk of MGUS progression, such as paraprotein levels ≥15g/L, high-risk paraprotein type and SFLC ratio ≥1.65 were not associated with progression in the MGUS cohort analysed in our study. We acknowledge that our analysis presented here may be hampered by small sample size.

Moreover, while on a population-wide basis, follow-up of 1,129 MGUS patients for an average of 34.1 years (range: 0.0-43.6 years) showed that advanced age (≥ 60 years) was associated with elevated risk of progression to MM [41], the association between patient age and risk of progression was not statistically significant in our study. This may be attributed to the significantly smaller sample size (n=28) of our patient cohort. Furthermore, this also illustrates the fact that while advanced age is associated with increased risk of progression on a population-wide basis, age alone is not sufficient to predict an individual's risk of progression.

In conclusion, we have shown that the senescent phenotype of BM-MSCs of MGUS and MM patients is similar to that of age-matched controls and is primarily related to patient age rather than disease stage. The observed BM-MSC senescence at MGUS suggests that stromal senescence occurs prior to the development of overt MM. Importantly, we have shown, for the first time, that elevated levels of BM-MSC senescence at MGUS is predictive of patient progression to MM. Further studies will explore whether BM-MSC senescence induction can promote the proliferation of MM PCs *in vitro* and *in vivo* and thereby directly contribute to PC outgrowth and progression to MM.

4 INVESTIGATING THE EFFECT OF BM-MSC SENESCENCE ON MM PC PROLIFERATION

4.1 Introduction

Several previous studies have suggested that senescent stromal cells may directly contribute to the proliferation of cancer cells [231, 266, 268, 271, 273, 274, 379]. In order to explore the effect of senescent stromal cells on cancer growth and progression *in vitro*, previous studies have utilised various *in vitro* senescence induction methods. One of the most common *in vitro* senescence induction methods is replicative exhaustion, which is achieved by sequential passaging of cells until they cease to proliferate [381]. This proliferative arrest is caused by progressive telomere shortening with each cell division [382]. Critically short telomeres are recognised by the DDR, which culminates in the induction of an irreversible proliferative arrest by activating the p53 pathway, which in turn leads to the upregulation of the CDK inhibitor $p21^{Cip1}$ (encoded by *CDKN1A*) [383]. In parallel with this, replicative senescence also results in the upregulation of expression at the *CDKN2A* locus, comprising $p14^{ARF}$ and $p16^{INK4A}$ CDK inhibitor genes [384, 385]. While $p14^{ARF}$ primarily works to support the function of $p21^{Cip1}$, the collective action of $p16^{INK4A}$ and $p21^{Cip1}$ leads to hypophosphorylation of the retinoblastoma protein, which sequesters E2F transcription factors and leads to permanent cell cycle arrest [386, 387]. Consequently, quantitation of the gene and protein expression of these $p14^{ARF}$ and $p16^{INK4A}$ CDK inhibitors is commonly utilised to confirm induction of replicative senescence [385, 388-390].

As replicative senescence may require prolonged *in vitro* passaging depending on cell type, alternative senescence induction methods that aim to trigger the DDR have been established, termed stress-induced premature (SIP) senescence. For example, hydrogen peroxide (H_2O_2) treatment is commonly used to induce stromal cell senescence [271, 391, 392]. Primarily, H_2O_2 treatment generates large amounts of ROS, which directly induce DNA damage by oxidising nucleoside bases, thereby inducing DNA breaks and triggering the DDR [393]. Furthermore,

treatment with chemotherapeutic drugs, such as doxorubicin is also commonly used to induce cellular senescence [275, 394-397]. Doxorubicin exerts its action by intercalating into DNA and disrupting the function of topoisomerase II, thereby halting DNA repair and inducing DNA damage, culminating in DDR [398]. Alternatively, gamma irradiation, which exerts direct high-energy damage to the phosphodiester backbone of DNA and leads to single and double stranded breaks with subsequent upregulation of $p21^{Cip1}$ expression, is also widely used to induce stromal cell senescence *in vitro* [390, 399-401].

Importantly, studies utilising *in vitro* replicative and SIP senescence induction techniques have revealed that stromal cell senescence has been implicated in promoting proliferation, invasiveness and chemotherapy resistance in premalignant and malignant cells *in vitro*. For example, co-culture studies suggest that replicatively senescent WI-38 fibroblasts significantly induce the proliferation of malignant breast cancer cell line MDA-MB-231, relative to co-culture with non-senescent controls [266]. Additionally, the proliferation rate of MDA-MB-231 breast cancer cells was also significantly increased upon co-culture with senescent primary human mammary fibroblasts, where senescence was induced with low-dose radiation, compared with co-culture with non-irradiated control fibroblasts [267]. Similar findings were observed by Coppe *et al.*, where direct co-culture of weakly tumorigenic Eph4-v epithelial cells with irradiation-induced and or replicatively senescent fibroblast cell lines WI-38 and hBF promoted their proliferation *in vitro* relative to co-culture with non-senescent control fibroblasts [268]. Moreover, senescent fibroblasts have also been shown to induce the proliferation of premalignant cells in direct co-culture. Namely, HaCAT human epidermal keratinocytes, S1 human mammary epithelial cells and Scp2 mammary epithelial preneoplastic cell lines, all which harbour p53 mutations but do not form tumours *in vivo*, proliferate significantly more in direct co-culture with replicatively senescent WI-38 fibroblasts compared

with non-senescent controls [266, 268]. Similarly, Lawrenson *et al.* showed that H_2O_2-mediated senescence induction in primary ovarian fibroblast cells significantly promoted the proliferation of partially transformed primary ovarian surface epithelial cells compared with co-culture with non-senescent cells in a 3-dimensional (3D) spheroid culture system [269]. Importantly, while senescent fibroblasts promoted the outgrowth of premalignant and malignant cells *in vitro*, this effect was not observed with normal, untransformed epithelial and ovarian fibroblast cells, suggesting that senescent cells can only promote the proliferation of partially transformed, preneoplastic cells [266, 269]. As senescent cells accumulate with age, this may contribute to the age-related progression from cancer precursor conditions to malignancy.

Aside from proliferation, stromal cell senescence has also been linked to conferring other advantages for malignant cells *in vitro*. For example, co-culture of Suit-2 and Capan-1 pancreatic cancer cell lines with irradiated MRC-5 fibroblasts, or irradiated primary pancreatic fibroblasts, significantly enhanced the Matrigel invasion of the cancer cells when compared with co-culture with non-senescent controls [270]. Furthermore, co-culture of MDA-MB-231 and MCF-7 breast cancer cell lines with radiation-induced senescent fibroblasts was shown to protect them from chemotherapy and radiotherapy induced apoptosis compared with co-cultures with non-senescent fibroblasts [267].

Additionally, senescent stromal cells have also been implicated in creating a microenvironment supportive of tumour growth of preneoplastic and neoplastic cells *in vivo*. For example, while injection of premalignant HaCAT or SCp2 epithelial cell lines alone does not result in tumour development in *nu/nu* mice, co-injection of these cells in combination with equal numbers of senescent WI-38 fibroblasts resulted in significant tumour development compared with co-

injection with non-senescent controls [266]. In line with this, co-injection of weakly tumorigenic EpH4-v mouse mammary epithelial cells with irradiation-induced senescent murine mammary fibroblasts into mammary fat pads of female *nu/nu* mice significantly promoted tumour formation and vascularisation relative to co-injection with non-senescent fibroblasts or EpH4-v cells alone [268]. Likewise, co-injection of malignant Ha(Pk) epithelial or MDA-MB-231 breast cancer cell lines in combination with senescent WI-38 fibroblasts also significantly promoted tumorigenesis in *nu/nu* mice compared with co-injection with non-senescent cells or tumour cells alone [266]. Similarly, injection of MDA-MB-231 breast cancer cells in nude mice, in combination H_2O_2-treated senescent umbilical cord MSCs, significantly promoted tumour initiation, accelerated tumour growth and led to a significant increase in tumour xenograft size and weight and tumour vascularisation compared with co-injection with non-senescent MSCs or the injection of tumour cells alone [271]. Analogously, co-injection of MDA-MB-231 cells or PC-3 prostate cancer cells, in combination with HCA2 fibroblasts treated with bleomycin to facilitate senescence induction, in *scid* mice significantly promoted the xenograft tumour growth compared with co-injection with non-senescent controls [272]. Co-transplantation of PC-3 cells with irradiation-induced senescent PSC27 fibroblast cells has also been reported to significantly increase xenograft size in *scid* mice compared with co-transplantation with non-irradiated PSC27 fibroblasts [273].

Importantly, the tumour supportive properties of senescent cells in the bone marrow microenvironment have also been explored *in vivo*. For example, Luo *et al.* used a FASST (fibroblasts accelerate stromal supported tumorigenesis) model that utilises a stromal-specific Cre-recombinase, driven by the collagen-I promoter, to induce targeted stromal senescence in the murine BM by inducing the expression of $p27^{Kip1}$ cell cycle inhibitor [274]. Indeed, when these mice were used in an intracardiac NT2 murine breast cancer model, significantly higher

tumour burden was detected in bones of FASST mice compared with littermate controls, suggesting that the accumulation of senescent stromal cells in the bone marrow microenvironment is sufficient to create a hospitable niche for breast cancer cell outgrowth [274]. In line with this, BM-MSC senescence has been shown to play a role in tumour growth of acute myeloid leukaemia cells in a p16-3MR mouse model. The p16-3MR mice contain a transgene, comprised of the $p16^{INK4A}$ regulatory elements driving the expression of herpes simplex virus thymidine kinase, which enables selective elimination of $p16^{INK4A}$ expressing cells following administration of ganciclovir [402]. Strikingly, the ablation of senescent cells in a p16-3MR mice was shown to significantly reduce tumour growth of MN-1 acute myeloid leukaemia cells and subsequently increase murine survival [300].

Collectively, the induction of stromal cell senescence by SIP or replicative means, has been shown to promote the proliferation of premalignant and malignant cells in direct co-culture *in vitro* and *in vivo*. Importantly, senescent stromal cells have also been implicated in facilitating tumour growth in the bone marrow microenvironment *in vivo*. The age-related accumulation of senescent stromal cells, including BM-MSCs, may play a role in promoting the outgrowth of malignant cell clones in the BM and promote the progression of haematological cancers such as MM. In Chapter 3, we showed that BM-MSC senescence precedes overt MM development and is evident at the MGUS stage and strongly correlates with patient age. Importantly, we also showed that BM-MSC senescence, at MGUS, is predictive of subsequent patient progression to MM. While it has been suggested that MM PCs may induce senescence in BM-MSCs [231], our results suggest that increasing BM-MSC senescence with age is associated with increased risk of progression from MGUS to MM. Therefore, in this chapter we firstly evaluated the MM tumour cell supporting properties of MGUS and MM BM-MSCs. Moreover, we also tested both replicative and SIP methods of senescence induction of murine and human BM-MSCs to

directly investigate whether contact co-culture of senescent BM-MSCs enabled MM plasma cell proliferation *in vitro*.

4.2 Results

4.2.1 Analysis of MM growth supporting properties of BM-MSCs from non-cancer donors and MGUS and MM patients

As we have shown that BM-MSC senescence at MGUS was associated with progression to active MM, we investigated the capacity of MGUS and MM BM-MSCs to support the proliferation of MM PC *in vitro*. Firstly, we assessed the behaviour of MM PCs in direct co-culture with non-senescent BM-MSCs. Human and murine MM cell lines KMM1 and 5TGM1, respectively, were transduced to express luciferase (KMM1-luc and 5TGM1-luc) to enable cell number quantification by bioluminescence. Direct co-culture of KMM1-luc cells with human BM-MSCs obtained from young (<35 years of age) non-cancer donors for 72 hours significantly suppressed KMM1 proliferation by 47.4%, relative to monoculture controls (p=0.0010; unpaired t-test; Figure 4.1A). Similarly, direct co-culture of 5TGM1-luc cells with murine BM-MSCs significantly suppressed 5TGM1-luc proliferation by 92.9% when compared with 5TGM1-luc cells cultured alone (p<0.0001; unpaired t-test; Figure 4.1B).

Figure 4.1 BM-MSCs suppress the proliferation of MM cell lines *in vitro.* For all co-culture experiments, BM-MSCs were seeded at $2.5x10^4$cells/cm^2 in triplicate in a 96 well plate and allowed to adhere overnight. Luciferase-expressing MM PCs were seeded at $1x10^4$cells/well the following day and the number of MM PC cells/well was quantified after 3-days of co-culture by bioluminescence imaging. (**A)** Co-culture of human KMM1-luc MM cells with BM-MSCs from healthy non-cancer controls <35 years of age, n=3. (**B)** Co-culture of murine 5TGM1-luc MM cells with KaLwRij BM-MSCs, n=4. *p<0.05, ****p<0.0001, unpaired t-test. Graphs depict mean + SEM.

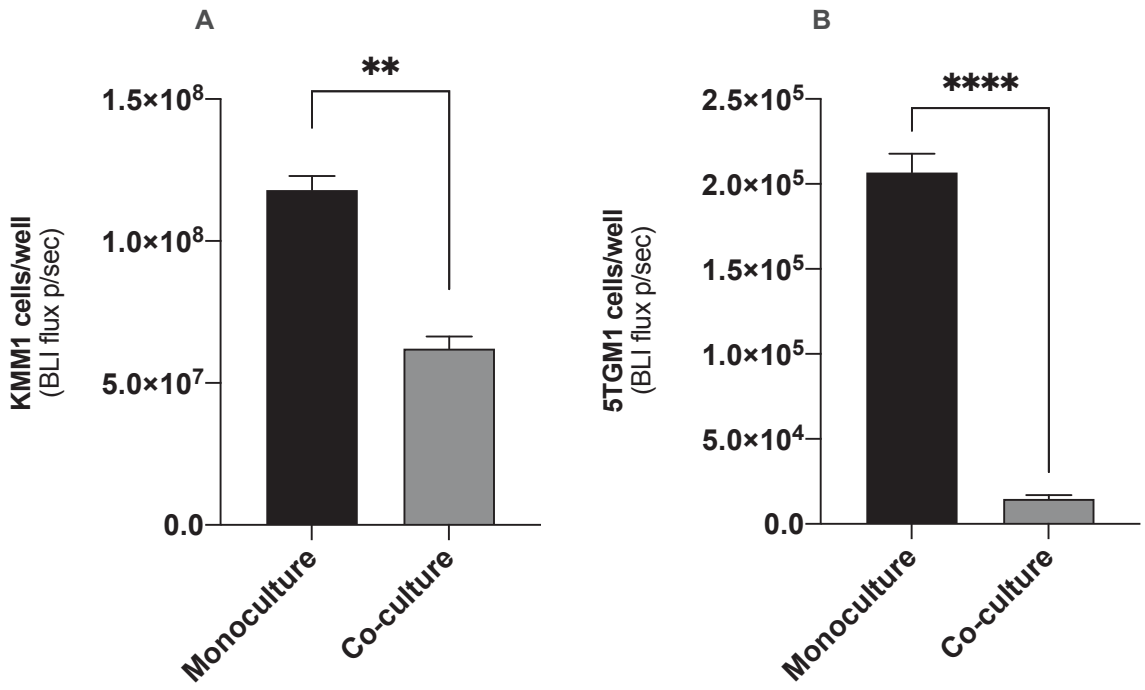
A
**
1.5×10^8
1.0×10^8
5.0×10^7
0.0
KMM1 cells/well
(BLI flux p/sec)
Monoculture
Co-culture
B
****
2.5×10^5
2.0×10^5
1.5×10^5
1.0×10^5
5.0×10^4
0.0
5TGM1 cells/well
(BLI flux p/sec)
Monoculture
Co-culture

Next, to determine the effect of BM-MSCs from different disease settings on MM PC proliferation, KMM1-luc cells were co-cultured in direct contact with BM-MSCs isolated from young (<35 years of age) and aged (60+ years of age) non-cancer individuals, newly diagnosed MGUS or MM patients. The proliferation of KMM1-luc cells was decreased by 42.3% and 42.0%, relative to KMM1-luc proliferation in monoculture, after 72hr co-culture with BM-MSCs from young (median: 42.3%; range: 33.6%-49.0%) and aged (median: 42%; range: 17.5%-53.7%) non-cancer control BM-MSCs, respectively (Figure 4.2A). The level of proliferative suppression of KMM1-luc cells in co-culture with BM-MSCs from MGUS patients was similar to that observed with aged non-cancer controls, with a 32.0% reduction in cell number compared with KMM1-luc cells in monoculture (median: 32.0%; range: 5.00%-43.0%). Moreover, the suppressive effect was further reduced in co-culture with MM BM-MSCs, with a 14.0% reduction in KMM1-luc cell numbers, compared with KMM1-luc monocultures (median: 14.0%; range: 5.00%-45.0%). Indeed, KMM1-luc cell numbers were significantly higher in co-culture with MGUS and MM BM-MSCs than in those with control BM-MSCs from young non-cancer patients (p=0.044 and p=0.034 respectively; Kruskal-Wallis test with Dunn's multiple comparisons test; Figure 4.2A).

Next, we investigated whether the ability of BM-MSCs from MGUS patients to support KMM1-luc cells in direct co-culture *in vitro* was linked to the rate of MGUS-to-MM disease progression in these MGUS donors. ROC analysis suggested that the extent of growth suppression that BM-MSCs exerted on KMM1-luc cell proliferation could be used to differentiate patients who were likely to progress to MM compared with those who were likely to have stable disease (AUC: 0.69; 95% CI: 0.41-0.96; p=0.19; Figure 4.2B). The selected cut-off of ≥0.686 (≥68.6% of the proliferation level observed in KMM1-luc monoculture) showed predictive power for MGUS-to-MM progression with a true positive rate of 60% and a false

positive rate of 14% (sensitivity: 0.60 and specificity: 0.86; Figure 4.2B). Three out of 12 MGUS patients in the KMM1-prolif^{lo} group progressed to overt MM during follow up, while 6 of 7 patients in the KMM1-prolif^{hi} group progressed. Kaplan-Meier analysis revealed that MGUS patients whose BM-MSCs had a greater capacity to support KMM1-luc proliferation in co-culture (KMM1-prolif^{hi}) were 4.1 times (95% CI: 1.018-16.5) more likely to progress to MM compared with those whose BM-MSCs had a lower capacity to promote KMM1-luc proliferation (KMM1-prolif^{lo}) (p=0.02; log-rank test; Figure 4.2C). The median time to progression of KMM1-prolif^{hi} patients was 142.4 weeks, while median survival of KMM1-prolif^{lo} patients was 514.3 weeks. Collectively, these data suggest that BM-MSCs isolated from patients with MM display a reduced capacity to suppress the growth of MM PCs in co-culture *in vitro* when compared with aged non-cancer BM-MSCs. Furthermore, there was an inverse association between the capacity of BM-MSCs from MGUS patients to suppress MM PC growth *in vitro* and risk of progression to MM in these patients. Consequently, these studies highlight that changes in the BM microenvironment, specifically in BM-MSCs, may play a role in promoting MM PC tumour outgrowth and progression from MGUS to MM.

Figure 4.2 MM PC growth supporting properties of BM-MSCs from non-cancer controls, MGUS and MM patients *in vitro*. (A) BM-MSCs obtained by plastic adherence from *n*=10 young (<35) and *n*=10 aged (60+ years) non-cancer controls and *n*=18 newly diagnosed MGUS and *n*=6 MM patients were cultured *in vitro* for 3 weeks and used in experiments at the start of week 3 (passage 5). For co-culture experiments, BM-MSCs were seeded at $2.5x10^4$cells/cm^2 in triplicate and allowed to adhere overnight. Luciferase-expressing KMM1 cells were seeded at $1x10^4$cells/well the following day and the number of MM PCs was quantified after 3-days of co-culture by bioluminescence imaging. Bioluminescent signal was normalised to that of KMM1-luc cells in monoculture. Graph depicts the median and interquartile range, **p*<0.05, Kruskal-Wallis test with Dunn's multiple comparisons post-test. **(B)** ROC analysis was conducted to stratify MGUS patients on their ability to allow KMM1-luc proliferation in direct culture. **(C)** MGUS patients were stratified into those that enabled KMM1-luc proliferation of <68.6% of KMM1-luc monocultures (KMM1-$prolif^{lo}$) (*n*=12) and those that enabled KMM1-luc proliferation of ≥68.6% relative to monoculture levels (KMM1-$prolif^{hi}$) (*n*=7). Progression to MM was plotted using Kaplan-Meier curves and curves were compared with the log-rank test. MGUS progression defined as time of commencement of treatment for their myeloma disease; patients were censored at time of last follow-up.

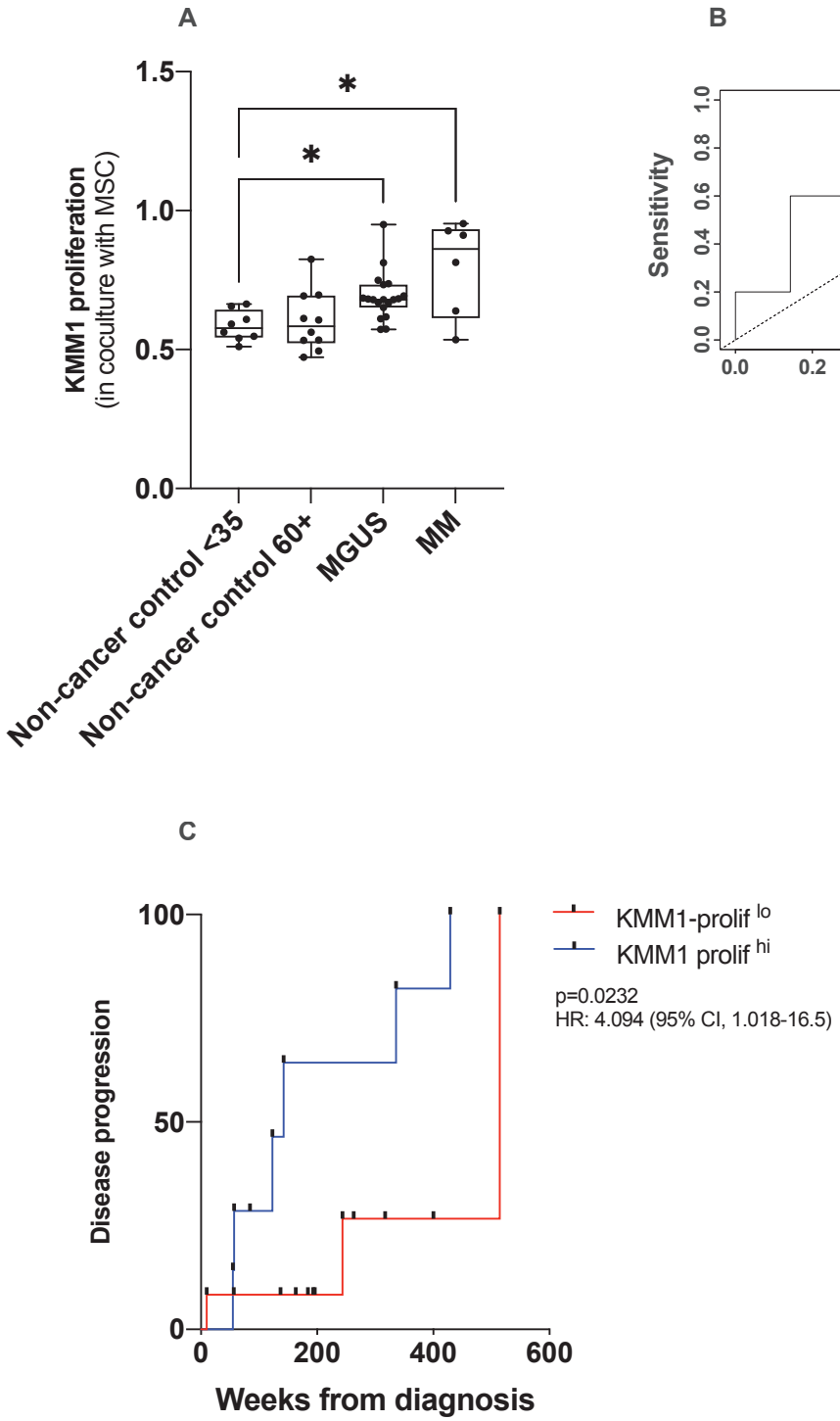
A
B
C
KMM1 proliferation
(in coculture with MSC)
1.5
1.0
0.5
0.0
*
*
Non-cancer control <35
Non-cancer control 60+
MGUS
MM
Sensitivity
1-specificity
0.0
0.2
0.4
0.6
0.8
1.0
KMM1
Disease progression
100
50
0
0
200
400
600
Weeks from diagnosis
KMM1-prolif lo
KMM1 prolif hi
p=0.0232
HR: 4.094 (95% CI, 1.018-16.5)

4.2.2 BM-MSCs senescence with biological age in KaLwRij mice and promote tumour cell proliferation in direct culture *in vitro*.

We have shown that both BM-MSC senescence and the ability of BM-MSCs to support KMM1-luc growth in co-culture at MGUS was predictive of progression to overt MM. This led us to hypothesise that increasing senescent BM-MSCs numbers with age could enable PC outgrowth and progression from MGUS to MM. In order to further validate that the age-associated increased senescent BM-MSC numbers could enable MM PC proliferation, we initially assessed BM-MSC senescence in ageing mice. In these studies, we investigated whether BM-MSCs isolated from 18-month-old KaLwRij mice displayed increased senescence, relative to young 8-week-old control mice. Consistent with what has been shown in the literature in other mouse strains [244], BM-MSCs isolated from KaLwRij aged mice displayed increased β-gal staining and enlarged, flattened cell morphology relative to BM-MSCs isolated from young 8-week-old mice, indicative of increased senescence (Figure 4.3A). In keeping with this observation, gene expression analysis revealed that mRNA expression levels of *Cdkn2a* ($p14^{INK4A}$) were elevated 2-fold in BM-MSCs from 18-month-old mice (mean: 0.008; SEM: 0.0017) compared with 8-week-old mice (mean: 0.004; SEM: 0.0010), albeit not significantly (Figure 4.3B). Similarly, there was a 1.8-fold increase in *Cdkn2a* ($p16^{INK4A}$) mRNA expression levels in 18-month-old mice (mean: 0.0079; SEM: 0.0020) relative to 8-week old mice (mean: 0.0046; SEM: 0.0013), but this did not reach statistical significance (Figure 4.3C). Intriguingly, the number of 5TGM1-luc cells increased significantly by 20.8-fold in co-culture with BM-MSCs isolated from 18-month-old mice relative to BM-MSCs isolated from 8-week-old mice (p=0.011; unpaired t-test; Figure 4.3D). This suggests that the onset of age-induced BM-MSC senescence reduced the proliferative suppression exerted by KaLwRij BM-MSCs on MM PCs. Collectively, we show that BM-MSCs senesce with advancing biological age in KaLwRij mice and allow the proliferation of murine MM PCs in co-culture *in vitro*.

Figure 4.3 Murine BM-MSCs senesce with biological ageing and are less suppressive of 5TGM1-luc proliferation in direct co-culture compared with BM-MSCs from young mice *in vitro*. BM-MSCs were isolated by plastic adherence from long bones from 8-week-old and 18-month-old KaLwRij mice, cultured for 2 weeks *in vitro* and senescent features were analysed at the start of week 2 in culture (passage 3). **(A)** Cells were stained for senescence-associated β-galactosidase activity (blue). Representative images are shown. Scale bar: 300 μm. RNA was extracted and expression of **(B)** *Cdkn2a* $p14^{INK4A}$ and **(C)** *Cdkn2a* $p16^{INK4A}$ mRNA levels was analysed by real time PCR. Data are presented as mRNA expression normalised to *Gapdh*, n=4-6. **(D)** For all co-culture experiments, BM-MSCs were seeded at $2.5x10^4$cells/cm^2 in triplicate in a 96 well plate and allowed to adhere overnight. Luciferase-expressing MM PCs were seeded at $1x10^4$cells/well the following day and the number of MM PC cells/well was quantified after 3-days of co-culture by bioluminescence imaging. Proliferation of 5TGM1-luc cells co-cultured with BM-MSCs from 8-week-old and 18-month-old KaLwRij mice, n=4-5; *p<0.05, unpaired t-test. Graphs depict median and interquartile ranges.

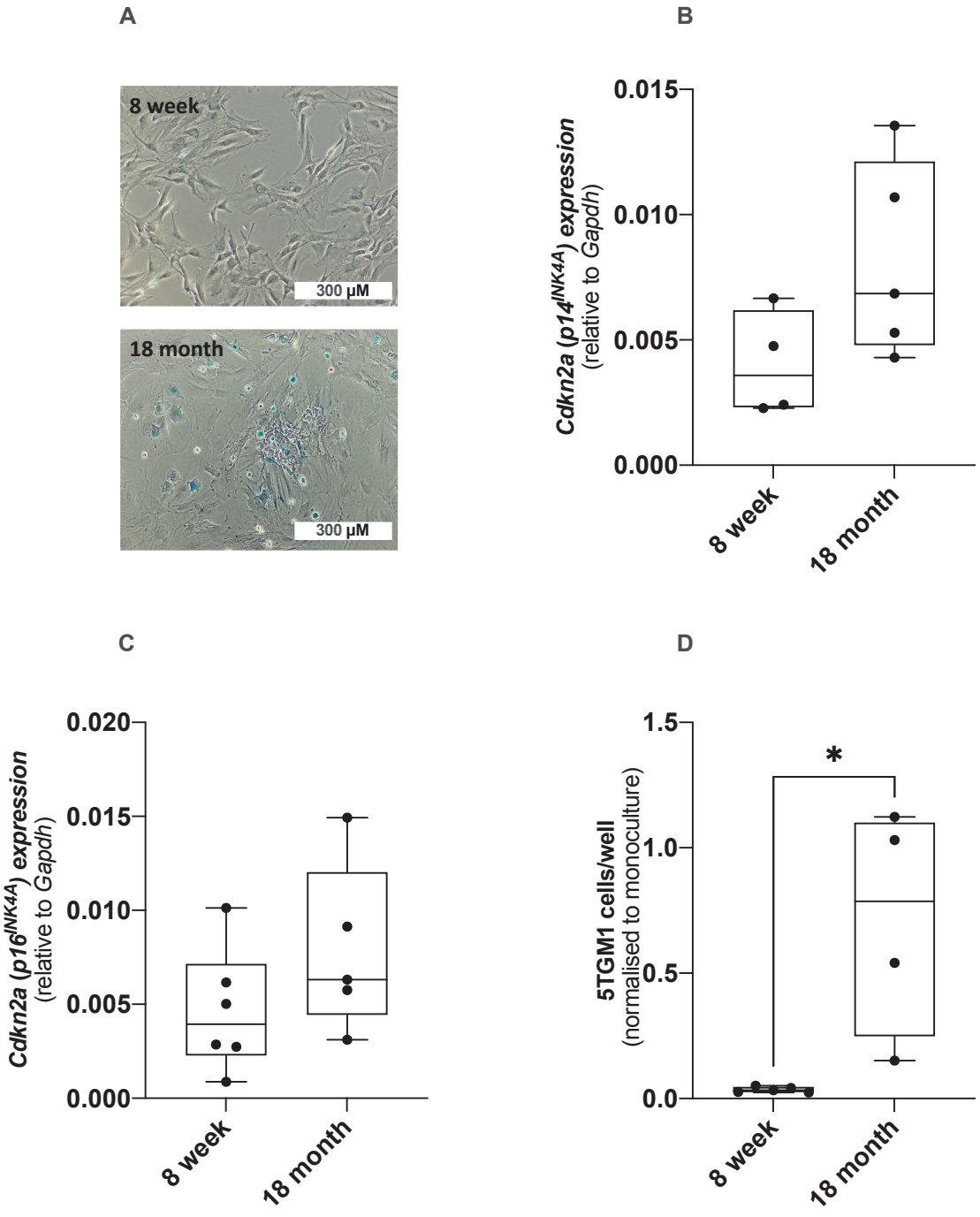
A
8 week
300 µM
18 month
300 µM
B
Cdkn2a (p14INK4A) expression
(relative to Gapdh)
0.015
0.010
0.005
0.000
8 week
18 month
C
Cdkn2a (p16INK4A) expression
(relative to Gapdh)
0.020
0.015
0.010
0.005
0.000
8 week
18 month
D
5TGM1 cells/well
(normalised to monoculture)
1.5
1.0
0.5
0.0
*
8 week
18 month

4.2.3 Validation of senescence induction methods in human and murine BM-MSC senescence *in vitro*

To further investigate whether senescent BM-MSCs could enable PC outgrowth, we set out to directly induce senescence, *in vitro,* in human and murine BM-MSCs and use these cells in co-cultures with MM cell lines to assess their proliferation compared with co-culture with non-senescent control BM-MSCs. Firstly, we evaluated hydrogen peroxide (H_2O_2) treatment as a method of BM-MSC senescence induction, as H_2O_2 treatment has been widely reported in the literature to lead to oxidative stress-induced, premature senescence in fibroblastic cells [403, 404] including BM-MSCs [405]. BM-MSCs obtained by plastic adherence from non-cancer donors <35 years of age and KaLwRij mice were cultured *in vitro* for 2 weeks and used in experiments at the start of week 2 (passage 3). Both human and murine BM-MSCs were treated with 600 μM or 800 μM H_2O_2 for 2 hours to facilitate senescence induction. The onset of senescence was evaluated after 96 hours. Although an increase in β-gal staining was observed in both human and murine BM-MSCs, with increasing concentration of H_2O_2, the treated cells did not show morphological features of senescence and remained spindle shaped, much like the untreated controls (Figures 4.4A and 4.4B). Accordingly, mRNA expression levels of senescence associated *CDKN2A* and *CDKN1A* did not significantly differ in human BM-MSCs treated with 600 μM or 800 μM or untreated controls (*CDKN2A* $p14^{INK4A}$ p=0.50 [Figure 4.4C*i*]; $p16^{INK4A}$ p=0.63 [Figure 4.4C*ii*]); *CDKN1A* p=0.14 (Figure 4.4C *iii*); one-way ANOVA). Similarly, in the murine setting, mRNA expression levels of *Cdkn2a* $p14^{INK4A}$ and $p16^{INK4A}$ were not significantly affected by treatment with 600 μM and 800 μM H_2O_2, when compared with untreated control BM-MCs ($p14^{INK4A}$ p=0.40; $p16^{INK4A}$ p=0.67; one-way ANOVA; Figure 4.3D*i-ii*). Consequently, as we did not observe the induction of a senescent phenotype with H_2O_2 treatment in both human and murine BM-MSCs this senescence induction technique was not used in further studies.

Figure 4.4 H_2O_2 treatment does not lead to senescence induction of human and murine BM-MSCs. BM-MSCs obtained by plastic adherence from non-cancer patients <35 years of age and KaLwRij mice were cultured *in vitro* for 2 weeks and used in experiments at the start of week 2 (passage 3). BM-MSCs were seeded at $6x10^3$cells/cm^2 in 6 well plates, allowed to adhere overnight and cultured for 2 days to achieve 60-70% confluence. Subsequently, BM-MSCs were treated with 0-800 μM H_2O_2 for 2 hours in normal media (α-MEM with 10% FCS with additives and ascorbate-2-phosphate). Treatment was aspirated and wells washed twice with PBS. Cells were then cultured in normal media for 96 hours. β-galactosidase activity (blue) was evaluated in **(A)** healthy non-cancer patients <35 years of age and **(B)** murine KaLwRij BM-MSCs. Representative images are shown. Scale bar: 300 μm. **(C)** RNA was extracted from H_2O_2-treated BM-MSCs from healthy non-cancer patients <35 years of age and mRNA expression levels of**(i)** *CDKN2A* $p14^{INK4A}$, **(ii)** *CDKN2A* $p16^{INK4A}$ and **(iii)** *CDKN1A* were analysed by real time PCR. Data are presented as mRNA expression normalised to *ACTB*. **(D)** RNA was extracted from H_2O_2-treated BM-MSCs from KaLwRij mice and mRNA expression levels of *Cdkn2a* **(i)** $p14^{INK4A}$ and **(ii)** $p16^{INK4A}$ were analysed by real time PCR. Data are presented as mRNA expression normalised to *Gapdh*, *n*=3, one-way ANOVA. Graphs depict mean + SEM.